SINET: Ethiop. J. Sci., 24(1):1–15, 2001
 ISSN: 0379–2897

ON THE EQUATION XY = Z (Y - X^2) OVER A UNIQUE FACTORIZATION DOMAIN

Yismaw Alemu

Department of Mathematics, Faculty of Science, Addis Ababa University
PO Box 1176, Addis Ababa, Ethiopia, E-mail: maths.aau@telecom.net.et

ABSTRACT: The article gives the parametric solutions of $xy = z(y - x^2)$ over any unique factorization domain. An application of the obtained characterization to Diophantine equations is demonstrated.

1. INTRODUCTION

b = 5 and a = 2 are natural numbers such that the decimal representation of b/a is $(a.b)_{ten}$. In an informal discussion, L. Kadosh* asks whether there are other natural numbers b and a such that $b/a = (a.b)_{ten}$.

To fix notations, let a, b and g be natural numbers with $g \geq 2$. Put

$$a = \sum_{i=0}^{k} a_i g^i \text{ and } b = \sum_{j=0}^{n-1} b_j g^j$$

with $0 \leq a_i, b_j < g$, k and n, whole numbers, $n > 0$ and $a_k b_{n-1} \neq 0$. The expression

$$\alpha = a + \frac{b}{g^n} = \sum_{i=0}^{k} a_i g^i + \sum_{j=0}^{n-1} b_j g^{-n+j}$$

* L. Kadosh says that he got the problem from a colleague. A reviewer has pointed out that the problem is due to Michael S. Runge (1991).

is called the representation of the rational number $\alpha = a + \frac{b}{g^n}$ in base g. For simplicity, we denote this representation of α by $(a.b)_g$.

Thus a generalization of the above posed problem is whether

$$b/a = (a.b)_g \tag{1}$$

holds for some other pair of natural numbers (b,a). Still more, the above problem is contained in a question that looks for natural numbers a and b, b not a multiple of a, such that

$$\frac{b}{a} = a + \frac{b}{h} \tag{2}$$

for some natural number h.

Our basic interest is on the solutions of (2) in natural numbers. On the other hand, the arguments developed to solve (2) in natural numbers also hold in unique factorization domains. Evidently (2) is equivalent to

$$ab = h(b - a^2) \tag{3}$$

with $ah \neq 0$, b is not a multiple of a, which is the title of the article with x = a, y = b and z = h over such domains. In the next two sections, we discuss (3) in any unique factorization domain. Theorem 1 gives the parametric solutions of (3). The particulars about natural numbers are indicated in the remarks. The last section gives positive answer to (1). The base ten problem in (1) shall be considered in a forthcoming article.

2. THE PRIMARY RESULTS

In the present article, D denotes a unique factorization domain (UFD) with $1 \neq 0$. If a, b, A, $B \in D\backslash\{0\}$, then a greatest common factor of a and b exists, denoted by (a , b), and is unique up to associates. We write (a, b) = (A, B) to mean that (a, b) and (A, B) are associates. Moreover (a, b) = 1 shall mean that a and b are relatively prime.

Suppose a, b$\in D$, b$\notin$aD such that

$$\frac{b}{a}=a+\frac{b}{h} \quad (4)$$

for some hϵD. Then h is a non-unit in D and (4) is equivalent to (3) over D. Put $c = b - a^2$ and let $d = (a, b)$. Then $a = da_1$ and $b = db_1$ with $a_1, b_1 \in D$ and $(a_1, b_1) = 1$. Therefore $c = dc_1$ with $c_1 = b_1 - da_1^2 \in D$. It is then clear that a_1 is a non-unit and relatively prime to b_1c_1. Unless otherwise stated, a, a_1, b, b_1, c, c_1, d and h refer to the notations defined above. For a prime p$\in D$ and x$\in D\backslash\{0\}$, $ord_p(x)$ is the largest integer n such that

$$x \equiv 0 \pmod{p^n}.$$

Lemma 1. Suppose a, b and h$\in D$ satisfying (4). Then, with the notations defined above, c_1 divides d^2. If D is the ring of rational integers, then h is odd iff c_1 is even and

$$ord_2(c_1) = 2\, ord_2(d).$$

Proof. If a, b, hϵD satisfy (4), then they satisfy (3).

Hence

$$h = \frac{ab}{c} = \frac{d^2a_1^3}{c_1} + a = a_1\left(\frac{d^2a_1^2}{c_1} + d\right) \quad (5)$$

Since $(a_1, c_1) = 1$, we conclude that $d_2 \equiv 0 \pmod{c_1}$.

To prove the second part, let a, b, h be rational integers satisfying (3). Suppose h is odd. Then from (5), we conclude that a_1 is odd, hence $\frac{d^2}{c_1}$ and d

**The fraction notation seems handier for this problem and we continue to use it.

have opposite parity. If $\frac{d^2}{c_1}$ were even, then d would be even. Hence $\frac{d^2}{c_1}$ is necessarily odd, and hence d is even. Therefore $\mathrm{ord}_2(c_1) = 2\ \mathrm{ord}_2(d) \geq 2$.

Conversely, if c_1 is even and $\mathrm{ord}_2(c_1) = 2\ \mathrm{ord}_2(d) \geq 2$, then d is even. But then $(a_1, c_1) = 1$, hence a_1 is odd. Therefore

$$h = a_1\left(\frac{d^2}{c_1}a_1^2 + d\right) \text{ is odd.}$$

Assume a, b, $h \in D$ satisfy (4). Then by Lemma 1, $d^2 = qc_1$ for some $q \in D$. Using (5), we have $h = qa_1^3 + a = a_1(qa_1^2 + d)$.

On the other hand, $b = a^2 + c = d^2a_1^2 + dc_1 = c_1(qa_1^2 + d)$.

Conversely, consider the following algorithm.

(2.1) Choose arbitrary but relatively prime $a_1, c_1 \in D\backslash\{0\}$, a_1 non-unit and $d \in D\backslash\{0\}$ such that $d^2 = qc_1$ for some $q \in D$.

(2.2) Put $a = da_1$, $c = dc_1$ so that $d^3 \equiv 0 \pmod{c}$.

(2.3) Set $b = a^2 + c = c_1(qa^2{}_1 + d)$
$h = qa_1^3 + a = a_1(qa_1^2 + d)$

Then a, b and h satisfy the relation

$$\frac{b}{a} = a + \frac{b}{h}.$$

Hence we have proved the following.

Theorem 1. Suppose a, b, $h \in D$ such that $b \notin aD$ and $\frac{b}{a} = a + \frac{b}{h}$. Then $b = c_1(qa_1^2 + d)$ and $h = a_1(qa_1^2 + d)$, where $d^2 = qc_1$. Conversely, the solutions of $\frac{b}{a} = a + \frac{b}{h}$ are obtained by the algorithm **(2.1)** - **(2.3)**.

Remark 1

(1.1) Consider the partial ordering on D given by $x \leq y$ iff $y \in xD$, and $x < y$ iff $x \leq y$ but $x \notin yD$. If c_1 in Theorem 1 is a unit, then, with $u = c_1^{-1}$, $bu = qa_1^2 + d$. Thus the element $h = a_1(qa_1^2 + d) = ua_1b$ is such that $b < h$, in the sense of the partial ordering just indicated. However, if c_1 is not a unit, it is immediate from the Theorem that neither $h \leq b$ nor $b \leq h$ holds.

(1.2) If a, b and h are natural numbers satisfying (4), it follows from Theorem 1 that $b < h$ iff $c_1 < a_1$, where $<$ is the usual (natural) order on the set of rational integers.

(1.3) In the choice of parameters in the above algorithm, it could happen that $h = g^n$ for some $g \in D$ and natural number $n > 1$. If a,b and h are natural numbers, then $h = g^n$, $n > 1$, could happen only if $d = (a, b) > 1$. Indeed, otherwise $d = 1$ and $c \mid d^2$ gives that $c = 1$. But then $b = a^2 + 1$ and $ab = h = g^n$ gives that $b = A^n$ and $B^n = a$ with natural numbers A, B each greater than 1. Consequently $1 = b - a^2 = A^n - B^{2n}$, which obviously does not hold for $n > 1$.

(1.4) If D is the ring of rational integers and c_1 in the above algorithm is odd, then by Lemma 1, h is necessarily even. This in particular holds when $d = c$. On the other hand, if c_1 is even such that $\mathrm{ord}_2(c_1) = 2\ \mathrm{ord}_2(d)$, then h is necessarily odd. For instance with $c_1 = 4$, $a_1 = 7$, $d = 2(5) = 10$, we have $a = 70$, $c = 40$, $b = 4940$, $h = 8645$ and

$$\frac{4940}{70} = 70 + \frac{4940}{8645}\ .$$

Corollary 1. If c_1, a_1, q and d are natural numbers with $c_1 < a_1$ and $d^2 = qc_1$, then $a = da_1$, $b = c_1(qa_1^2 + d)$ and $h = a_1(qa_1^2 + d)$ satisfy the relation

$$\frac{b}{a} = a + \frac{b}{h} = (a.b)_h$$

Proof. By Theorem 1 and Remark (1.2),

$b = c_1 (qa_1^2 + d) < a_1 (qa_1^2 + d) = h$

satisfy (4). Thus a and b are one digit natural numbers in base h, and the result follows.

3. THE CASE $h = g^n$

In this section for a, b, h satisfying (4), we formulate necessary and sufficient conditions for $h = g^n$ for some $g \in D$ and natural number $n > 1$. We need the following Lemma.

Lemma 2. Suppose e, $f \in D\backslash\{0\}$ are relatively prime and for some $g \in D$ and natural number $n > 1$, $ef = g^n$. Then

$e = uB^n$, $f = u^{-1}A^n$ and $g = AB$

for some u, A, $B \in D$, with unit u and (A, B) = 1.

Proof. The assertion is obvious if both e and f are units. Hence assume, without loss of generality, that e is a non-unit. Then g is non-unit. Since D is a UFD,

$$g = wp_1^{\alpha_1} p_2^{\alpha_2} \dots p_k^{\alpha_k}$$

with primes $p_1, p_2, \dots p_k$ in D, pairwise relatively prime, $\alpha_i > 0$ and unit $w \in D$. If need be by reindexing, let $p_1, p_2, \dots, p_t$ be the only prime factors of e, up to associates. If t = k, then f is a unit and we can set A = 1 and B = g. Otherwise t < k. In any of the cases, put

$$B = wp_1^{\alpha_1} \dots p_t^{\alpha_t} \text{ and } A = p_{t+1}^{\alpha_{t+1}} \dots p_k^{\alpha_k}$$

so that AB = g and (A, B) = 1. It follows that

$ef = B^nA^n$.

Since (e, A) = 1 = (B, f), it is clear from the last equation that

$e = uB^n$ and $f = u^{-1}A^n$

for some unit $u \in D$.

3.1 The case (a, b) is an associate of b - a^2

Suppose d = (a, b) is an associate of c = b - a^2. Then c = dw for some unit w $\in D$. But then

$$hc = ab = a(a^2 + c) = da_1(d^2a_1^2 + dw) \text{ implies that } hw = da_1(da_1^2 + w).$$

Therefore $g^n = h = w^{-1}da_1\ (da_1^2 + w)$. Since $(w^{-1}da_1,\ da_1^2 + w) = 1$, by Lemma 2, we get $w^{-1}da_1 = uB^n$ and $da_1^2 + w = u^{-1}A^n$ for some unit $u \in D$, g = AB, A, B $\in D$ and (A, B) = 1. Multiplying the first equation by w and the second by d, we respectively get

$$a = da_1 = wuB^n \text{ and } b = (da_1)^2 + dw = u^{-1}dA^n \tag{6}$$

with units u, w $\in D$, A, B $\in D$, (A, B) = 1, dw = c = b - a^2, d = (a, b), a_1 non-unit in D and $h = (AB)^n$.

3.2 The case (a, b) is not an associate of b - a^2

Suppose (a, b) is not an associate of b - a^2. Then c_1 is not a unit in D. Recall that

$$\frac{c_1}{a_1} = \frac{c}{a} = \frac{b-a^2}{a} = \frac{b}{a} - a = \frac{b}{h} = \frac{db_1}{h} \tag{7}$$

As $b_1 - da_1^2 = c_1$ and $(a_1, b_1) = 1$, it is clear that c_1 divides d iff c_1 divides b_1. We now consider two cases.

Case 1: Suppose c_1 divides d. Then $d = c_1d_1$ and (7) reduces to

$$\frac{1}{a_1} = \frac{d_1b_1}{h}\ . \tag{8}$$

Since D is a UFD, set $d_1 = d_{11}d_{12}$ such that every prime factor of d_{11} is a factor of a_1 and $(a_1, d_{12}) = 1$. Thus (8) reduces to

$g^n = h = (a_1d_{11})\ (d_{12}b_1)$.

Since $(a_1d_{11},\ d_{12}b_1) = 1$, by Lemma 2, we have

$$a_1d_{11} = uB^n \text{ and } d_{12}b_1 = u^{-1}A^n \tag{9}$$

with $g = AB$, $(A, B) = 1$ and unit $u \in D$. Multiplying the first equation in equ. (9) by c_1d_{12} and the second by c_1d_{11}, we respectively obtain

$$a = da_1 = c_1d_{12}uB^n \text{ and } b = u^{-1}c_1d_{11}A^n \tag{10}$$

with $(A, B) = 1$, u unit, $c_1d_{11}d_{12} = d = (a, b)$, a_1 and c_1 non-units $dc_1 = c = b - a^2$ and $h = (AB)^n$.

Case 2: Suppose c_1 does not divide d. Then, as remarked in the first paragraph of the section, c_1 does not divide b_1 too. However from (7), since $(a_1, c_1) = 1$, c_1 divides db_1. Then put $c_1 = c_{11}c_{12}$ so that $b_1 = c_{11}b_2$ and $d = c_{12}d_2$ with $d_2 \notin c_{11}D$ and $b_2 \notin c_{12}D$. Hence (7) reduces to

$$\frac{1}{a_1} = \frac{d_2b_2}{h} . \tag{11}$$

Since b_2 is a factor of b_1 and $(a_1, b_1) = 1$, we have $(b_2, a_1) = 1$. Express $d_2 = d_{21}d_{22}$ such that every prime factor of d_{21} is a factor of a_1 and $(d_{22}, a_1) = 1$. Thus equ. (11) is equivalent to $g^n = h = (a_1d_{21})(b_2d_{22})$ with $(a_1d_{21}, b_2d_{22}) = 1$. By Lemma 2, we have

$$a_1d_{21} = uB^n \text{ and } d_{22}b_2 = u^{-1}A^n \tag{12}$$

for some u, A, $B \in D$ unit u, $g = AB$ and $(A, B) = 1$. Multiplying the first in equ. (12) by $c_{12}d_{22}$ and the second by $c_{11}c_{12}d_{21}$, we respectively obtain
$a_1c_{12}(d_{21}d_{22}) = c_{12}d_{22}\, uB^n$ and $(b_2c_{11})(d_{21}d_{22})c_{12} = (c_{11}c_{12})d_{21}u^{-1}A^n$.

But $d_{21}d_{22} = d_2$, $b_2c_{11} = b_1$, $d_2c_{12} = d$, $da_1 = a$, $db_1 = b$ and $c_{11}c_{12} = c_1$. Thus the above equations respectively reduce to

$$a = c_{12}d_{22}\, uB^n \text{ and } b = c_1d_{21}\, u^{-1}A^n \tag{13}$$

for some unit u, $(a, b) = d = c_{12}d_{21}d_{22}$, $c_1 = c_{11}c_{12}$, $d_2 = d_{21}d_{22} \notin c_{11}D$, $\frac{b}{dc_{11}} = b_2 \notin c_{12}D$ and $b - a^2 = c = dc_1$. Thus we have almost justified the following.

Theorem 2. Suppose a, b, h $\in D$ satisfy (4). Then $h = g^n$ for some $g \in D$ and natural number $n > 1$ iff the following respective cases hold with $g = AB$, $(A, B) = 1$, $A, B \in D$.

(2.1) When c is an associate of d, a and b are given by the relations in (6) satisfying the condition $c = b - a^2$.

(2.2) When $d \in c_1D$, c_1 non-unit, a and b are given by the relations in (10) satisfying the condition $c = b - a^2$.

(2.3) When $d \notin c_1D$, a and b are given by the relations in (13) satisfying the condition $c = b - a^2$.

Proof. The forward implications have already been shown in the subsections (3.1), (3.2) case 1 and case 2, respectively.

The converses are immediate. For instance, if a and b satisfy (6) with $c=b-a^2$, then

$$\frac{b}{a} - a = \frac{u^{-1}dA^n - w^2u^2B^{2n}}{a} = \frac{c}{uwB^n} = \frac{(cw^{-1})u^{-1}A^n}{B^nA^n} = \frac{du^{-1}A^n}{h} = \frac{b}{h}.$$

The other cases are similarly shown.

Of course the equations arising from (6), (10) and (13) with the condition $c=b-a^2$ are not manageable in their generalities. One may set some additional conditions on the parameters.

One such condition is to set $u = w = 1$, which necessarily holds if a, b and h are natural numbers. So, if we set $u = w = 1$, the equations in (6), (10) and (13), respectively reduce to

$$a = da_1 = B^n \text{ and } b = (da_1)^2 + d = dA^n \tag{14}$$

$$a = da_1 = c_1d_{12}B^n \text{ and } b = d_{11}c_1A^n \tag{15}$$

and

$$a = da_1 = c_{12}d_{22}B^n \text{ and } b = c_1d_{21}A^n \tag{16}$$

From the pair of equations in (14), we get

$$A^n - a_1B^n = 1 \tag{17}$$

with $B^n \in a_1D$, which we shall use in the next section to exhibit solutions for (1).

From the pair of equations in (15) and parameters defined under case 1 in (3.2), $c = b - a^2$ gives

$$d = c_1d_{11}d_{12} = d_{11}A^n - c_1d_{12}^2B^{2n} \tag{18}$$

and from the pair of equations in (16) and parameters defined under case 2 in (3.2), $c = b - a^2$ gives

$$(c_{11}c_{12})d_2 = c_{11}c_{12}d_{21}d_{22} = c_{11}d_{21}A^n - c_{12}d_{22}^2B^{2n} \tag{19}$$

Lemma 3. Consider the equation $fe = k_1k_2A^n - fB^{2n}$ for any natural number n and indeterminates A, B, e, f, k_1, k_2 over a commutative ring **R** with unity. For any e, $B \in \mathbf{R}$, the equation has a solution in **R**.

Proof. Choose any two elements e, $B \in \mathbf{R}$ and natural number n. Put

$$B^{2n} + e = k_1A^m$$

for some k_1, $A \in \mathbf{R}$ and natural number $m \leq n$. Then with $f = k_2A^{n-m}$ for some $k_2 \in \mathbf{R}$, we have

$$k_1k_2A^n = (k_1A^m)(k_2A^{n-m}) = (B^{2n} + e)f = fB^{2n} + ef.$$

Thus

$$k_1k_2A^n - fB^{2n} = ef,$$

completing the proof of the Lemma.

Corollary 2

(2.1) Suppose $d_{11} = d_{12} = 1$ in (18). Then $d = c_1$ and the equation has a solution for any $B \in D$ and natural number n. In particular, for any non-unit $B \in D\backslash\{0\}$ and natural number $n > 1$ such that $B^{2n} + 1 = A^m$ for some $A \in D$ and natural number $m < n$,

$a = B^nA^{n-m}$, $b = A^{2n-m}$ and $h = (AB)^n$ satisfy (4).

(2.2) Suppose $d_{21} = d_{22} = 1$ and $c_{12} = qc_{11}$ for some $q \in D\backslash\{0\}$ in (19). Then the equation has a solution for any c_{11}, $B \in D$ and natural number n. In particular, for any non-units c_{11}, $B \in D\backslash\{0\}$, $(c_{11}, B)=1$ and natural number $n > 1$ such that $B^{2n} + c_{11} = A^m$ for some $A \in D$ and natural number $m < n$,

$a = A^{n-m}B^n(A^m-B^{2n})$, $b = A^{2n-m}(A^m-B^{2n})^2$ and $h = (AB)^n$ satisfy (4).

Proof. If $d_{11} = d_{12} = 1$ in (18), then $d_1 = d_{11}d_{12} = 1$, $d = c_1d_1 = c_1$. The equation may be written as

$$A^n - dB^{2n} = d \tag{20}$$

With $f = d$, $e = 1 = k_1 = k_2$ in Lemma 3, for arbitrary natural number n and $B \in D$, (20) has a solution in D.

If we choose a non-unit $B \in D\backslash\{0\}$ and $n > 1$ such that $B^{2n} + 1 = A^m$ for some $A \in D$ and natural number $m < n$, which is always a possible construction, and set $d = A^{n-m}$, then $A^n - dB^{2n} = d$. For these choices, using (10), we have

$$\begin{aligned} c &= dc_1 = d^2 = A^{2(n-m)} \\ a &= da_1 = c_1d_{12}uB^n = A^{n-m}B^n \\ b &= c_1d_{11}u^{-1}A^n = A^{n-m}A^n = A^{2n-m} \\ h &= (AB)^n \end{aligned} \tag{21}$$

with $(A, B) = 1$. Hence a, b, h given by (21) satisfy (4).

To prove the second part, suppose $d_{21} = 1 = d_{22}$ and $c_{12} = qc_{11}$ for some $q \in D$ holds in (19). Then the equation reduces to

$$qc_{11} = A^n - qB^{2n} \tag{22}$$

Then, with $e = c_{11}$, $f = q$, $k_1 = k_2 = 1$ in Lemma 3, the last equation has a solution for any c_{11}, $B \in D$ and natural number n.

If we choose non-units $c_{11}, B \in D\backslash\{0\}$, $(c_{11}, B) = 1$ and natural number $n > 1$ such that $B^{2n} + c_{11} = A^m$, $A \in D$ and natural number $m < n$, again always possible, and set $q = A^{n-m}$, then (22) holds. For these choices, using (13),

$$\begin{aligned} c_{12} &= qc_{11} = A^{n-m}(A^m - B^{2n}) \\ c_1 &= c_{11}c_{12} = qc_{11}^2 = A^{n-m}(A^m - B^{2n})^2 \\ a &= c_{12}d_{22}uB^n = A^{n-m}(A^m - B^{2n})B^n \\ b &= c_1d_{21}u^{-1}A^n = A^{2n-m}(A^m - B^{2n})^2 \\ h &= (AB)^n \end{aligned} \tag{23}$$

with $(A, B) = 1$. Hence a, b and h given by (23) satisfy the relation in (4). This completes the proof of the Corollary.

4. APPLICATION

One may impose additional conditions on the parameters in (17), (18) or (19). Some of the resulting equations arising from such a process are challenging Diophantine equations. This will be elaborated more in a forthcoming article. In this section, we demonstrate two different situations.

Assume, henceforth, that a, b and h are natural numbers satisfying (2) and $h = g^n$ for some natural number $g > 1$ and $n > 1$. In view of Remark (1.3), we necessarily have $(a, b) = d > 1$. Moreover, $u = 1 = w$ necessarily holds. Consequently the equations in (6), (10) and (13) with $c = b - a^2$ are respectively equivalent to the equations in (17), (18) and (19). Besides, it is clear that the parameters in these equations represent natural numbers.

Corollary 3. For natural numbers a, b, h as above, suppose in (18), $d_{11} = d_{12} = 1$ and $c_1 = A^\beta$ for some natural number β. Then $\beta = n - 1$ and $A = B^{2n} + 1$.

Proof. Since $d_{11} = d_{12} = 1$ and $c_1 = A^{\beta}$ the equation in (18) reduces to

$$A^{n-\beta} - B^{2n} = 1 \tag{24}$$

If $n - \beta > 1$, it is evident that $n - \beta$ is odd, hence $n - \beta \geq 3$. Moreover B is even, hence $B \geq 2$. But then a result of V.A. Lebesgue (see Mordell, 1969) shows that the Diophantine equation in (24) has no solution. Hence $n - \beta \leq 1$. Therefore $n = \beta + 1$ and $A = B^{2n} + 1$.

Under the assumptions of Corollary 3, since $c_1 = d$, equation (10) yields $a = A^{n-1}B^n$, $b = A^{2n-1}$, $c = dc_1 = A^{2(n-1)}$ and $h = (AB)^n$ satisfying (2). However, since $B^n < B^{2n} + 1 = A \leq A^{n-1}$, it is clear that $h < b$, for this case.

Remark 2. It was indicated in Remark (1.2) that for natural numbers satisfying (2), $b < h$ iff $c_1 < a_1$. Specially when (a, b) and $b - a^2$ are associates, hence $d = c$, we have $c_1 = 1$ and thus $c_1 = 1 < 2 \leq a_1$. Thus all the solutions of (2) under this case satisfy the relation $c < a < b < h$. Notice that these solutions are related by the equations in (6) which are equivalent to (17) with the condition $c = b - a^2$.

For natural numbers a, b, h satisfying (2), consider the equation in (17)

$$\text{i.e } A^n - a_1B^n = 1 \tag{25}$$

with $B^n \equiv 0 \pmod{a_1}$. In particular $2 \leq a_1 \leq B^n$. Hence positive solutions of (25) satisfy $c_1 = 1 < a_1 \leq B^n$.

First of all the condition $B^n \equiv 0 \pmod{a_1}$ in (25) is quite restrictive. For instance $(x,y) = (3,2)$ is a solution of

$$x^4 - 5y^4 = 1 \tag{26}$$

with $5 < 2^4$. However the equation has no solution in natural numbers x and y with $y \equiv 0 \pmod 5$. Indeed, Cohn (1965) has shown that $(x, y) = (\pm 1, 0)$, $(\pm 3, \pm 2)$ are the only solutions of the Diophantine equation in (26).

Assume now that a_1 in (25) is not a perfect square and $n = 2$. Adopting standard techniques to construct the set of units of the ring of integers with

norm 1 in the number field $Q(\sqrt{a_1})$ (Borevich and Shafarevich, 1966), or using the explicit result in Carmichael (1959) the Diophantine equation

$$x^2 - a_1y^2 = 1 \tag{27}$$

has a solution with natural numbers x and y.

Let $\alpha + \beta\sqrt{a_1}$ be such a solution of (27). For each natural number m, let $\alpha_m + \beta_m\sqrt{a_1} = (\alpha + \beta\sqrt{a_1})^{ma_1}$ with natural numbers α_m and β_m. Evidently β_m is a multiple of a_1 and hence $a_1 \leq \beta_m$. Besides $(x, y) = (\alpha_m, \beta_m)$ satisfies the equation in (25) with $n = 2$.

For each natural number m, let

$$d = c = \beta_m^2/a_1 > 1 .$$

Then

$$a = da_1 = \beta_m^2, \quad b_1 = da_1^2 + 1 = \beta_m^2 a_1 + 1 = \alpha_m^2 .$$

Consequently, the natural numbers

$$a = \beta_m^2, \quad b = db_1 = \beta_m^4 + c, \quad h = (\alpha_m \beta_m)^2$$

satisfy the relation

$$\frac{b}{a} = a + \frac{b}{h} .$$

In fact, since $a_1 \leq \beta_m < b < (\alpha_m \beta_m)^2 = g^2 = h$.

Therefore,

$$b = b_1g + b_0,$$

with $0 < b_0, b_1 < g$. Hence

$$\frac{b}{a} = (a.b_1b_0)_g = (a.b)_g .$$

The following Theorem is now immediate from the above illustration, thus giving a stronger positive answer to (1).

Theorem 3. There are infinitely many triples of natural numbers (b,a,g) with (a, b) = $b\text{-}a^2 > 1$, b not a multiple of a, and $h = g^2$, g a natural number, $g < b < g^2$ such that

$$a + \frac{b}{h} = \frac{b}{a} = (a.b)_g .$$

ACKNOWLEDGEMENTS

This article was completed at The Abdul Salam International Centre for Theoretical Physics and financed by the Swedish Agency for Research Cooperation with Developing Countries. The author is grateful for the financial support and comfortable working conditions at the Centre. The author would like to thank two anonymous referees of *SINET* for their invaluable and constructive suggestions on the original version of the article.

REFERENCES

1. Borevich, Z.I. and Shafarevich, I.R. (1966). *Number Theory*, Academic Press, New York.
2. Carmichael, R.D. (1959). *The Theory of Numbers and Diophantine Analysis*, Dover Publications, Inc., New York.
3. Cohn, J.H.E. (1965). Lucas and Fibonacci numbers and some diophantine equations, *Proc. Glasgow Math. Assoc.* **7**:24–28.
4. Mordell, L.E. (1969). *Diophantine Equations*, Academic Press, London.
5. Runge S.M. (1991). "Problem 1862: Simple Arithmetic", *Journal of Recreational Mathematics* **23**(1):28.

SINET: Ethiop. J. Sci., 24(1):17–33, 2001
 ISSN: 0379–2897

THE EFFICIENCY OF OLS ESTIMATOR IN THE LINEAR REGRESSION MODEL WITH SPATIALLY CORRELATED ERRORS

Butte Gotu

Department of Statistics, Faculty of Science, Addis Ababa University
PO Box 1176, Addis Ababa, Ethiopia, E-mail: Sinet-aau@telecom.net.et

ABSTRACT: Bounds for the efficiency of ordinary least squares estimator relative to generalized least squares estimator in the linear regression model with first-order spatial error process are given.

Key words/phrases: Efficiency, generalized least squares, ordinary least squares, spatial error process, spatial correlation

INTRODUCTION

Let the relationship between an observable random variable y and k explanatory variables $X_1,\ldots,X_k$ in a T-county system be specified in linear regression form

$$y = X\beta + u, \tag{1}$$

where X is a $T\times k$ matrix of known constants with full column rank $k < T$, and ß is a $k\times 1$ vector of unknown parameters. The vector u is a disturbance term with $E(u) = 0$ and $Cov(u) = \sigma_\epsilon^2 V_*$, where σ_ϵ^2 is a positive unknown scalar and V_* a $T\times T$ positive definite matrix with identical diagonal elements. The assumption that the diagonal elements of V_* are all identical indicates that we consider only homoscedastic disturbances $u'_i s$ which are correlated.

The ordinary least squares (OLS) and the generalized least squares (GLS) estimators of ß in model (1) are given by $\hat{\beta} = (X'X)^{-1}X'y$ and $\tilde{\beta} = (X'V_*^{-1}X)^{-1}X'V_*^{-1}y$, respectively, with covariance matrices $Cov(\hat{\beta}) = \sigma_\epsilon^2(X'X)^{-1}X'V_*X(X'X)^{-1}$ and $Cov(\tilde{\beta}) = \sigma_\epsilon^2(X'V_*^{-1}X)^{-1}$.

When the covariance of the disturbance vector u is not a scalar multiple of the identity matrix, that is $Cov(u) \neq \sigma_\epsilon^2 I$ as in model (1), it is well known that the GLS estimator provides the best linear unbiased estimator (BLUE) of β in contrast to OLS (see Fomby *et al.*, 1984, p. 17).

But in applications, Cov(u) usually involves unknown parameters like a spatial correlation coefficient, so one has to look for another estimator, OLS, say. In cases where Cov(u) does not involve unknown parameters, one problem facing a researcher dealing with model (1) is how to measure the efficiency of OLS estimator $\hat{\beta}$ relative to GLS estimator $\tilde{\beta}$. For spatial case, this question can be expressed as: what can we gain by estimating β in the regression model based on spatial assumptions instead of using simple standard regression specifications?

A number of authors have investigated the efficiency of OLS relative to GLS estimator when the errors are serially or spatially correlated by using various efficiency criteria (see Bloomfield and Watson, 1975; Krämer, 1980; Krämer and Donninger, 1987; Haining, 1990; Griffith, 1988; Cordy and Griffith, 1993; Krämer and Baltagi, 1996). The most remarkable feature of the results obtained is that the relative efficiency depends mainly on the error process considered, the regressor matrix X and the degree of correlation. The relevant literature can be grouped into two, namely papers which assume X as given and seek bounds for the efficiency as the covariance matrix varies, and papers which take the covariance matrix as given and consider bounds for the efficiency as X varies. Another aspect of the resulting analysis shows the behaviour of the relative efficiency of OLS when the correlation parameter tends toward the boundary of the parameter space.

In this paper, bounds for the efficiency of OLS relative to GLS estimator of β in model (1) under first-order spatial error process, that is under the assumption that the covariance matrix is given, are constructed by using the measures of efficiency based on

- the euclidean norm of the difference $P_X V_* - V_* P_X$, $P_X = X(X'X)^{-1}X'$
- the ratio of the traces of the covariance matrices of $X\tilde{\beta}$ and $X\hat{\beta}$
- the ratio of the determinants of the covariances of $\tilde{\beta}$ and $\hat{\beta}$.

The bounds obtained can then be used to decide whether to apply OLS method or GLS method based on the assumptions of first-order spatial process.

LINEAR REGRESSION WITH FIRST-ORDER SPATIAL ERROR PROCESSES

In order to analyze the efficiency of OLS relative to GLS estimator given specific error process, one needs the structure of the covariance matrix of the disturbance vector u. So, we start by specifying first-order spatial error processes.

Let the components of u follow a first-order spatial moving average (MA(1)) process

$$u_i = \rho \sum_{j=1}^{T} w_{ij} \epsilon_j + \epsilon_i$$

or, in matrix form

$$u = \rho W \epsilon + \epsilon \qquad (2)$$

where ρ denotes a spatial correlation coefficient for a given county system and ϵ is an error term with $E(\epsilon) = 0$ and $Cov(\epsilon) = \sigma_\epsilon^2 I$ (I is the T-dimensional identity matrix). W is a $T \times T$ matrix whose elements are known non-negative weights defined by (Cliff and Ord 1981, pp. 17–19):

$$w_{ij} \begin{cases} >0, & \textit{if } i \textit{ and } j \textit{ are neighbours } (i \neq j) \\ =0, & \textit{otherwise.} \end{cases}$$

The element w_{ij} of the weights matrix W measures the strength of the effect of county j on county i.

Under first-order spatial autoregressive (AR(1)) process, the components of u follow the pattern

$$u_i = \rho \sum_{j=1}^{T} w_{ij} u_j + \epsilon_i$$

or, in matrix form

$$u = \rho W u + \epsilon \,. \tag{3}$$

Equations (2) and (3) can be written as

$$u = (I + \rho W)\epsilon \quad \text{and} \quad u = (I - \rho W)^{-1} \epsilon \,, \tag{4}$$

respectively, where in the AR(1) case the matrix $I - \rho W$ must be non-singular. From (1) and (4), we obtain four possible structures of $Cov(u) = \sigma_\epsilon^2 V_*$ for the first-order spatial error process:

$$V_* = \begin{cases} (I+\rho W)(I+\rho W') & : \ MA(1) \\ (I+\rho W) & : \ MA(1) - conditional \\ (I-\rho W)^{-1}(I-\rho W')^{-1} & : \ AR(1) \\ (I-\rho W)^{-1} & : \ AR(1) - conditional. \end{cases} \tag{5}$$

The conditional cases are special cases of the unconditional process (Bartlett, 1971; Besag, 1974). To ensure that V_* is positive definite, the possible values of ρ must be identified (see Horn and Johnson, 1985, p. 301). Once the structure of the covariance matrix is specified the next step will be to analyze the efficiency of OLS estimator by using different efficiency measures. Before we analyze efficiency, let us introduce a general expression of the covariance matrix of the disturbance vector and give some general assumptions used throughout the paper.

According to the assumptions given in model (1) the matrix V_* has identical diagonal elements, and denoting this element by υ, we get

$$Cov(u) = \sigma_\epsilon^2 V_* = (\upsilon \sigma_\epsilon^2) V = \sigma_u^2 V, \tag{6}$$

where $V = (1/\upsilon) V_*$ and $\sigma_u^2 = \upsilon \sigma_\epsilon^2$ is the variance of the disturbances u_i, $i = 1, \ldots, T$. Using the above assumptions under spatial process we can now write model (1) as the familiar general linear regression model

$$y = X\beta + u, \quad E(u) = 0, \quad Cov(u) = \sigma_u^2 V. \tag{7}$$

We assume that $X'X = I$. For the matrix X with full column rank, there is no loss of generality in assuming that $X'X=I$ because under the transformation

$$y = \tilde{X}\delta + u \tag{8}$$

with $\tilde{X} = X(X'X)^{-1/2}$ and $\delta = (X'X)^{1/2}\beta$ the condition $\tilde{X}'\tilde{X} = I$ is valid for all X, and the OLS and GLS estimators of β are given by $\hat{\beta} = (X'X)^{-1/2}\hat{\delta}$ and $\tilde{\beta} = (X'X)^{-1/2}\tilde{\delta}$, respectively. $\hat{\delta}$ and $\tilde{\delta}$ are the estimators of δ in (8). Furthermore, we impose the following assumptions on the weight matrix W throughout or when needed (see Appendix regarding examples):

- W is symmetric.
- W is symmetric and orthogonal.
- W is symmetric with row sums equal to one.

EFFICIENCY BASED ON THE EUCLIDEAN NORM

Consider the measure of efficiency based on the euclidean norm of the difference $P_X V - VP_X$ defined by (see Bloomfield and Watson, 1975)

$$\begin{aligned} e_1(\rho) &:= \tfrac{1}{2} \| P_X V - VP_X \|^2 \\ &= \tfrac{1}{2} tr((P_X V - VP_X)'(P_X V - VP_X)) \\ &= tr(P_X V^2) - tr(P_X V)^2 \ . \end{aligned} \tag{9}$$

When $e_1(\rho) = 0$, the OLS estimator $\hat{\beta}$ can be applied without loss of efficiency whereas a loss of efficiency is expected if $e_1(\rho) \neq 0$. In what follows $\mu_i(A)$ denotes the i-th eigenvalue of a $T \times T$ matrix A.

Theorem 1 (Bloomfield and Watson, 1975)

Assume that $\mu_1(V) \leq \ldots \leq \mu_T(V)$. Under the assumptions that $X'X = I$, V positive definite and $T \geq 2k$, we have

$$e_1(\rho) \leq \frac{1}{4}\sum_{i=1}^{k} (\mu_i(V) - \mu_{T-i+1}(V))^2 \quad (10)$$

Remarks:
When there are big differences within the k pairs $(\mu_i(V), \mu_{T-i+1}(V))$ *of the eigenvalues of V, then the bound in (10) will be large. The restriction* $T \geq 2k$ *by Bloomfield and Watson allows to take pairs at a time.*

Based on the theorem by Bloomfield and Watson the following result can be stated.

Theorem 2
Let $\mu_1(V) \leq \ldots \leq \mu_T(V)$. Under the assumptions that $X'X = I$, V positive definite and $T \geq 2k$, we obtain

$$e_1(\rho) \leq \frac{1}{4\upsilon^2}\sum_{i=1}^{k} (\mu_i(V_*) - \mu_{T-i+1}(V_*))^2 , \quad (11)$$

Proof:
By inserting $V = (1/\upsilon)V_*$ in (9), we have

$$e_1(\rho) = \frac{1}{\upsilon^2}\{tr(P_X V_*^2) - tr(P_X V_*)^2\} . \quad (12)$$

The result follows then by applying Theorem 1. ◇

In the following the upper bounds of $e_1(\rho)$ will be given by applying the relationship given in (11) under some assumptions on the weights matrix.

Corollary 1
Let $X'X = I$ and $T \geq 2k$. When the components of the disturbance vector u in model (7) follow a conditional spatial $MA(1)$ process, then

$$e_1(\rho) \leq \frac{\rho^2}{4}\sum_{i=1}^{k} (\mu_i(W) - \mu_{T-i+1}(W))^2 . \quad (13)$$

Proof:
For a conditional spatial moving average process of order one the matrix V_* is given by $V_* = (I + \rho W)$, with W being symmetric. The diagonal elements of V_* are all equal to one because the respective elements of the weights matrix are all equal to zero. This implies that $v = 1$. Furthermore,

$$\mu_i(V_*) = 1 + \rho\, \mu_i(W) \ , \tag{14}$$

where the eigenvalues $\mu_i(V_*)$ and $\mu_i(W)$, $i=1, \ldots, T$ are in ascending order. Inserting (14) in (11) completes the proof. ◇

The bound in (13) will be large when there are large differences within the k pairs of eigenvalues $(\mu_i(W),\mu_{T-i+1}(W))$ of the matrix W. That is, the efficiency of OLS relative to GLS estimator will be lower when the differences within the pairs of eigenvalues of W are large.

If the row sums of W are equal to one, then $e_1(\rho) \leq k\rho^2$ because the absolute value of the eigenvalue $\mu_i(W)$ is less than or equal to one for all i (see Graybill, 1983, p. 98).

Remark:
The result of Corollary 1 also holds for a conditional spatial AR(1) process if W is orthogonal.

Corollary 2
Assume that W is orthogonal and symmetric. Let $X'X = I$ and $T \geq 2k$. When the components of the disturbance vector u in model (7) follow a spatial $MA(1)$ or $AR(1)$ process, then

$$e_1(\rho) \leq \frac{4k\rho^2}{(1+\rho^2)^2} \ .$$

Proof:

***MA*(1) process:**

Under a spatial $MA(1)$ process we have

$$V_* = (I + \rho W)(I + \rho W').$$

From the assumption that the weights matrix W is orthogonal and symmetric it follows that

$$V_* = (1 + \rho^2)I + 2\rho W ,$$

implying $v = 1 + \rho^2$ and $\mu_i(V_*) = (1 + \rho^2) + 2\rho\mu_i(W)$. Inserting these eigenvalues in (11) we get

$$e_1(\rho) \leq \frac{\rho^2}{(1 + \rho^2)^2} \sum_{i=1}^{k} (\mu_i(W) - \mu_{T-i+1}(W))^2$$

Since W is orthogonal and symmetric we have $\mu_i(W) \in\{-1,1\}$, which gives $e_1(\rho) \leq (4k\rho^2)/(1 + \rho^2)^2$

AR(1) process:

Under a spatial $AR(1)$ process the matrix V_* is given by

$$V_* = (I - \rho W)^{-1}(I - \rho W')^{-1}.$$

When the weights matrix W is assumed to be symmetric and orthogonal, we obtain $(I - \rho W)^{-1} = (1/(1 - \rho^2))(I + \rho W)$ (see Searle, 1982, p. 137), and V_* has the form

$$V_* = \frac{1}{(1-\rho^2)^2}((1+\rho^2)I + 2\rho W))$$

This implies that $v = (1 + \rho^2)/(1 - \rho^2)^2$ and

$$\mu_i(V_*) = \frac{1}{(1-\rho^2)^2}((1+\rho^2) + 2\rho\mu_i(W)) , \qquad (15)$$

where the eigenvalues are in ascending order. Inserting (15) in (11) and using the fact that $\mu_i(W) \in \{-1,1\}$ completes the proof. ◇

The following result shows that the OLS estimator can be applied without loss of efficiency as ρ goes to one.

Theorem 3
Let $\Re(X)$ be the k-dimensional space spanned by the columns of X, and let $\ell := (1,\ldots,1)' \in \Re(X)$. If $\lim_{\rho\to 1} V = c\ell\ell'$, $c \in \mathbb{R}$, then $\lim_{\rho\to 1} e_1(\rho) = 0$.

Proof:
The efficiency $e_1(\rho)$ can be written as:

$$e_1(\rho) = tr(P_X V^2) - tr(P_X V)^2 = tr(P_X V(V - P_X V))$$
$$=^{*} tr(P_X V M_X V).$$

When the condition $\lim_{\rho\to 1} V = c\ell\ell'$ holds, we have

$$\lim_{\rho\to 1} e_1(\rho) = c^2 tr(P_X \ell\ell' M_X \ell\ell')$$

Since $\ell \in \Re(X)$ we get $M_X\ell = (I - P_X)X\gamma = 0$, γ being a $k \times 1$ vector, and this implies $\lim_{\rho\to 1} e_1(\rho) = 0$. ◇

EFFICIENCY BASED ON THE RATIO OF TRACES

If the ratio of the mean squared errors is used to define the measure of efficiency of OLS relative to GLS estimator, then we have (see Krämer, 1980)

$$e_2(\rho) := \frac{tr(Cov(X\tilde{\beta}))}{tr(Cov(X\hat{\beta}))}$$

with $Cov(X\tilde{\beta}) = \sigma_u^2 X(X'V^{-1}X)^{-1}X'$ and $Cov(X\hat{\beta}) = \sigma_u^2 P_X V P_X$. Using this measure of efficiency a number of papers investigate the efficiency of OLS relative to GLS estimator under stationary AR(1) process in time series and

spatial models (see Krämer, 1980, 1984; Krämer and Donninger, 1987; Krämer and Baltagi, 1996).

The following theorem gives a lower bound for $e_2(\rho)$ which holds for all covariance structures under general linear regression model (7).

Theorem 4

Let $X'X = I$. Then

$$\frac{\sum_{i=1}^{k} \mu_i(V)}{\sum_{i=1}^{k} \mu_{T-k+i}(V)} \leq e_2(\rho) \leq 1 \ . \tag{16}$$

Proof:

Since σ_u^2, in $e_2(\rho)$, cancels out, we set $\sigma_u^2 = 1$ in calculating covariances. Under the assumption $X'X = I$, we have

$$tr(Cov(X\hat{\beta})) = tr(P_X V P_X) = tr(X'VX) \tag{17}$$

and

$$\begin{aligned} tr(Cov(X\tilde{\beta})) &= tr(X(X'V^{-1}X)^{-1}X') = tr(X'V^{-1}X)^{-1} \\ &= \sum_{i=1}^{k} \mu_i((X'V^{-1}X)^{-1}) \\ &= \sum_{i=1}^{k} \frac{1}{\mu_i(X'V^{-1}X)} \ . \end{aligned} \tag{18}$$

Applying Poincaré separation theorem we obtain the following inequalities (see Horn and Johnson, 1985, p. 190):

$$\begin{aligned} &\sum_{i=1}^{k} \mu_i(V) \leq tr(Cov(X\hat{\beta})) \leq \sum_{i=1}^{k} \mu_{T-k+i}(V) \\ &\mu_i(V^{-1}) \leq \mu_i(X'V^{-1}X) \leq \mu_{T-k+i}(V^{-1}) \ . \end{aligned} \tag{19}$$

The second inequality in (19) implies

$$\frac{1}{\mu_i(X'V^{-1}X)} \geq \frac{1}{\mu_{T-k+i}(V^{-1})}, \quad i=1,\ldots,k .$$

Using (17) to (19) we have

$$\begin{aligned} tr(Co\,v(X\tilde{\beta})) &\geq \sum_{i}^{k} \frac{1}{\mu_{T-k+i}(V^{-1})} \\ &= \sum_{i}^{k} \mu_i(V) \\ tr(Co\,v(X\hat{\beta})) &\leq \sum_{i=i}^{k} \mu_{T-k+i}(V) . \end{aligned} \tag{20}$$

From (20) it is clear that

$$\frac{\sum_{i=1}^{k} \mu_i(V)}{\sum_{i=1}^{k} \mu_{T-k+i}(V)} \leq e_2(\rho) .$$

The inequality $e_2(\rho) \leq 1$ follows from the optimality of GLS estimator (see Krämer, 1980). ◇

If there is a large difference between the sum of the k smallest and k largest eigenvalues of V, then the efficiency of OLSE will significantly be smaller, but never less than the ratio of the smallest and the largest eigenvalues $\mu_{min}(V)/\mu_{max}(V)$.

Remark:

If the diagonal elements of V_* are not identical, meaning that the $u'_i s$ have different variances, then we get

$$e_2(\rho) \geq \frac{\sum_{i=1}^{k} \mu_i(V_*)}{\sum_{i=1}^{k} \mu_{T-k+i}(V_*)} .$$

For spatial models with first-order spatial error process the following result is obtained.

Corollary 3
Assume that the matrix X fulfils $X'X = I$. Let the weights matrix W be symmetric with row sums equal to one. If the components of the disturbance vector u follow a spatial $MA(1)$ or $AR(1)$ process, then

$$e_2(\rho) \geq \frac{(1-\rho)^2}{(1+\rho)^2}, \qquad \rho > 0 . \tag{21}$$

Proof:
MA(1) process
Under a spatial $MA(1)$ process with symmetric weights matrix the eigenvalues of V_* are given by

$$\mu_i(V_*) = (1 + \rho\,\mu_i(W))^2 , \qquad i = 1,\ldots,T ,$$

where the eigenvalues of W and V_* are in ascending order. When the row sums of W are all equal to one, then the absolute value of $\mu_i(W)$ is less than or equal to one for all i (see Graybill, 1983, p. 98). This implies

$$\frac{1}{\upsilon}(1-\rho)^2 \leq \mu_i(V) \leq \frac{1}{\upsilon}(1+\rho)^2 , \qquad \rho > 0 , \tag{22}$$

so that applying Theorem 4 gives (21).

AR(1) process
Using the same reasoning as in the $MA(1)$ case we obtain the following bounds for the eigenvalues of V:

$$\frac{1}{\upsilon(1+\rho)^2} \leq \mu_i(V) \leq \frac{1}{\upsilon(1-\rho)^2} , \qquad \rho > 0 \tag{23}$$

and (21) follows by applying Theorem 4.

In what follows we use a measure of efficiency which is based on the determinants of the covariances of the least squares estimators, and give a lower bound for the efficiency of OLS relative to GLS estimator.

EFFICIENCY BASED ON THE RATIO OF DETERMINANTS

Consider the measure of efficiency given by (see Watson, 1955)

$$e_3(\rho) := \frac{|Cov(\tilde{\beta})|}{|Cov(\hat{\beta})|} = \frac{|X'X|^2}{|X'VX||X'V^{-1}X|},$$

where $|.|$ stands for determinant. The matrices $X'VX$ and $X'V^{1}X$ are positive definite because V is positive definite and X of full column rank. This implies that $e_3(\rho) > 0$.

Let A and B be T x k matrices and assume that $B'B$ is non-singular. The well known Cauchy-Inequality concerning the determinants of two matrices A and B states that $|A'B|^2 \leq |A'A|\ |B'B|$ (see Basilevsky, 1983, p. 167). Using $A=V^{1/2}X$ and $B=V^{-1/2}X$, we get $|X'X|^2 \leq |X'VX|\,|X'V^{-1}X|$. This implies, under the assumption $X'X = I$, $e_3(\rho) \leq 1$.

The following theorem gives a lower bound for $e_3(\rho)$.

Theorem 5
Let $X'X = I$. Then

$$e_3(\rho) \geq \prod_{i=1}^{k} \frac{\mu_i(V)}{\mu_{T-k+i}(V)}. \tag{24}$$

Proof:
By applying Poincaré separation theorem we get

$$\prod_{i=1}^{k} \mu_i(V) \le \prod_{i=1}^{k} \mu_i(X'VX) \le \prod_{i=1}^{k} \mu_{T-k+i}(V)$$
$$\prod_{i=1}^{k} \mu_i(V^{-1}) \le \prod_{i=1}^{k} \mu_i(X'V^{-1}X) \le \prod_{i=1}^{k} \mu_{T-k+i}(V^{-1}) ,$$

where the eigenvalues are in ascending order. This implies

$$|X'VX| = \prod_{i=1}^{k} \mu_i(X'VX) \ge \prod_{i=1}^{k} \mu_i(V) ,$$

so that

$$\frac{1}{|X'VX|} \le \prod_{i=1}^{k} \frac{1}{\mu_i(V)} .$$

Furthermore,

$$|X'VX| \le \prod_{i=1}^{k} \mu_{T-k+i}(V)$$
$$|X'V^{-1}X| \le \prod_{i=1}^{k} \mu_{T-k+i}(V^{-1}) .$$

This implies

$$\frac{1}{|X'VX|} \ge \prod_{i=1}^{k} \frac{1}{\mu_{T-k+i}(V)}$$
$$|X'V^{-1}X| \le \prod_{i=1}^{k} \frac{1}{\mu_i(V)} . \qquad (25)$$

According to the definition, we have

$$e_3(\rho) = \frac{1/|X'VX|}{|X'V^{-1}X|} ,$$

and using (25) yields the asserted result. ◇

Remark:
Bloomfield and Watson (1975) give a narrower lower bound for $e_3(\rho)$ under the additional assumptions that $T \geq 2k$ and $k > 1$.

Under first-order spatial error process we get the following result.

Corollary 4
Assume that $X'X=I$. Let the weights matrix W be symmetric with row sums equal to one. If the components of the disturbance vector u follow a spatial $MA(1)$ or $AR(1)$ process, then

$$e_3(\rho) \geq \frac{(1-\rho)^{2k}}{(1+\rho)^{2k}}, \quad \rho > 0 .$$

Proof:
The proof follows by applying Theorem 5 using the bounds of the eigenvalues of the matrix V given in (22) and (23). ◇

Remark:
When the diagonal elements of V_* are not identical, meaning that the u_i's have different variances, we get

$$e_3(\rho) \geq \prod_{i=1}^{k} \frac{\mu_i(V_*)}{\mu_{T-k+i}(V_*)} .$$

REFERENCES

1. Bartlett, M.S. (1971). Physical nearest neighbour models and non-linear time series. *Journal of Applied Probability* **8:**222–232.
2. Besag, J.E. (1974). Spatial interaction and statistical analysis of lattice systems, *Journal of Royal Statistical Society* B **36:**192–236.
3. Basilevsky, A. (1983). *Applied Matrix Algebra in the Statistical Sciences*. Elsevier Science Publishing, New York.
4. Bloomfield, P. and Watson, G.S. (1975). The inefficiency of least squares. *Biometrika* **62:**121–128.
5. Cliff, A.D. and Ord, J.K. (1981). *Spatial Processes: Models and Applications*. Pion, London.

6. Cordy, C.B. and Griffith, D.A. (1993). Efficiency of least squares estimators in the presence of spatial autocorrelation. *Communications in Statistics, Simulation and Computation* **22**:1161–1179.

7. Fomby, T.B., Hill, R.C. and Johnson, S.R. (1984). *Advanced Econometric Methods*. Springer-Verlag, New York.

8. Graybill, F.A. (1983). *Matrices with Applications in Statistics*. 2nd ed., Wadsworth, Belmont.

9. Griffith, D.A. (1988). *Advanced Spatial Statistics*. Kluwer, Dordrecht.

10. Haining, R. (1990). *Spatial Data Analysis in the Social and Environmental Sciences*. Cambridge University Press, Cambridge.

11. Horn, R.A. and Johnson, C.R. (1985). *Matrix Analysis*. Cambridge University Press, Cambridge.

12. Krämer, W. (1980). Finite sample efficiency of ordinary least squares in the linear regression model with autocorrelated errors. *Journal of the American Statistical Association* **75**:1005–1009.

13. Krämer, W. (1984). High correlation among Errors and the efficiency of ordinary least squares in the linear models. *Statistical Papers* **25**:135–142.

14. Krämer, W. and Donninger, C. (1987). Spatial autocorrelation among errors and the relative efficiency of OLS in the linear regression model. *Journal of the American Statistical Association* **82**:577–579.

15. Krämer, W. and Baltagi, B. (1996). A general condition for an optimal limiting efficiency of OLS in the general linear regression model. *Economic Letters* **50**:13–17.

16. Searle, S.R. (1982). *Matrix Algebra Useful for Statistics*. Wiley, New York.

17. Watson, G.S. (1955). Serial correlation in regression analysis. *Biometrika* **42**:327–341.

Appendix

Examples for orthogonal and symmetric weight matrices.

$$W_1 = \begin{pmatrix} 0&0&0&1 & & & & \\ 0&0&1&0 & & & & \\ 0&1&0&0 & & \bigcirc & & \\ 1&0&0&0 & & & & \\ & & & & 0&0&0&1 \\ & & & & 0&0&1&0 \\ & \bigcirc & & & 0&1&0&0 \\ & & & & 1&0&0&0 \end{pmatrix}$$

$$W_2 = \begin{pmatrix} 0&1&0&0 & & & & \\ 1&0&0&0 & & & & \\ 0&0&0&1 & & \bigcirc & & \\ 0&0&1&0 & & & & \\ & & & & 0&1&0&0 \\ & & & & 1&0&0&0 \\ & \bigcirc & & & 0&0&0&1 \\ & & & & 0&0&1&0 \end{pmatrix}$$

Examples for symmetric weight matrices with row sums equal to one.

$$W_3 = \frac{1}{2}\begin{pmatrix} 0&1&0&0&1 & & & & & \\ 1&0&1&0&0 & & & & & \\ 0&1&0&1&0 & & \bigcirc & & & \\ 0&0&1&0&1 & & & & & \\ 1&0&0&1&0 & & & & & \\ & & & & & 0&1&0&0&1 \\ & & & & & 1&0&1&0&0 \\ & & \bigcirc & & & 0&1&0&1&0 \\ & & & & & 0&0&1&0&1 \\ & & & & & 1&0&0&1&0 \end{pmatrix}$$

$$W_4 = \frac{1}{4}\begin{pmatrix} 0&1&1&1&1 & & & & & \\ 1&0&1&1&1 & & & & & \\ 1&1&0&1&1 & & \bigcirc & & & \\ 1&1&1&0&1 & & & & & \\ 1&1&1&1&0 & & & & & \\ & & & & & 0&1&1&1&1 \\ & & & & & 1&0&1&1&1 \\ & & \bigcirc & & & 1&1&0&1&1 \\ & & & & & 1&1&1&0&1 \\ & & & & & 1&1&1&1&0 \end{pmatrix}$$

SINET: Ethiop. J. Sci., 24(1):35–49, 2001

 ISSN: 0379–2897

GROWTH PERFORMANCE OF CROSSBRED DAIRY CATTLE AT ASELLA LIVESTOCK FARM, ARSI ETHIOPIA

Abdinasir Ibrahim [1,*] and Eskil Brännäng [2]

[1] Awassa College of Agriculture, PO Box 5, Awassa, Ethiopia

[2] Dept of Animal Breeding and Genetics, Swedish University of Agricultural Sciences, Box 7023, S-75007 Uppsala, Sweden

ABSTRACT: Genetic and non-genetic factors affecting growth traits and growth performance at 50% and 75% upgrading levels were studied, in the Arsi highland, Ethiopia. The traits studied were: weight at birth, 6, 12, 18, 24 and 36 months. The analyses were carried out using Harvey's Mixed Model Least-squares and Maximum Likelihood Computer Program. The breed groups compared were: 1/2 Friesian 1/2 Arsi (F1FA), 1/2 Friesian 1/2 Zebu (F1FZ), 1/2 Friesian 1/4 Jersey 1/4 Arsi (F(JxA)), 3/4 Friesian 1/4 Arsi (75%FA) and 3/4 Friesian 1/4 Zebu (75%FZ). The 75% FA were significantly heavier than F1FA at birth, 6 and 30 months. No significant differences were found between F1FZ and 75%FZ at all ages. The differences between F(JxA) and F1FA were not significant except at 6 months. The 75% FA were significantly heavier than the F(JxA) at birth, 30 and 36 months. However, 75% FA were significantly lighter than 75% FZ at 12 and 36 months. No significant effect of sex were observed at birth, though males were slightly heavier. Parity of the dam did not show significant influence on body weight except at birth and 24 months. Year of birth of the calf did not have significant effect except at 12 months. The effect of season of birth was significant at birth and 12 months. Animals born during the main rains were the heaviest at birth. Heritability estimates for weights at birth, 6, 12, 18 and 24 months were: 0.20 ± 0.15, 0.14 ± 0.23, 0.04 ± 0.21, 0.68 ± 0.34 and 0.33 ± 0.29, respectively. From the results obtained, it may be concluded that the management and feeding conditions at Asella Livestock Farm would warrant the limitation of upgrading level to 50% exotic inheritance. The smaller weights for the three-breed crosses, *i.e.*, (F(JxA), may be advantageous

* Current address: Humboldt Universität zu Berlin, Institute für Tierzucht in den Tropen und Subtropen, Philippstr. 13, Haus 9, 10115 Berlin, Germany.

to the smallholder, as such animal could be maintained by smallholder farmers as they have lower maintenance requirement as compared to the larger animals.

Key words/phrases: Crossbred, dairy cattle, growth, heritability

INTRODUCTION

Poor genetic potential of indigenous cattle for milk production, low level of animal husbandry practices, inadequate feed supply and prevalence of a variety of diseases and high rate of mortality are among other factors that limit animal performance in Ethiopia.

The indigenous cattle are smaller in size and produce less milk and meat than European cattle. On the other hand, indigenous cattle often exhibit remarkable heat tolerance, has the ability to maintain body condition on poor quality feedstuffs and also exhibit a certain degree of resistance to diseases (Ansell, 1985).

In order to improve animal production, improvement of both genetic and environmental factors are important. To improve animal performance through genetic means, the breeder has two tools; either to carry out selection within indigenous breeds or crossbreed the indigenous breeds with the high yielding exotic animals.

It is generally agreed that genetic improvement through selection is a slow process. Even though all the selection pressure is put on milk yield and it is supported by well organised recording system and progeny testing, the progress will not be more than 1–2% per year and since this is too slow a task, other methods of breed improvement are often preferred (Brännäng and Persson, 1990).

Through crossbreeding milk yield per lactation could be increased considerably and age at first calving could often be reduced by one year or more in first crosses (Rendel, 1974). According to McDowell (1982), more than 60 phenotypic traits have been identified that could be improved through cross-breeding.

Optimum proportion of genes from temperate and tropical breeds may be different for various dairy production systems (McDowell, 1996). A low proportion of improved temperate breeds may be required to suit limited feed resource in traditional production systems (Sendros Demeke and Tesfaye Kumsa, 1998). Studies on smallholder farms in Ethiopia have shown that first generation between Friesian or Jersey and indigenous Zebu breeds had performed well under farmers' conditions in terms of milk yield and reproduction while maintaining good health (Tesfay Kumsa, 1993).

Since growth, milk production and reproduction are closely related traits, the required aim in dairy cattle production should be to improve all these traits. Growth studies based on body weight performance are especially important because they provide the basis for production traits such as milk, meat and work (Dhumal *et al.*, 1988).

Therefore, generating information on growth performance could help provide valuable documentation for developing a future national breeding policy. In order to achieve specific objectives and to assure full advantages of crossbreeding as well, evaluation of the performance of the crossbreeds, including different levels of exotic inheritance, is important.

It was with this justification that the present study was undertaken with the following objectives:

1. to compare the growth performance of crossbreeds with different levels of exotic inheritance;

2. to investigate genetic and environmental factors affecting growth traits.

MATERIALS AND METHODS

Description of the study area

The Asella Livestock Farm is located about 3 km south of Asella town at an altitude of 2400 m. The station has a mild sub-tropical climate, with maximum and minimum temperature ranging from +18 to +22°C and +5 to +10°C,

respectively. The average annual precipitation from 1969–1982 ranged between 1013 to 1500 mm. The vegetation consists of annual legumes and perennial grasses. The natural pasture includes: *Chlorius gayana, Setaria sphacelata, Panicum coloratum* and legumes such as *Trifolium semipilosum, Glycine wightii and Trifolium burchellianum* (Kiwuwa *et al.*, 1983).

Seasonal classification

Systematic factors such as season and year of birth could cause variation in the performance of animals born in different seasons and years. Kiwuwa *et al.* (1983), who evaluated productivity of crossbred cows in the Arsi region reported significant influence of season of birth on milk production. The authors also reported significant influence of year of calving on reproductive performance of crossbred cows. In order to quantify the effect of year and season of birth on the growth traits, it was important to include them in the analyses. Based on the rainfall records and pasture condition, the months of the year were grouped into three seasons, short rains was defined as months from March to May, the main rainy season covered the months of June to September and the dry season was from October to February.

Herd management

Animals were grazed on natural pasture, and supplementary hay or concentrate consisting of 48% niger seed cake, 48% wheat bran, 3.5% bone meal and 0.5% salt were provided. Cows were fed 2 to 4 kg of concentrates per day depending on the level of milk yield. New born calves were separated from their dams immediately after birth and were bucket-fed up to weaning between 49 to 79 days of age. Colostrum and whole milk substitute were fed to calves twice daily at the rate of 1.0 kg to 2.5 kg of milk equivalent. All animals were vaccinated against anthrax, rinderpest, blackleg, pleuropneumonia and brucellosis and were regularly drenched against internal parasites (Kiwuwa *et al.*, 1983).

Data recording

All animals were ear tagged for identification. At each calving, the date, sire number, dam number, breed and sex of the calves were recorded. Birth weight was taken within 24 hours after parturition and subsequent weights were taken in three weeks interval. Unfortunately, there were periods when no weighing

seemed to have been done and incomplete sets of growth data were excluded from the analyses.

Data preparation

Since most crossbred animals were produced from Arsi cattle, other crosses from the indigenous dam breeds, *i.e.,* Fogera, Borana and Barka were grouped as Zebu crossbreeds, because of the small number of crosses available during the study period. There were uneven distribution of crosses over the study period, since F1 crosses naturally appear at the beginning and crossbreeds with higher exotic inheritance were available during later years. As this could cause a confounding effect between years and breed groups, data from crossbreeds that have been taken during the same year have been used. For first generation (F1) animals, only parity of their dams recorded at the farm were considered. Neither age nor parities of local animals at the time of purchase were known. However, only rather young animals were bought.

Breed groups

The growth performances of five breed groups, namely 1/2 Friesian 1/2 Arsi(F1FA), 1/2 Friesian 1/2 Zebu(F1FZ), 3/4 Friesian 1/4 Arsi(75%FA), 3/4 Friesian 1/4 Zebu(75%FZ) and 1/2 Friesian 1/4 Jersey 1/4 Arsi(F(JxA)) were analyzed and compared.

Traits

Birth weight, 6, 12, 18, 24, 30, 36 month weights were analyzed using the following statistical model.

Statistical model

$Y_{ijklmno} = \mu + S_i + B_j + X_k + P_l + Y_m + E_n + e_{ijklmno}$

$Y_{ijklmno}$ = the observation on weight at birth, 6, 12, 18, 24, 30 and 36 months

μ = a constant common to all observation (overall mean)

S_i = the random effect of i^{th} sire normally and independently distributed with $(0, \sigma^2 s)$

B_j = the fixed effect of j^{th} breed group or grade

X_k = the fixed effect of k^{th} sex**
P_l = the fixed effect of l^{th} parity
Y_m = the fixed effect of m^{th} birth year
E_n = the fixed effect of n^{th} birth season
$e_{ijklmno}$ = the random error associated with $Y_{ijklmno}{}^{th}$ observation which is assumed to be normally and independently distributed with $(0,\sigma^2 e)$

Preliminary analyses for all traits showed non-significant interactions (breed x year of birth and breed x season of birth), and therefore were excluded from the model. Harvey's Mixed Model Least-squares and Maximum Likelihood Computer Program (Harvey, 1990) was used for the analyses. Heritability estimates were from the sire component by using paternal half-sib correlation method (Harvey's Model 2).

RESULTS AND DISCUSSION

A comparative study was made among five breed groups, namely F1FA, F1FZ, F(JxA), 75%FA and 75%FZ crosses. The least-squares means with their standard errors for weights at birth, 6, 12, 18, 24, 30 and 36 months are presented in Tables 1 and 2. The analyses of variance for the above weight traits are shown in Table 3.

The coefficient of determination of the models explained between 56% and 69% of the variation in the body weights of the animals (Table 3). The breed group had a significant influence on body weights at birth, 6, 12, 30 and 36 months of age (Table 3). Regarding the birth weight, F1FZ, 75%FZ and 75%FA grades were significantly heavier than F1FA and F(JxA) crossbreeds (Table 1). Increase in Friesian inheritance tended to increase birth weight in Friesian-Arsi crossbreeds. This might be due to the better maternal environment provided by the F1 dams and also the increased proportion of Friesian genes. The present

** The effect of sex was included only for birth weight, for older weights, the analyses were exclusively based on female animals.

observation is in line with the observation of Taneja and Bhat (1972); Naryanswamy *et al.*, (1984) and Kano Banjaw and Mekonnen Haile-Mariam (1994). The F1FA and F(JxA) were comparable at birth. The 75% FA were significantly heavier than F1FA at birth, 6 and 30 months. Increase in Friesian inheritance tended to increase body weights up to 30 months. The relatively smaller differences at 36 months, might be due to unfavourable conditions for the 75%FA at later ages (Table 2).

The 75%FZ and F1FZ had comparable performance throughout as differences in body weights were not significant at all ages (Tables 1 and 2). Hence, increase in the Friesian inheritance did not increase body weights linearly. The lack of significant difference between those genetic groups suggests the management at the farm was more suited to the intermediate cross, i.e. F1FZ. The present results are, in agreement to the report of Taneja and Bhat (1972) and Singh *et al.*, (1985) who noted an increase in body weight of crosses of only up to 50% Friesian inheritance. Similarly, kano Banjaw and Mekonnen Haile-Mariam (1994) observed no significant difference in weaning weight between F1 and three-quarter crosses between Friesian and Borana cattle in Ethiopia. F1 calves grew 12.2% faster than Borana and had comparable growth rate with the three-quarter cross.

The three-breed crosses with 75% exotic inheritance, F(JxA) had comparable performance with F1FA at all ages, however, were heavier significantly only at 6 months of age suggesting that the management and feeding conditions were not optimum for animals with 75% exotic inheritance. It could also be due to an effect of different growth curves, as Jersey is known as early maturing breed (Tables 1 and 2). Saha and Parekh (1988) reported that Friesian x Gir were superior to Friesian-Jersey-Gir crosses between 3 to 24 months.

The 75%FA were significantly heavier than the F(JxA) grades, at birth, 30 and 36 months. Thus, reflecting the influence of Jersey germplasm on the growth performance. Under peasant management and feeding conditions, such apparent lower weights could be advantages, as they could be maintained more easily by small farmers. The 75%FA were significantly lighter than 75%FZ at 12 and 36 months. This trend was consistent at almost all ages, indicating heavier body weight of Zebu than of the Arsi animals (Tables 1 and 2).

Table 1. Least squares means (LSM) and standard errors (SE) of effects influencing body weight traits (kg).

Variable	n	Birth weight LSM ± SE	n	6 months weight LSM ± SE	n	12 months weight LSM±SE	n	18 months weight LSM±SE
Overall breed	347	23.7±0.4	206	91.8±1.4	213	160.2± 2.1	164	220.1± 4.3
F1FA	101	21.5±0.5^{a}	73	80.6±2.7^{a}	73	149.6± 4.5^{c}	63	207.7± 6.9^{a}
F1FZ	63	24.6±0.5^{b}	36	94.3±2.7^{b}	37	165.3± 4.4^{ab}	28	224.2± 6.6^{a}
F(JxA)	64	21.9±0.6^{a}	34	93.4±2.9^{b}	34	155.9± 4.9^{bc}	27	216.5± 7.0^{a}
75%FA	89	24.6±0.6^{b}	47	93.4±2.7^{b}	51	157.7± 4.6^{bc}	35	214.3± 7.4^{a}
75%FZ	30	25.7±0.8^{b}	16	97.2±4.1^{b}	18	172.4± 6.6^{a}	11	237.8±10.0^{a}
Sex								
Male	120	23.9±0.5^{a}	-	-	-	-	-	-
Female	227	23.4±0.4^{a}	-	-	-	-	-	-
Parity								
1	149	22.9±0.4^{b}	95	88.9±2.0^{a}	98	152.8± 3.2^{a}	73	209.6± 5.4^{a}
2	82	23.5±0.5^{ab}	47	90.6±2.4^{a}	48	157.8± 4.0^{a}	35	216.5± 6.4^{a}
3	72	24.7±0.5^{a}	38	90.3±2.7^{a}	39	162.7± 4.3^{a}	34	226.9± 6.4^{a}
4+	44	23.6±0.9^{ab}	26	97.2±3.1^{a}	28	167.4± 5.1^{a}	22	227.4± 7.7^{a}
Birth year								
71	72	22.3±1.0^{a}	64	92.5±5.0^{a}	64	164.4± 8.4^{a}	53	229.7±12.2^{a}
72	98	23.9±0.6^{a}	49	98.2±3.6^{a}	51	187.0± 5.9^{b}	47	239.2± 8.6^{a}
73	117	24.4±0.6^{a}	65	94.4±3.5^{a}	69	152.0± 5.8^{c}	37	214.1± 9.0^{a}
74	60	24.2±1.0^{a}	28	81.9±6.5^{a}	29	137.3±11.1^{d}	27	197.4±15.3^{a}
Birth season								
Short rains	121	23.2±0.5^{a}	81	93.1±2.1^{b}	84	163.2± 3.5^{a}	73	225.8± 5.6^{b}
Rainy season	87	24.5±0.5^{b}	49	93.9±2.4^{b}	50	168.0± 3.9^{a}	39	224.7± 6.1^{b}
Dry season	139	23.2±0.5^{a}	76	88.3±2.2^{b}	79	149.4± 3.5^{b}	52	209.7± 5.9^{b}

Within variables means followed by the same letter are not significantly different ($P > 0.05$).

Table 2. Least squares means (LSM) and standard errors (SE) of effects influencing body weight traits (kg).

Variable	n	24 months weight LSM ± SE	n	30 months weight LSM ± SE	n	36 months weight LSM ± SE
Overall Breed	170	259.7± 3.3	157	278.0± 9.0	143	284.2± 4.5
F1FA	67	252.1± 5.6^{a}	59	259.4± 7.4^{b}	51	274.2± 8.7^{ab}
F1FZ	28	264.7± 5.9^{a}	28	292.4± 8.1^{a}	27	306.6± 8.7^{c}
F(JxA)	27	257.5± 6.1^{a}	29	260.5± 8.1^{b}	28	249.4± 9.2^{a}
75%FA	35	265.5± 5.9^{a}	33	289.6± 8.6^{a}	31	277.0± 9.1^{b}
75%FZ	13	258.8± 8.4^{a}	8	287.8±15.4^{a}	6	314.0±18.1^{c}
Parity						
1	81	248.0± 4.3^{c}	73	271.4± 6.0^{a}	68	287.7± 6.5^{a}
2	36	267.6± 5.3^{a}	33	280.3± 7.4^{a}	30	280.1± 8.4^{a}
3	31	257.1± 6.0^{abc}	30	274.9± 8.0^{a}	25	288.0± 9.2^{a}
4+	22	266.1± 6.5^{ab}	21	285.2± 9.1^{a}	20	281.2± 9.5^{a}
Birth year						
71	61	273.8± 9.9^{b}	55	278.8±13.6^{b}	51	284.7±15.5^{b}
72	40	276.4± 7.5^{b}	33	282.8± 9.7^{b}	24	301.1±11.9^{b}
73	48	253.1±13.1^{b}	51	277.3± 9.5^{b}	52	301.0±10.6^{b}
74	21	235.1±13.1^{b}	18	264.0±18.2^{b}	16	250.1±22.4^{b}
Birth season						
Short rains	71	261.9± 4.6^{a}	60	274.9± 6.1^{a}	60	280.0± 6.7^{a}
Rainy season	39	259.2± 5.2^{a}	34	280.6± 7.1^{a}	28	283.7± 8.4^{a}
Dry season	60	258.0± 4.9^{a}	63	278.4± 6.0^{a}	55	289.0± 6.7^{a}

Within variables means followed by the same letter are not significantly different ($P>0.05$).

Table 3. Least squares analysis of variance for body weight traits.

Source of variation	Mean squares						
	Traits						
	Birth	6 m	12 m	18 m	24 m	30 m	36 m
Sire	13.9ns	228.2ns	600.8ns	1324.2*	879.3ns	1156.4ns	1232.5ns
	(39)	(35)	(37)	(36)	(34)	(34)	(36)
Breed	127.5***	910.4**	1631.7*	1652.3ns	661.4ns	4811.7**	8662.4**
	(4)	(4)	(4)	(4)	(4)	(4)	(4)
Sex	15.3ns	n.a.	n.a.	n.a.	n.a.	n.a.	n.a.
	(1)						
Parity	25.6*	343.0ns	1370.2ns	1995.5ns	2766.4**	754.8ns	343.3ns
	(3)	(3)	(3)	(3)	(3)	(3)	(3)
Birth year	14.8ns	382.7ns	5720.1**	1810.5ns	1346.7ns	271.0ns	2315.1ns
	(3)	(3)	(3)	(3)	(3)	(3)	(3)
Birth season	42.7*	363.2ns	3743.7**	2267.2ns	141.3ns	264.5ns	585.2ns
	(2)	(2)	(2)	(2)	(2)	(2)	(2)
Remainder	10.0	193.3	576.3	749.9	641.8	1171.2	1253.2
	(294)	(158)	(163)	(115)	(123)	(110)	(94)
R^2	0.56	0.60	0.62	0.67	0.66	0.69	0.68

*, $P<0.05$; **, $P<0.01$; ***, $P<0.001$; ns, not significant ($P>0.05$); (), degrees of freedom; n.a., not available.

Due to the scarcity of information on male animals, which in the first year of the project were normally slaughtered at lower ages, the effect of sex could not be included in the model except for birth weights. Non-significant effect of sex was observed at birth (Table 3). Similar results were reported by various authors (Govindaijah *et al.*, 1979; Trail and Gregory, 1982; Nicholson, 1983; Maarof and Arafat, 1985; Sharma *et al.*, 1986 and Rege *et al.*, 1993). The results were, however, in contrast to other reports in which males were significantly heavier than females at birth (Ghosh *et al.*, 1979; Aman *et al.*, 1985; Saeed *et al.*, 1987 and Kano Banjaw and Mekonnen Haile-Mariam, 1994).

The effect of parity of the dam was found to have significant influence only at birth and 24 months (Table 3). At birth, animals born to the third parity were significantly heavier than those born to the first parity. At 24 months, animals born to the fourth and above parities were significantly heavier than those born to the first parity (Tables 1 and 2).

The year of birth did not contribute any significant variation at all phases of age, except at 12 months (Table 3). However, there was a clear trend at all ages that the weights go down from birth year 1972 to 1974. This trend may indicate a deterioration in management and feeding conditions over these years. The effect year of birth on body weights has been attributed to the wide variation in the availability of feed and fodder and management practices over the years in India (Naryanswamy *et al.*, 1984; Nautiyal and Bhat, 1989).

Season of birth had significant influence on weights at birth and 12 months (Table 3). Calves born during the main rains had the heaviest birth weight and were significantly different from those born in the small rains and dry seasons. At 12 months, calves born in the short and main rains were significantly heavier than those born in the dry season. Animals born during the rainy seasons were kept in door in the dry season and had the advantage or better chance of utilising pasture of good quality and quantity in the subsequent small and main rainy seasons. It is generally observed that season of birth had little effect at older ages, which is substantiated by the observations of Naryanswamy *et al.* (1984); Singh *et al.* (1985); Venugopal *et al.* (1986); Singh and Bhat (1987), who noted significant effect of season of birth on body weights between 6 to 12 months of age.

In order to estimate heritabilities of body weight traits, sires were included in the model as a random effect. All Friesian sires were not progeny tested bulls, however, brought from different sub-population in Kenya, Sweden and Israel. This will give estimates of heritabilities based on crossbred progeny, F1 and 75% upgraded offsprings. In cases where the aim is to establish a crossbred population, in which selection could be carried out for different traits, the estimation of genetic parameters is necessary for the population in question.

The variation associated with sire was only significant at 18 months (Table 3). Johnson and Gambo (1975); Naryanswamy *et al.* (1984), who reported non-significant effect of sire except at birth, concluded that sires were not important in enhancing the growth of their offsprings.

Heritability estimates for weights at birth, 6, 12, 18 and 24 months are presented in Table 4. The value for birth weight is lower than most values reported in the literature and so are heritabilities for 6 and 12 months. In general, the lower heritabilities for these traits may indicate lower additive genetic variation in this population. The estimates for 18 and 24 months were higher and agree well with the ranges reported in the literature. The increase in value with age is logical as the first part of the growth period is more affected by environmental variations than the older ages. Although the higher heritability estimates may suggest better scope of improvement through selection, the values showed high standard error mainly due to the small number of offsprings per sire. It is, therefore, necessary to verify the magnitude of the additive genetic variation of these traits on large crossbred population.

Table 4. Heritability estimates for different body weight traits.

Traits	$h^2 \pm SE$
Birth weight	0.20 ± 0.15
6 months weight	0.14 ± 0.23
12 months weight	0.04 ± 0.21
18 months weight	0.68 ± 0.34
24 months weight	0.33 ± 0.29

CONCLUSIONS

Increase in Friesian inheritance did not increase body weights linearly as expected, suggesting apparently unfavourable conditions for the genetically superior animals, *i.e.*, 75%FA and 75%FZ. Therefore, it may be concluded that management and feeding at Asella Livestock Farm would warrant limitation of level of upgrading to 50% of exotic inheritance.

The three-breed cross, F(JXA) had comparable body weights to F1FA. The positive effect of upgrading on growth performance was also not observed in this group. However, smaller weights of F(JXA) may be advantageous to smallholder farmers, as such animals could be maintained more easily than larger animals with higher levels of Friesian inheritance.

The implication of current results to smallholder dairy farmers in the region is that continuous upgrading may not lead to linear increase in production under farmers conditions, therefore, intermediate grades which can best fit into the available resources at farm level are more appropriate.

ACKNOWLEDGEMENTS

We would like to thank the Ministry of Agriculture, the Southern Agricultural Development (SEAD) Zone office, Asella, Ethiopia, for allowing us to use the data from Asella Livestock Farm. Many thanks are also due to the Swedish Agency for Research Co-operation with Developing Countries (SAREC) for its technical and material support.

REFERENCES

1. Aman A., Kamal, K.M., Arief, O.M. and Shokri, O.A. (1985). Variation in weights of Kadah-Kelantan cattle from birth to one year of age. *MARDI Research Bullelin* **13**:81–86.
2. Ansell, R.H. (1985). Cattle breeding in the tropics. *World Animal Review* **54**:30–38.
3. Brännäng, E. and Persson, S. (1990). *Ethiopian Animal Husbandry. A Handbook.* Uppsala, Sweden.

4. Dhumal, M.V., Sakaree, P.G. and Deshpande P. (1988). Factors affecting growth rate of local and Jersey x Local calves. *Indian J. Anim. Sci.* **58**:855–859.

5. Ghosh, D., Choudhury, G., Banerjee, G.C. and Ghosh, M.N. (1979). Studies on the growth pattern and factors affecting it in the Holstein x Hariana crossbred calves. *Indian vet. J.* **56**:656–659.

6. Govindaijah, M.G., Singh, B.P., Singh, M.R., Tyagi, J.C. and Saxena, R.P. (1979). Factors affecting birth weight in Hariana cattle. *Indian Vet. J.* **56**:300–305.

7. Harvey, W.R. (1990). User's Guide for PC-2 Version. Mixed Model Least-Squares and Maximum Likelihood Computer Program.

8. Johnson, A.O. and Gambo, A. (1975). Growth performance of dairy crossbred calves at Shika Research Station. *Samaru Agricultural News Letter (Nigeria)* **17**:41–45.

9. Kano Banjaw and Mekonnen Haile-Mariam (1994). Productivity of Borana cattle and their Friesian crosses at Abernosa Ranch, Rift Valley of Ethiopia. II. Growth performance. *Trop. Anim. Hlth Prod.* **26**:49–57.

10. Kiwuwa, G.H., Trail, J.C.M., Kurtu, M.Y., Getachew Worku, Anderson F.M. and Durkin, J. (1983). Crossbred dairy cattle productivity in Arsi Region, Ethiopia. ILCA Research Report No. 11. ILCA, Addis Ababa, Ethiopia.

11. Maarof, N.N. and Arafat, I.A. (1985). Some factors affecting birth and weaning weights in Friesian cattle. *World Review Anim. Prod.* 21:37–40.

12. McDowell, R.E. (1982). Crossbreeding as a system of mating for dairy production. South-Coop. Ser. Bull. No. 259. Lousiana Agri. Stn, Baton Rouge.

13. McDowell, R.E. (1996). The economic viability of crosses of *Bos taurus* and *Bos indicus* for dairying in warm climates. *J. Dairy Sci.* **79**:1292–1303.

14. Naryanswamy, M., Balaine, D.S. and Ram, S. (1984). Studies on growth efficiency in Friesian x Sahiwal crosses. *Indian J. Dairy Sci.* **37**:44–49.

15. Nautiyal, C.P. and Bhat, C.P. (1989). Body weight of Hariana crosses. *Indian J. Anim. Sci.* **59**:1007–1010.

16. Nicholson, M.J. (1983). Calf growth, milk offtake and estimated lactation yields of Borana cattle in the Southern rangelands of Ethiopia. Joint ILCA/RDP Ethiopian Pastoral System Study Program. ILCA/JEPSS, Research Report No. 6. ILCA, Addis Ababa, Ethiopia.

17. Rege, J.E.O., Von Kaufmann, R.R., Mwenya, W.N.M., Otchere E.O. and Mani, R.I. (1993). On-farm performance of Bunaji (White Fulani) cattle. Growth, reproductive performance, milk offtake and mortality. *Anim. Prod.* **57**:211–220.

18. Rendel, J. (1974). The role of breeding and genetics in animal production improvement in developing countries. *Genetics* **78**:563–575.

19. Saeed, A.M., Ward, P.N., Light D., Durkin, J.W. and Wilson, R.T. (1987). Characterisation of Kenana cattle at Um Banein, Sudan. ILCA Research Report No. 16. International Livestock Centre for Africa, Addis Ababa, Ethiopia.

20. Saha, D.N. and Parekh, H.K.B. (1988). Factors affecting body weight in half and three fourth crossbred cattle. *Indian J. Dairy Sci.* **41**:394–397.

21. Sendros Demeke and Tesfaye Kumsa (1998). Factors to be considered in the formulation of livestock breeding policy. **In**: *Proceedings of Fifth National Conference of Ethiopian Society of Animal Production*, 15–17 May 1997. Ethiopian Society of Animal production. Addis Ababa, Ethiopia.

22. Sharma, L.D., Lohmi, P.C. and Gupta, A. (1986). Non-genetic factors affecting birth weight in Jersey calves. *Indian Vet. J.* **63**:158–159.

23. Singh, S.R., Mishra, H.R. and Singh, S.K. (1985). Factors affecting six monthly body weights in Friesian x Sahiwal females. *Indian Vet. Med. J.* **9**:199–204.

24. Singh, B. and Bhat, P.N. (1987). Effect of crossbreeding on body weight changes in Holstein x Sahiwal crossbreeds. *Indian Vet. J.* **64**:52–57.

25. Taneja, V.K. and Bhat, P.N. (1972). Genetic and non-genetic factors affecting body weights in Sahiwal x Friesian crosses. *Anim. Prod.* **14**:295–298.

26. Tesfaye Kumsa (1993). Small holder dairy in Ethiopia. **In**: *Future of Livestock Industries in East and Southern Africa*. Proceedings of the Workshop held at Kadama Ranch Hotel, Zimbabwe, 20–23 July 1992. International Livestock Centre for Africa, Addis Ababa, Ethiopia.

27. Trail, J.C.M. and Gregory, K.E. (1982). Production Characters of the Sahiwal and Ayrshire breeds and their crosses in Kenya. *Trop. Anim. Hlth. Prod.* **14**:45–57.

28. Venugopal, G., Bhattacharyya, N.K and Bisht, G.S. (1986). Birth weight and weight gains of Brown Swiss-Zebu crosses in Kerala. *Indian Vet. J.* **63**:479–483.

SINET: Ethiop. J. Sci., 24(1):51–68, 2001
 ISSN: 0379–2897

SURFACE KINETIC TEMPERATURE MAPPING USING SATELLITE SPECTRAL DATA IN CENTRAL MAIN ETHIOPIAN RIFT AND ADJACENT HIGHLANDS

Tenalem Ayenew

Department of Geology and Geophysics, Faculty of Science, Addis Ababa University
PO Box 1176, Addis Ababa, Ethiopia, E-mail: dgg@telecom.net.et

ABSTRACT: Remotely sensed thermal-infrared spectral data can be used to derive surface temperature of any object if the optical and thermal properties are known. In this study TM band six has been used to assess the spatial variability of the kinetic temperature of the central Ethiopian rift lakes and adjacent highlands. NOAA-AVHRR data have been used to understand the relative differences of the monthly lake surface kinetic temperatures. The result revealed that despite the limited topographic differences of the rift lakes and their proximity, the surface kinetic temperature difference is high, mainly due to groundwater and surface water fluxes. From thermal signature analysis two hot springs below the lake bed of Ziway were discovered. The various hot springs around three of the lakes have limited role in the overall water budget of these lakes as compared to the total surface water and cold groundwater fluxes. Temperature from the land surface shows also large variations with altitude and land cover types.

Key words/phrases: Kinetic temperature, rift lakes, spectral data, thematic mapper, thermal infra-red

INTRODUCTION

One of the first uses of thermal images in hydrogeology is to detect temperature contrasts due to up-welling groundwater in water bodies using Thematic Mapper (TM) data (Meijerink; 1996). In some later studies, such contrasts are associated with groundwater discharge areas (Bobba *et al.*, 1992; Batelaan *et al.*, 1993; Tenalem Ayenew, 1998). Short-wave thermal infra-red data have also been used

to discover high temperature thermal events and for geothermal resources assessment (Rothery *et al.*, 1988).

The use of thermal infra-red data is becoming increasingly useful for measuring different surface flux densities and temperatures (Menenti, 1984; Bastiaanssen, 1995; Pelgrum and Bastiaanssen, 1996). Lagouarde (1991) suggests the possibility of using the National Oceanic and Atmospheric Administration (NOAA) Advanced Very High Resolution Radiometer (AVHRR) for a radiation balance. He proposed a simple algorithm for estimating the upward long-wave component of the surface radiation balance from only one surface measurement derived from NOAA. TM and NOAA-AVHRR have also been used for evapotranspiration mapping (Kerr *et al.*, 1992, Parodi, 1993; Timmermans, 1995; Tenalem Ayenew, 1998).

Cloud free multi-temporal spectral data of TM and NOAA can be of great help in assessing the temporal variation of temperature and evapotranspiration from the land and water bodies (Parodi, 1993). However, due to the high cost of TM images, its application in multi-temporal analysis of hydrometeorlogical process is very limited.

In this study, thermal infra-red TM band 6 data of a single scene were used for different purposes. Temperature contrasts in the lakes are of interest in the area to detect whether hydrothermal activities occur and if so, the relative importance of the discharges. Hydrothermal water could also influence the temperature of river water discharging into the lakes.

A second application is to assess the differences in temperature of the lakes, which are associated with different evaporation rates. Since there are no field data available on lake evaporation, ancillary information for this important factor of the water budget is useful. In this connection, in addition to TM, the NOAA-AVHRR data was used to derive the mean monthly surface kinetic temperatures of the lakes using cloud free images at the National Meteorological Services Agency.

The third application is to study the geothermal manifestations in relation to the rift geologic structures; the study area is characterized by many hot springs and fumaroles associated with geothermal fields. This helps to detect possible

migration routes of groundwater. Spring discharges emanating below the lakes could also be estimated from thermal images.

The TM image was taken on 21 November 1989 (satellite overpass at 10:00 AM local time). TM band six operates between the wave length range of 10.4 μm and 12.5 μm of the thermal infra-red region with a ground resolution of 120 m. For monthly lake surface temperature estimation, the NOAA-AVHRR data (1994–1995) were used based on the method described by Bastiaanssen (1995). It acquires images with a swath width of 2,700 km and a ground resolution of 1,100 by 1,100 metres. The raw TM spectral data were converted to surface kinetic temperature by image processing techniques using the Integrated Land and Water Information System (ILWIS) software developed at the International Institute for Aerospace Survey and Earth Sciences (ITC), The Netherlands.

THE STUDY AREA

The basin studied is part of the Ethiopian Rift system bounded within the limits of 38°00'-39°30' east longitude and 7°00'–8°30' north latitude, and covers a total area of 13,000 km^2 of which 1,265 km^2 is permanent open water body. The central part is the floor of the rift occupied by four major lakes: Ziway, Langano, Abiyata and Shala, having average depths of 2.4, 21.9, 8.9 and 8.6 metres respectively (Table 1). Shala and Abiyata are highly alkaline terminal lakes with no surface water outlets fed by perennial rivers coming from the eastern and western highlands (Fig. 1). Hot springs emanating from the southern, southeastern and eastern shores feed Shala, Langano from springs located on the northern shore and in one of the northern islands. A low discharge hot spring exists in one of the southern islands of Ziway. Fig. 1 shows the main sites of geothermal manifestations.

The altitude ranges from a little over 3,000 meters above mean sea level (m.a.s.l) in large part of the surface water divide to 1,600 m.a.s.l around the rift lakes. The average altitude of the rift is about 1,700 m.a.s.l. The altitude ranges from 2,000 to 3,000 m.a.s.l in the western highland and 2,100 to 3,200 m.a.s.l in the eastern highlands. There are volcanic summits having an altitude of more than 4,000 m.a.s.l to the east (Tesfaye Chernet, 1982).

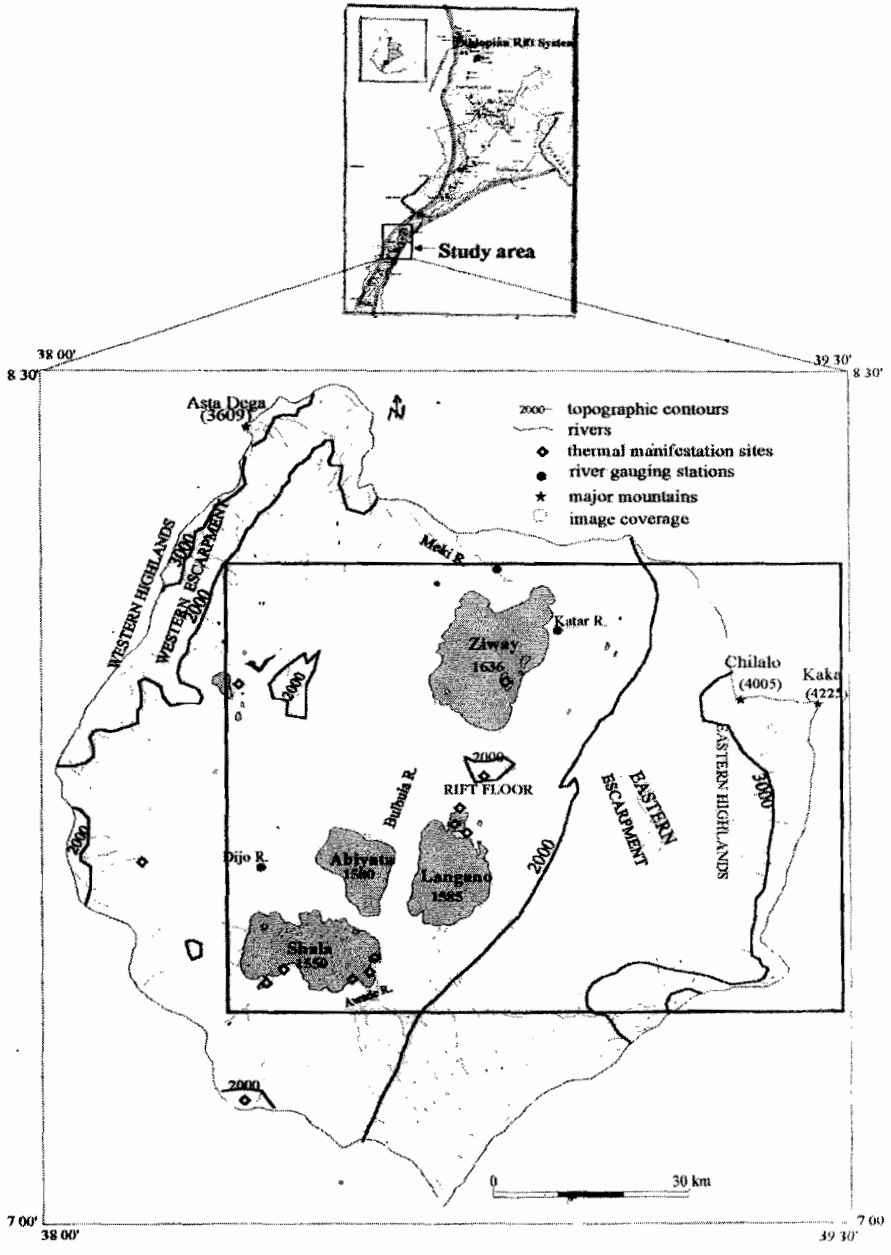

Fig. 1. Location map of the study area.

Geologically these lakes are situated in tectonically active rift volcanic terrain. The present day geologic and geomorphic features are the result of Cenozoic volcano-tectonic and sedimentation processes. Faulting was accompanied by extensive basaltic and silicic volcanism restricted to separate centres aligned along the NE-SW trending rift axis. Several shield volcanoes were developed in the plateaux; the different volcanic episodes formed thick rock sequences (Di Paola, 1972; Giday Woldegebriel *et al*, 1990). The major rock types in the rift are: ignimbrite, basalt, tuff, trachyte and pumice, associated with lacustrine, volcano-clastic, alluvial and colluvial deposits. Large-scale block faulting has disrupted these rocks and formed step-faults. As a result, the rift is distinctly separated from the highlands by a series of normal faults mainly trending parallel and sub-parallel to the axis of the rift. The floor of the rift is marked by a persistent belt of intense and active faulting and volcanic centres characterized by presence of hot springs and fumaroles.

The climate is humid to sub-humid in the highlands and semi-arid in the rift. Mean annual temperature is about 15°C in the highlands and around 20°C in the rift (HALCROW, 1989). The average annual rainfall ranges from about 1,150 mm in the eastern and western highlands to around 650 mm in the rift floor. At the top of large volcanic summits the annual rainfall can be as high as 1400 mm (Tenalem Ayenew, 1998). The main rainy season is between June and September. The dry season lasts from October to February. Temperature and rainfall show strong altitudinal variations (Tesfaye Chernet, 1982).

Most of the basin is moderately cultivated and, in major mountainous areas there is no much agriculture due to topographic and climatic constraints. Afro-montane forest lies between 2,000 and 3,000 m.a.s.l, above which alti-montane vegetation is found. The top of mountains is covered by afro-alpine vegetation. The escarpment is characterized by acacia and deciduous trees, evergreen and semi-evergreen bush land. On the southeastern escarpment large forested area exists (represented by black tone in Fig. 2). The remaining highland and escarpment is farmland with scattered trees and grazing land. Except few irrigated fields around lake Ziway, the rift is covered by grass, bushes and shrubs. Soda grounds and lacustrine soils in the rift floor are represented by strong white tone in Fig. 2. Table 2 shows the land cover types derived from multi-spectral classification of TM bands 2,3 and 4.

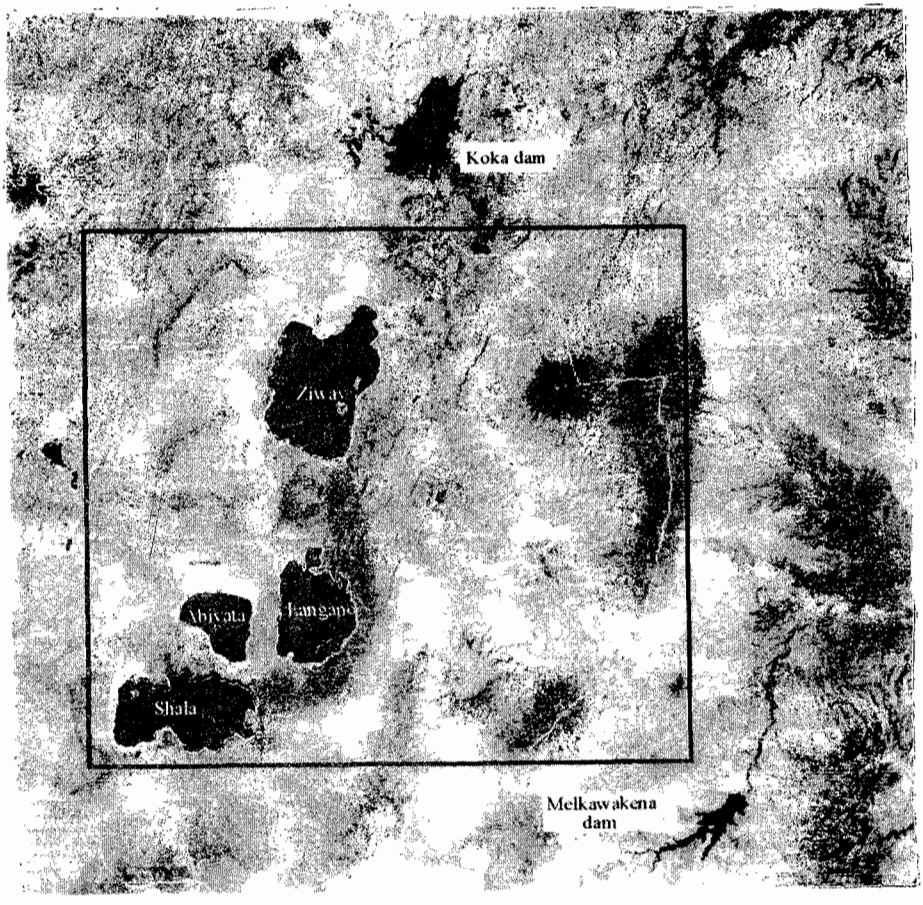

Fig. 2. Panchromatic TM image showing part of the basin and adjacent areas. The white line is the surface water divide of the basin. The thick black line indicate the scene chosen for the analysis.

Table 1. Basic hydrologic data of the major lakes (modified from HALCROW, 1989).

Lake	Altitude (m.a.s.l)	Lake area (km^2)	Catchment area (km^2)	Maximum depth (m)	Mean depth (m)	Volume (mcm)
Abiyata	1580	180	10740	14.2	7.6	954
Langano	1585	230	2000	47.9	17	3800
Shala	1550	370	2300	266	8.6	37000
Ziway	1636	440	7380	8.9	2.5	1466

Table 2. Areal coverage of land cover units in the basin.

Class	Land cover types	Areal coverage (%)	Area (km^2)
1	Permanent open water body	11.1	1443
2	Marshy areas, swamps and seasonal ponds	1.4	182
3	irrigated agricultural fields	0.7	91
4	large-scale rain-fed agriculture	1.2	156
5	pasture and farm plots with scattered trees and orchards	66.1	8593
6	dominantly grassland	3.6	468
7	bushes, shrubs and grassland with rare farm plots	7.3	949
8	woodland and afro-alpine vegetation	8.4	1092
9	settlement areas	0.2	26

METHODOLOGY

The radiant temperature of a given surface can be derived from the TM band 6 pixel values or digital number (DN) using the following relation developed by Markham and Barker (1986).

$$L_i = L_{\min,i} + \frac{L_{\max,i} - L_{\min,i}}{DN_{\max}} \cdot DN \qquad (1)$$

where, Li : spectral radiance in band i ($mW/cm^2.str.\mu m$)
$L_{min,i}$: spectral radiance at DN = 0 ($mW/cm^2.str.\mu m$)
$L_{max,i}$: spectral radiance at DN = max ($mW/cm^2.str.\mu m$)
DN : digital number
DN_{max} : grey level for the analyzed pixel

Once the spectral radiance is computed, it is possible to calculate the radiant temperature using the relation:

$$T_R = \frac{K_2}{\ln(\frac{K_1}{L_1} + 1)} \quad (2)$$

where, TR : radiant temperature (°K)
K_1 : calibration constant (60.776 mW/cm^2.str.μm)
K_2 : calibration constant (1260.56 mW/cm^2.str.μm, °K)
L_i : spectral radiance in band i (mW/cm^2/str/μm)

From the radiant temperature the kinetic temperature (T_{toa}) at the top of the atmosphere can be calculated by:

$$T_{toa} = \varepsilon^{0.25} T_R \quad (3)$$

The ε term represents the spectral emissivity. Since the emissivity of pure water is 1, the relation between the recorded signal at the satellite and the relative surface water temperature is a simple one. However, for conversion to absolute temperature, the effect of the atmosphere has to be accounted for. For land surfaces the interpretation of thermal imagery is not so simple, because the emissivity of the various land covers vary in a wide range due to variable thermal properties of soil-vegetation complexes. Topographic conditions, which determine slope exposure in relation to the sun's path prior to satellite overpass, also play a role.

A simplified approach to estimate the emissivity of the land using Normalized Difference Vegetation Index (NDVI) suggested by Griend *et al.* (1993) is

$$\varepsilon = 1.009 + 0.047 \ln(\text{NDVI}). \quad (4)$$

The above relation does not give the actual land surface temperature. It has to be converted to surface kinetic temperature (T_o) after corrections for atmospheric effects (Roerink, 1995). The general relation is given by:

$$T_o = \sqrt[4]{\frac{\sigma T_o^{R4} - (1-\varepsilon) L^{\downarrow}}{\sigma \varepsilon}} \quad (5)$$

Where, TR : black body surface temperature (°K)

$L^{\downarrow}$: incoming long-wave radiation derived from spectral data (W/m^2)

σ : Stefan Boltzman constant (5.6697×10^{-8} $W.m^{-2}$. K^{-4})

RESULTS AND DISCUSSION

Figure 3 shows the classified surface kinetic temperature of the lakes and the surrounding landscape established after appropriate atmospheric corrections. Table 3 shows the instantaneous surface kinetic temperature of the lakes derived from TM. The monthly surface temperature of the lakes derived from NOAA is given in Table 4.

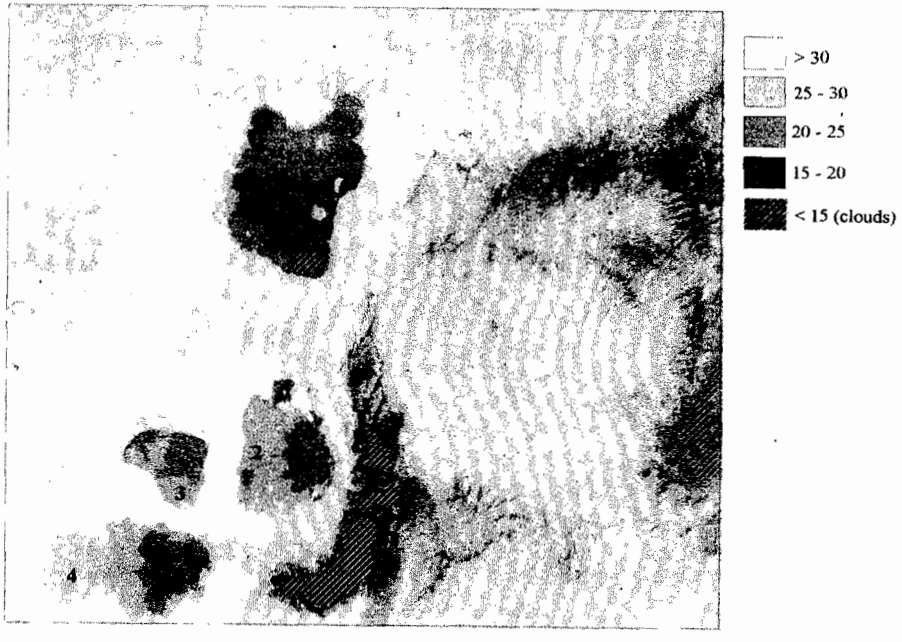

Fig. 3. Classified TM band six image showing surface kinetic temperature (°C) (1, Lake Ziway; 2, Lake Langano; 3, Lake Abiyata; 4, Lake Shala).

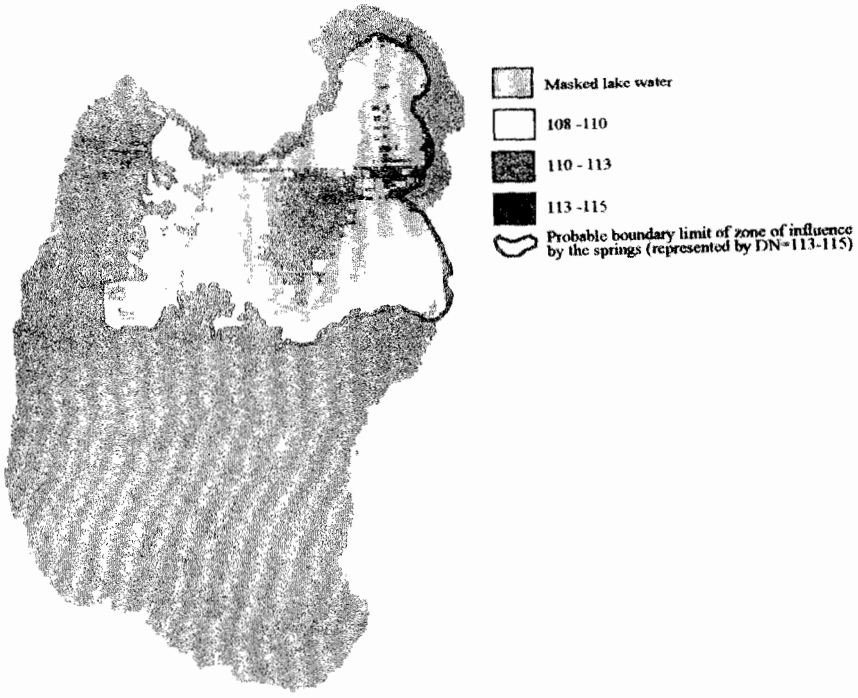

Fig. 4. Sites of hot spring emanation inside Lake Ziway (the highest DN value).

Table 3. Lake surface kinetic temperature (°C).

Basic statistics	Abiyata	Langano	Shala	Ziway
Average	22.9	22.5	23.2	20.9
Minimum	19.0	15.4	16.2	16.2
Maximum	27.4	27.0	26.9	26.8
Mode	20.9	21.8	22.7	20.4
St. deviation	0.9	1.1	1.2	0.9

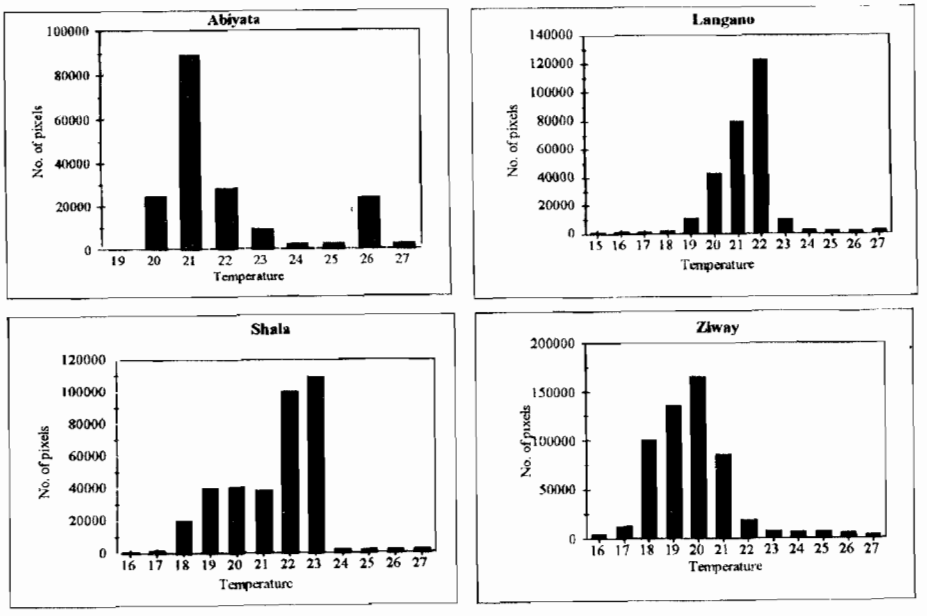

Fig. 5. Histograms of surface kinetic temperature of the lakes (°C).

Table 4. Surface temperature of the lakes derived from NOAA (°C). (min, minimum; avg, average; max, maximum.)

Lake		Jan	Feb	Mar	Apr	May	Jun	Jul	Aug	Sep	Oct	Nov	Dec
Ziway	min		17.8	15.6	16.8	21	18.6	17.6	17.8		18.2	19.2	19.6
	avg		18.4	18.8	23.2	23	20.6	19.2	18.4		20.4	22.6	23.2
	max		22	29.2	32	37	31	29.2	22		35.4	35.4	44.6
Langano	min		12.2	17	20.2	21.6	19.2	15.6	12.2		19	20.4	21.4
	avg		20	20.2	21.8	23.8	22	19.8	20		22.2	24.8	24.8
	max		22.6	29	29.8	33.8	31.8	29.2	22.6		33.6	37	40.4
Abiyata	min		13.8	16	20.4	22	16.6	17.2	13.8		19.2	20.2	20
	avg		19	20.8	22.6	25.4	21.2	20.6	19		22.8	26.6	25.4
	max		22.2	26.6	28.4	7.4	32.2	30	22.2		36.4	39.2	41
Shala	min		16.8	16	19.6	1.4	12.8	16.4	16.8		19	20.4	20.4
	avg		18.8	19.2	20.8	23	20.6	18.6	18.8		22	23.4	22.6
	max		21.8	24.8	26.8	32.2	30.8	23.6	21.8		34.2	34.8	32.2

Lake surface temperature

The result shows wide variation in the surface temperature of the lakes. This variation has resulted in large differences in the rates of open-water evaporation (Tenalem Ayenew, 1998). As illustrated in Fig. 3, not all the lakes have a uniform surface temperature. The lowest value usually exists far from the shores in the central and deeper part of the lakes. Locally this pattern is disrupted by the effect of inflowing rivers and groundwater fluxes. For example, there is a lower temperature at the confluence of Meki river with lake Ziway, and the rivers of Horakelo and Bulbula with lake Abiyata. Low temperature signature is evident close to the eastern shore where large rivers enter into lake Langano. These low temperature sites close to shores are also localities of large groundwater inflow; as identified from groundwater flow models simulations (Tenalem Ayenew, 2001).

The effect of the Katar river which comes from the eastern highlands entering lake Ziway from the northeastern side is not as important as the rivers coming to lakes Langano and Abiyata in affecting the temperature signature. Katar supplies the largest volume of cold water to lake Ziway. A large portion of the lake close to the confluence is very shallow; in the field it was found that there is no indication of geothermal manifestations around the lake. However, the hot springs emanating below the lake bed, a little south of the confluence (Fig. 4), might play a role in raising the temperature. Probably, the huge sediment of the mouth of the Katar delta at the confluence may reduce the water depth and consequently increase the surface temperature slightly.

The effect of known hot springs (Fig. 1) emanating close to shores on lake water temperature is not well pronounced. Although the points of emergence of hot springs is represented in local high temperature pixels to the south, southeast and east of lake Shala and north of lake Langano, there is little influence on the surface temperature. Lake surface temperature measurement was made in the field in these areas. There is only a rise of 1 to 2 °C from the normal colder lake water. This influence extends only up to a maximum of 20 to 30 meters far from the shores where these hot springs enter. In the presence of large hot spring fluxes, the rise in temperature would have been much higher. This implies that the role of these hot springs is small in terms of volume of water compared to the contribution of water from rivers and cold

groundwater system. Some hot springs are masked by the presence of local clouds, as in the case of south Ziway and the island in northern Langano. Some springs north of Langano are also masked by the presence of dense big trees.

From the histograms of kinetic temperature of the lakes (Fig. 5), the following generalizations can be made:

On the average, Abiyata and Shala have the highest surface temperature. In lake Abiyata the lower temperature of the histogram (19–21°C) is related to areas where rivers Bulbula and Horakelo enter into the lake from the north (Fig. 1), and the highest temperature distribution is related to areas in the southern tip and northern shallow part of the lake. The large number of pixels around 26°C refers to the southern tip and northern side of the lake where the water is extremely shallow. The shoreline in these areas is covered with white soda salts with very high temperature signature.

In lake Shala the lowest temperature corresponds to the deepest part of the lake and the small cloud covered areas (represented in less than 15°C in Fig. 3). The effect of the rivers coming from the southeastern highlands is represented by low temperature in the eastern half of the lake. The Dijo river, which comes from the western highlands into the lake, does not have a visible influence on temperature of the lake. This is due to upstream diversion of the river for irrigation. In Langano the lowest temperature (less than 19°C) is measured in the northern part around the island. The cloud cover areas are less than 15°C in Fig. 3. Very local highest temperature points are present on the northern shore where hot springs emanate. The 22–25°C value represents lake water influenced by incoming cold rivers.

Lake Ziway has the lowest temperature. This is partly related to the large quantity of cold water that comes from the two major rivers. High surface temperature exists close to the shallowest parts in the western and southern side where there are no inflowing rivers. Areas close to the small islands are represented by higher temperatures (25–27°C). This is probably due to the thermal exchange between the volcanic rocks and the lake water.

Geothermal fields and hydrothermal activities

A simple threshold value of the digital data allows discrimination of higher thermal signatures than the rest of the land. In this case the lowest kinetic temperature for geothermal manifestations on the land is 30°C. Although local geothermal manifestations are not clearly visible from the thermal images, in general they are aligned along active faults and recent central volcanic complexes. The soda salts around lakes Abiyata and Shala have also high temperatures. Not all regional faults are associated with geothermal fields. For example, the active regional faults of the eastern and western escarpment are devoid of geothermal manifestations or high temperature signatures. The most important geothermal fields are localized around and close to the Shala caldera and the northern shore of Langano. These are due to the presence of local active volcanic centres.

The NOAA image has little practical importance in showing local high temperature grounds due to the low resolution. Some high temperature grounds and associated hot springs were not detected also from the high resolution TM image due to forest cover. In such kind of terrain thermal signature analysis requires careful field investigations. Many hot springs, which are not observable from the satellite data, were identified in the field.

Inside lake Ziway, not far from the confluence with Katar river, there are sites of high DN value (Fig. 4). The thermal signature analysis allowed to discover at least two hot springs emanating below the bed of lake Ziway. The hot pixels inside lake Ziway have a surface temperature of 2 to 4°C greater than the surrounding colder lake water (with average temperature of around 22°C). The discharge of these springs were found to be low (Tenalem Ayenew and Gieske, 2001).

Land surface kinetic temperature

The classified image shows that there is a large temperature difference between the rift and the highlands; the zonation of temperature with altitude is locally disrupted by clouds. The dominant instantaneous kinetic temperature for most of the rift valley ranges from 26°C to 30°C. The temperature reaches locally more than 35°C in geothermal fields. In the highlands, the temperature ranges from a little above 15°C in high volcanic summits to 28°C in the rift plains.

The land cover types also have important influence on land surface kinetic temperature. For example, the rift floor lacustrine bare soil surface has high temperature compared to the grasslands and bush lands. The effect of land use on temperature is better represented in the rift. Whenever bare soil is present, the temperature is greater than the nearby land covered with crops or trees. The contrast is very high between forested land and bare soil; there is on average 5°C to 8°C difference between the acacia trees cover (around 21°C) and nearby lacustrine soils (more than 28°C). The soda salts around lake Abiyata have a very high temperature (around 30°C). As in the case of the lakes, the large differences in temperature resulted in wide variations in evapotranspiration from the land surface.

CONCLUSIONS AND RECOMMENDATIONS

The thermal signature analysis has demonstrated its importance in showing the relative spatial differences in temperature under data scarce conditions and has served as source of ancillary information in the process of actual evapotranspiration estimation and water balance study of the rift lakes. However, the instantaneous temperature value obtained from TM may not be good enough to show the long-term variability. The high cost of TM images limited its application for the study of temporal variations of temperature in this case. But, the NOAA-AVHRR allowed an estimate of a range of values of the monthly lake surface temperature. The relative differences of NOAA-derived lake surface temperatures agree with the results obtained from TM band 6.

In this study more confidence can be placed on lake surface temperature than the surrounding landscape, since the physical factors involved in lakes are easier to estimate using satellite spectral data than those for heterogeneous land surfaces.

Conventional open-water evaporation estimation methods usually assume that the surface temperature of lakes remains uniform and that evaporation proceeds more or less at the same rate over the total lake surface. However, this study clearly demonstrated that temperature varies widely depending on surface temperature and reflectance, and on the incoming fluxes from groundwater and

surface waters. The remote sensing approach helps to refine the results obtained from conventional open water simulations.

The result has revealed that with high resolution cloud free multi-temporal images and limited ground data; areal temperature can be estimated using thermal infra-red spectral data. This has important implications in future water resources studies in East African rift lakes associated with geothermal fields. The discovery of hot springs below the lake using the TM image has important implications in lake water balance studies.

Both the field measurements and the remotely sensed data in this study show that the most alkaline lake of Abiayta and Shala are hotter. Abiyata has a higher surface temperature than Shala, though they have comparable alkalinity, albido and located close to each other. This may be related to its shallow depth and the thermal properties of lake water and bottom sediments and the influence of the surrounding soda grounds. Ziway has the lowest temperature due to its relatively larger volume and the large contribution of cold fresh water from the two major feeder rivers of the basin.

Temperature from the land surface shows also large variations. This is due to the difference in altitude and land cover types. Generally forested areas have lower temperature than bare grounds. The highest temperature has been observed in rift soda grounds and local thermal manifestation areas.

With bathymetric maps of the lakes, better spatial temperature variations can be assessed in relation to depth. Temperature readings with depth is very important to discover more hot springs in deeper parts of the lakes which cannot be discriminated easily from thermal signature analysis using thermal infra-red images.

In areas where large groundwater enters into the lakes, the surface temperature is quite low. With seepage meter observations in the lake beds, better relation can be constructed between groundwater flux and surface temperature signatures. This method can be used to determine groundwater inflow sites from satellite observations in other large rift valley lakes.

ACKNOWLEDGEMENTS

The author is very grateful to Ato Tuffa Dinku and the staff of the Remote Sensing Laboratory of the National Meteorological Services Agency for providing the NOAA image to derive monthly lake temperature. The author would like to extend his appreciation to the Department of Geology and Geophysics, Addis Ababa University for providing logistic support for field checks.

REFERENCES

1. Bastiaanssen, W.G.M. (1995). Regionalisation of surface flux densities and moisture indicators in composite terrain. A remote sensing approach under clear skies in Mediterranean climates. Agricultural University of Wageningen. PhD Thesis, The Netherlands, 273 pp.
2. Bobba, A.G., Bukata, R.P. and Jerome, J.H. (1992). Digitally processed satellite data as a tool in detecting potential groundwater flow systems. *Journal of Hydrology* **131**:25–62.
3. Batelaan, O., de Smedt, F. and Otero Valle, M.N. (1993). Development and application of a groundwater model integrated in the GIS GRASS. **In:** *HydroGIS 93, International Association of Hydrological Sciences Publ.* no. 211, pp. 581–589.
4. Di Paola, G.M. (1972). The Ethiopian Rift Valley (between 7°00⅔ and 8°40⅔ Lat. North). *Bull. Volcanol.* **36**:517–560.
5. Giday Woldegebriel, Aronson, J.L. and Walter, R.C. (1990). Geology, geochronology, and rift basin development in central sector of the Main Ethiopian Rift. *Geol. Soc. Amer. Bull.* **102**:439–458.
6. Griend, A., Van de, A. and Owe, M. (1993). On the relationship between thermal emissivity and normalized difference vegetation index for natural surfaces. *J. Rem. Sens.*, **14**:1119–1131.
7. HALCROW (1989). Rift valley lakes integrated natural resources development master plan. Ethiopian Valleys Development Studies Authority, Unpub. Report, Addis Ababa, Ethiopia.
8. Kerr, Y.H., Lagourade, J.P. and Imbernon, J. (1992). Accurate land surface temperature retrieval from AVHRR data with use of an improved split–window algorithm. *Remote Sensing of the Environment* **41**:197–209.
9. Lagourade, J.P. (1991). Use of NOAA-AVHRR data combined with agrometeorological model for evapotranspiration monitoring. *J. Rem. Sens.* **12**:1853–1854.

10. Markham, B.L. and Barker, J.L. (1986). Landsat MSS and TM post-calibration dynamic ranges, exoatmospheric reflectance at satellite temperatures. EOSAT Landsat Technical Note 1. (new look-up tables), August 1986.

11. Meijerink, A.M.J. (1996). Remote sensing applications to hydrology: Groundwater. *J. Hydrol. Sci.* **41**(4):549–561.

12. Menenti, M. (1984). Physical aspects and determination of evaporation in deserts, applying remote sensing techniques. PhD Thesis, Wageningen Agr. Univ., ICW Publ. Wageningen. The Netherlands, 184 pp.

13. Parodi, G.N. (1993). An up to date inventory of remote sensing potentiality in the energy balance equation approach for actual evapotranspiration mapping. Basic theory and prospects. MSc thesis. ITC, Enschede, The Netherlands, 94 pp.

14. Pelgrum, J. and Bastiaanssen, W.G.M. (1996). An intercomparison of techniques to determine the area averaged latent heat flux from individual *in situ* observations: A remote sensing approach using the European field experiment in desertification-threatened area data. *Water Resources Research* **32**(9):2775–2786.

15. Roerink, G.J. (1995). SEBAL estimations of the areal patterns of sensible and latent heat fluxes over the HAPEX Sahel grid, Interne Mededling 364, DLO-Staring Centre, Wageningen, The Netherlands.

16. Rothery, D.A., Francis, P.W. and Wood, C.A. (1988). Volcano monitoring using short wavelength infrared data from satellite. *J. Geophys. Res.* **93**:7993–8008.

17. Tenalem Ayenew (1998). The hydrogeological system of the lake district basin, Central Main Ethiopian Rift. PhD Thesis, Free University of Amsterdam, The Netherlands, 259 pp.

18. Tenalem Ayenew and Gieske A.S.M. (2001). Determination of hot spring discharge in Lake Ziway (Ethiopia) by remote sensing. *ITC Journal*, (in press).

19. Tenalem Ayenew (2001). Numerical groundwater flow modelling of the Central Main Ethiopian Rift lakes basin, SINET: *Ethiop. J. Sci.* (in press).

20. Tesfaye Chernet (1982). Hydrogeology of the Lake Region, Ethiopia. Ethiopian Institute of Geological Surveys, Addis Ababa, Memoir N° 7.2

21. Timmermans, W. (1995). Remote sensing evapotranspiration. MSc thesis, Delft University of Technology. Delft, The Netherlands, 153 pp.

SINET: Ethiop. J. Sci., 24(1):69–91, 2001
 ISSN: 0379–2897

EPITHERMAL GOLD OCCURRENCES IN THE LAKES DISTRICT OF THE MAIN ETHIOPIAN RIFT AND TENDAHO AREA OF THE AFAR RIFT: DISCOVERY OF A METALLOGENIC PROVINCE

Solomon Tadesse

Department of Geology and Geophysics, Faculty of Science, Addis Ababa University, PO Box 1176, Addis Ababa, Ethiopia, E-mail: dgg@telecom.net.et

ABSTRACT: Plio-Quaternary volcanic products cover a large part of the Main Ethiopian Rift (MER). Epithermal gold occurrences related to Quaternary volcanics are at present being closely studied for their precious metal potential. Low sulphidation (Adularia-sericite-type) occurrences have been found. Analyses of 579 core and cutting samples collected for the purpose of exploratory geothermal studies from a number of localities (Gedemsa, Aluto and Corbetti calderas MER, and the Tendaho graben; Afar) were analyzed for gold. The results showed concentration of gold ranging from 100 ppb to 440 ppb. Values ranging between 200 and 300 ppb are very common. The overall characteristics of the known ore occurrences and the evolution of the Quaternary central volcanoes within the MER, and related epithermal processes seem to delineate an individual, homogeneous metallogenic province. A new field of investigation on epithermal ore occurrences which are unusual for the present Ethiopian metallogenic scenery is probably emerging. A study of these phenomena, in light of recent acquisitions in metallogenic knowledge, could be of interest not only for further scientific studies but also for new possibilities in mining activity. This study presents the occurrences of epithermal gold mineralization in the MER, the only one of its kind so far reported in the East African Rift System.

Key words/phrases: Caldera, epithermal gold, metallogeny, Plio-Quaternary, rift volcanics

INTRODUCTION

Epithermal precious metal mineralization is commonly associated with Cenozoic geothermal systems in areas of calc-alkaline volcanism. Much of this volcanism typically occurs above subduction zones along continental margins and in island arcs as well as along spreading mid-ocean ridges (*e.g.*, Burke *et al.*, 1981;

Harris *et al.*, 1986). Less commonly, economic mineralization may be associated with continental rift zones, such as the extensive rift system that cuts through south-western Asia and continues along the eastern side of Africa. This system already includes sectors that represent evolving oceanic basins (the Gulf of Aden and the Red Sea), but mostly it is comprised of subaerial intracratonic rifts, including the Ethiopian Rift Valley. Subaerial volcanism in the Ethiopian Rift Valley has caused hydrothermal activity, which is still active in several sites being investigated for geothermal energy. Extinct geothermal fields are also quite common. The possibility that these geothermal systems, related to the continental rifting, have been and may be ore-forming systems cannot be discarded a priori.

The Ethiopian Rift Valley in general held little more than an academic interest in scientific circles for a long period of time. Detailed geological studies and regional mapping of the rift valley have been conducted during the last 29 years (Di Paola, 1972). These have helped delineate specific industrial resources (*e.g.*, diatomite, bentonite, soda ash and geothermal steam), mainly through the work of the Ethiopian Institute of Geological Surveys. Studies aimed at identifying epithermal-type precious metal (mainly gold) resources within the Ethiopian Rift are relatively recent. The present work reports preliminary observations at selected sites within the Ethiopian Rift Valley and Afar where gold anomalies that are clearly associated with rift volcanism have now been found.

REGIONAL GEOLOGY OF THE ETHIOPIAN RIFT AND AFAR

The Ethiopian Rift is the northern most extension of the great East African Rift that extends from north-eastern Ethiopia to Mozambique in southern Africa, with a length of more than 4000 km. More than one-quarter of the rift system lies in Ethiopia (Fig. 1). The Ethiopian Rift is a large 1 km deep graben with an average width of about 70–80 km and a length of 700 km stretching from the Ethio-Kenyan border in the south to the Afar Depression in the north. The rift dissects the highlands of the country into the eastern and western plateaus and is bounded on two sides by a series of large normal (step) faults (Fig. 1). The eastern escarpment of the MER is characterised by step faults with significant throws in its northeastern sector exceeding 1500 m between the top of the plateau and the rift floor. The western margin is gradational and less marked thus accounting for the asymmetry of the MER. Continuous tectonic movements are confirmed by numerous young faults affecting Holocene rock units and by the intense seismicity of the whole region (Di Paola, 1972; Giday Woldegabriel *et al.*, 1990).

a)

b)

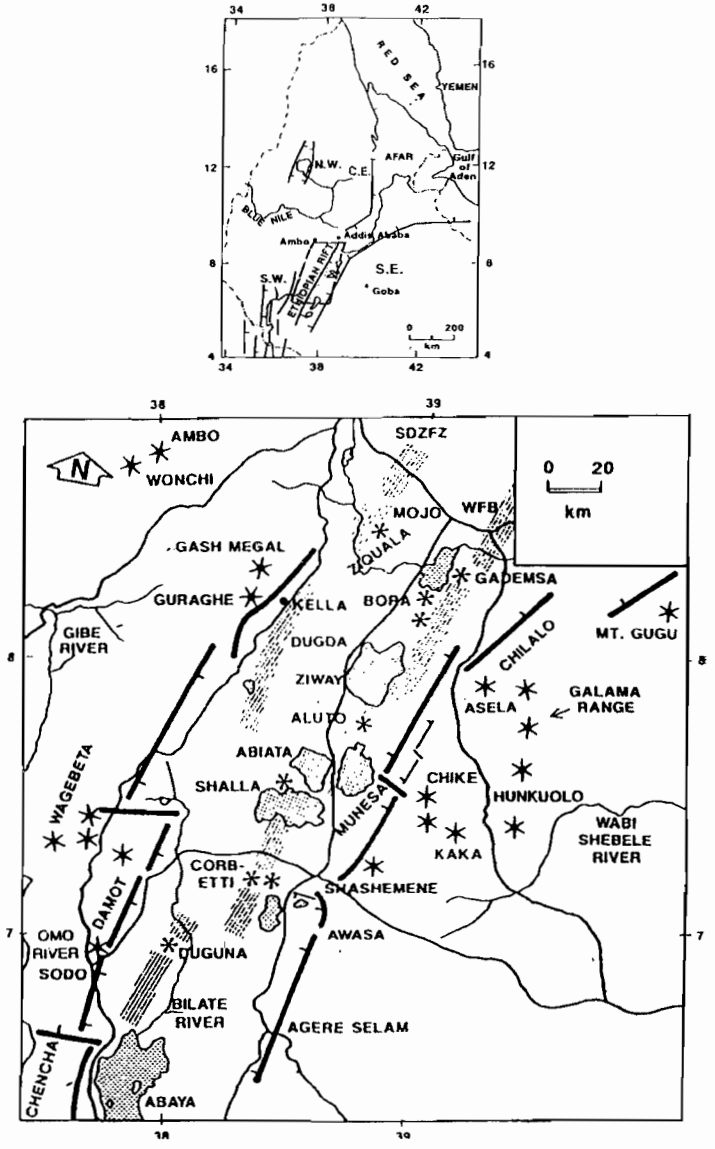

Fig. 1. a) Location of the Ethiopian and Afar rifts. b) The central sector of the MER and adjacent areas (modified after Giday Woldegabriel *et al.*, 1990). (Thick line segments represent rift margin faults with ticks on the downthrown side. Pointed stars represent rift-shoulder central volcanoes, and asterisks are Quaternary peralkaline rhyolite centres of the rift axis. The dual marginal Quaternary rift axes on the rift floor of the northern part of the central sector of the MER are expressed by tightly defined lines. Lakes are dotted, fine lines are rivers, and medium lines are major roads.)

The Ethiopian plateaus bordering the rift consist of a thick succession of flood basalts and subordinate amounts of rhyolites emplaced during Oligocene (Giday Woldegabriel *et al.*, 1990). The floor of the rift is commonly covered by Plio-Quaternary volcanic products and basin-fill volcanoclasic sediments. Basaltic volcanic rocks become progressively younger northwards to Afar, although young basaltic volcanism of minor volume is also common along the axial zone of the Ethiopian Rift. The main petrological feature of the MER is the abundance of silicic peralkaline volcanics (mainly pantallerites) related both to the fissural activity and to the several volcanoes rising from the rift floor. It has been suggested that east-west structures may be an important factor in controlling the locations of volcanism along the rift. Thick sediment accumulations of lacustrine origin cover large areas of the rift floor.

GEOLOGICAL SETTING AND EPITHERMAL MINERALIZATION OF THE PROSPECTING AREAS

A reconnaissance study of epithermal mineralization within the central sector of the Main Ethiopian Rift Valley has been conducted since 1997. Several central volcanoes are present along the axial portion of the rift and two of these, Corbetti and Gedemsa, were studied in detail because of the relatively abundant available bore hole data and better accessibility of the areas.

The Aluto volcanic complex is a Quaternary volcanic centre located along the Wonji Fault Belt (WFB) in the central sector of the MER. The Tendaho graben is found further north in the Afar depression. The evolution of associated calderas at Gedemsa, Aluto, and Corbetti is attributed to central-type eruptions, with subsequent volcano-tectonic collapses.

Epithermal mineral occurrences have been observed in these four localities (Corbetti, Gedemsa, Aluto and Tendaho). Associated features are found on the surface and at depth in drill core. These include alteration patterns that display characteristic low sulphidation type epithermal occurrences. The low sulphidation alteration commonly displays a broad propylitized (chlorite, epidote, quartz) area that envelopes a core of pervasive potassic alteration, together extending to as much as several kilometres. Locally, intermediate argillic alteration assemblages commonly overprint the potassic alteration. The alteration zone also displays broad propylitic zones, overprinted by advanced

argillic alteration (kaolinite). Mineral phases include chlorite, kaolin, calcite, quartz and epidote, adularia, iron oxides, smectite and albite.

The Corbetti caldera

Corbetti is a Holocene volcanic complex found in the central sector of the MER. The most abundant volcanic rocks are peralkaline pyroclastics (ignimbrite and pumice) which are attributed to central-type eruptions with subsequent volcano-tectonic collapse (Di Paola, 1972). The geometric outline of the resulting caldera is elliptical with its long axis measuring about 12 km. The wall of the caldera has a variable height between about 50 m and 200 m.

Post-caldera activity is represented by the emplacement of two very recent volcanic centres (Urji and Chabbi) (Fig. 2) situated on active faults that parallel the major structural zone of the rift system. The Urji and Chabbi centres have extended unwelded pumice flows and falls with minor obsidian flows. Both centres are at fumarolic stage. Several NNE trending minor normal faults cut all the volcanic rocks except the youngest products of the Urji and Chabbi centres. Eight shallow tempograd bore holes have been sunk at different locations in and outside the caldera ranging in depth from 50–200 m (Fig. 2). The bore holes were irregularly located but have enabled constructing shallow subsurface volcanic stratigraphy (Fig. 3).

The Corbetti caldera appears to be one of the most economically promising among the newly discovered occurrences. Altered rock forms a roughly north-south elongated area some two kilometres long and several hundred meters wide. Steam activity is apparent only along the extremities of this zone, but it is possible that thick soil cover may have masked the rest of the area. A low sulphidation (Adularia-sericite type) alteration processes are indicated by propylitic and advanced argillic assemblages in ignimbrite, pumice and rhyolite. The alteration is characterised by the presence of chlorite, kaolin, calcite and quartz. The metallic minerals found in the shallow drill-chip samples include Fe- and Ti-oxides, sulphide minerals including pyrite and chalcopyrite and possibly Pb-bearing sulphosalts. The propylitic alteration, which is largely overprinted by later intermediate argillic alteration, surrounds an elongated and discontinuous core of potassic alteration. Advanced argillic alteration is limited to areas in proximity to the vents. Crusts of salts and silica occur around the vents. Some of these salts are greenish in colour and appear to be ferrous iron and copper. Weakly developed surface alteration zones locally occur, with Fe and Ti-oxide.

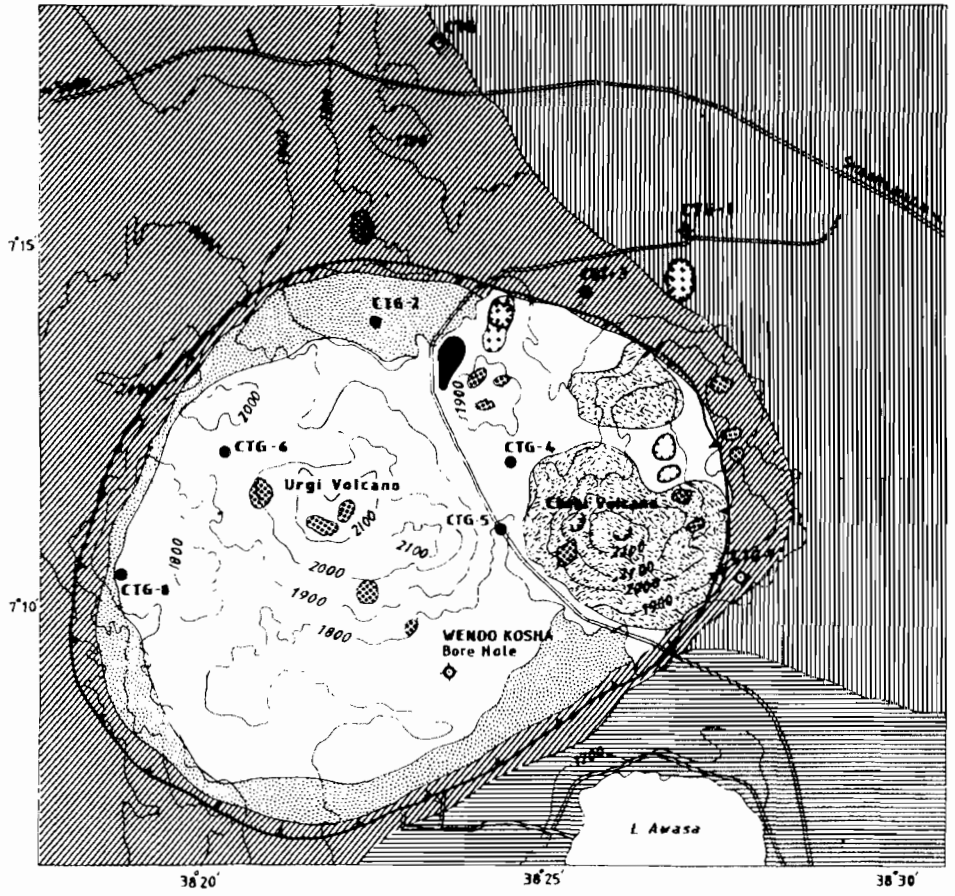

Lithology:
, Lacustrine deposits;
, Old layer pumice;
, Pumice and detritus;
, Basaltic flows and scoria cones;
, Obsidian lava flows;
, Ignimbrites;
, Recent pumice flows and falls;
, Alterations.

Topography:
, CTG drill holes analyzed;
, Contour;
, Other drill holes;
, All weather road;
, Crater;
, Lake;
, Corbetti caldera outer rim;
, Steaming ground.

Fig. 2. Geological sketch map of the Corbetti area (modified after Di Paola, 1972).

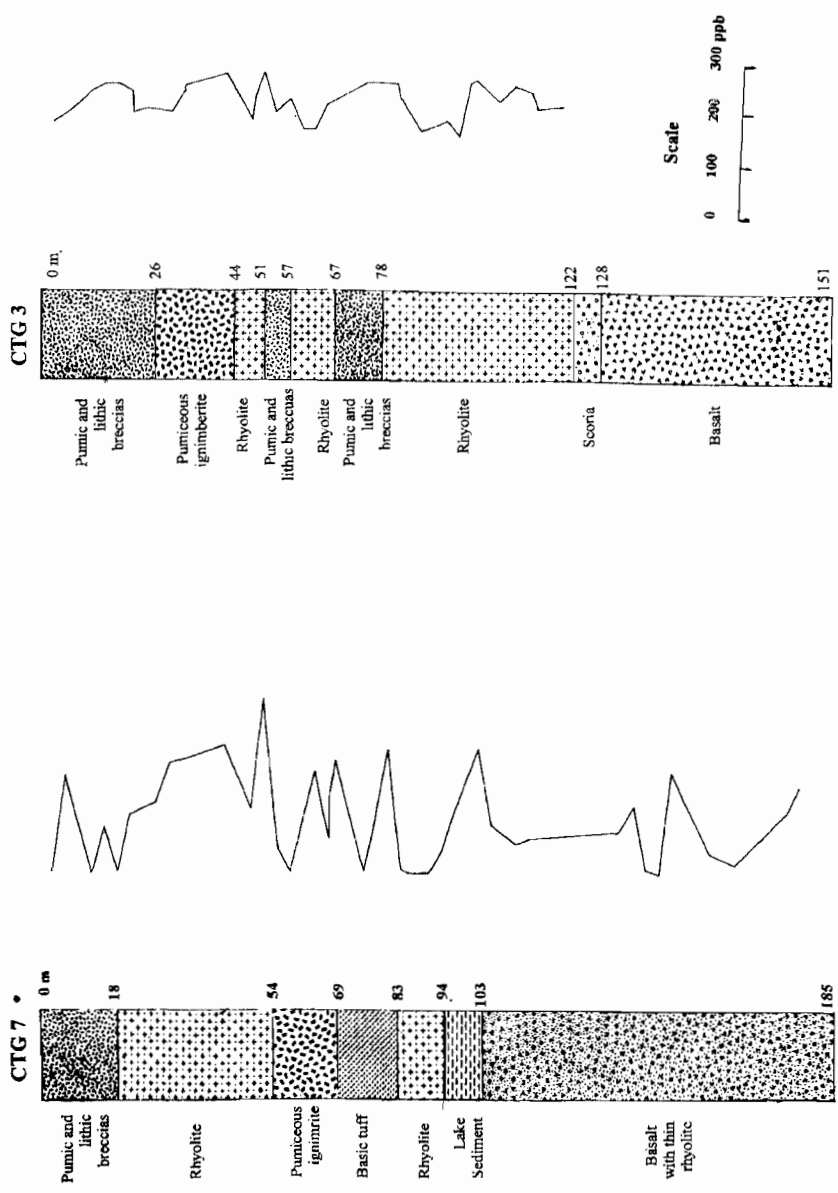

Fig. 3. Lithological columns of drill hole CTG-3 and CTG-7 with graph showing Au grade distribution.

Gedemsa caldera

Gedemsa is a recent (0.8 to 0.1 Ma) volcano in the central sector of the MER (Fig. 4). The lowest exposed products consist of acidic lavas, which in turn are covered by thick plinian unwelded pumice fall deposits. The pumice deposits are overlain by an ignimbrite sheet. Basic surge deposits are found lying on the ignimbrite in the northern part of the volcano. Postcaldera activity has resulted in the emission of acidic lava and interbedded pyroclastic products within the caldera itself. The volcanic products of Gedemsa consist mainly of peralkaline trachytes and rhyolites, mafic rocks being represented only by inclusion occurring within some of the post-caldera products (Peccerillo *et al.*, 1995).

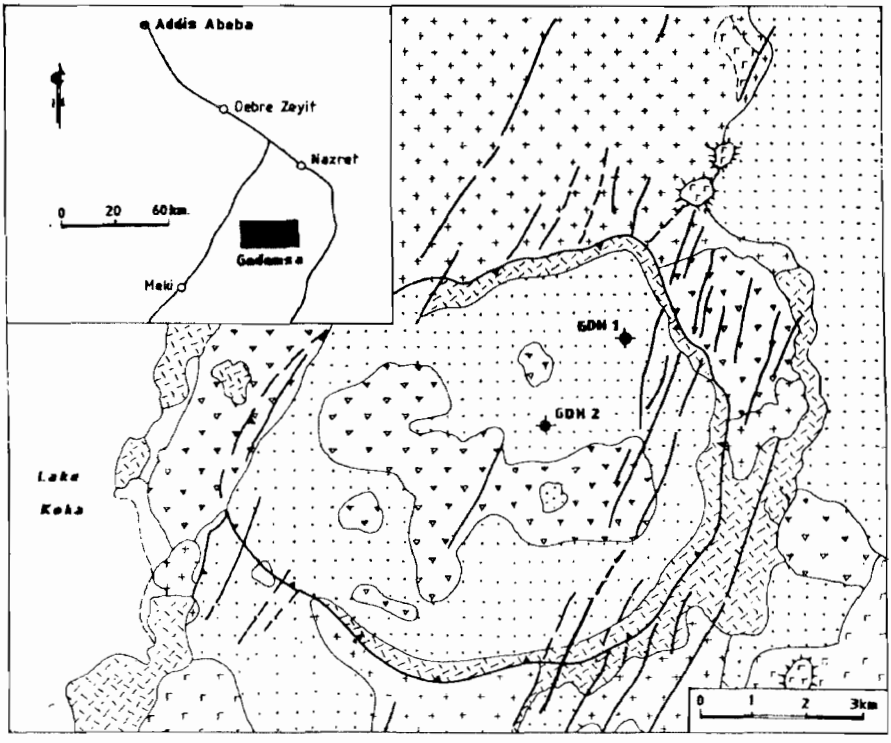

, Alluvium; , Recent basaltic flows; , Post cladéric pyroclastics and lava domes; , Rhyolitic lava flows and domes; , Gedemsa ingnimbrite and pyroclastics; , Caldera rim; —, Fauts; , Scoria cones.

Fig. 4. Geological sketch map and bore hole location of Gedemsa geothermal prospect (modified from Solomon Kebede, 1987).

The caldera itself is clearly a composite structure that resulted from repeated collapses following large plinian pyroclastic eruptions. The geometry of the caldera is almost circular, measuring about 10 kilometres in diameter. The whole caldera structure is strongly affected by many large closely-spaced NNE-SSW trending faults, especially at its eastern part. These faults belong to the Wonji Fault Belt and manifest active tectonics within the rift. Evidence for past hydrothermal activity is observed in the north-west caldera wall and on a small dome inside the caldera. Occurrences of several active thermal manifestations are also known along NNE fault lines immediately outside the caldera proper. The fossil manifestations have oxidised pumiceous deposits with some deposition of silica. Two shallow temperature gradient wells have been drilled within the Gedemsa caldera (Fig. 5) reaching depths of 190 and 200 meters, respectively with rock cutting samples taken every 3 meters.

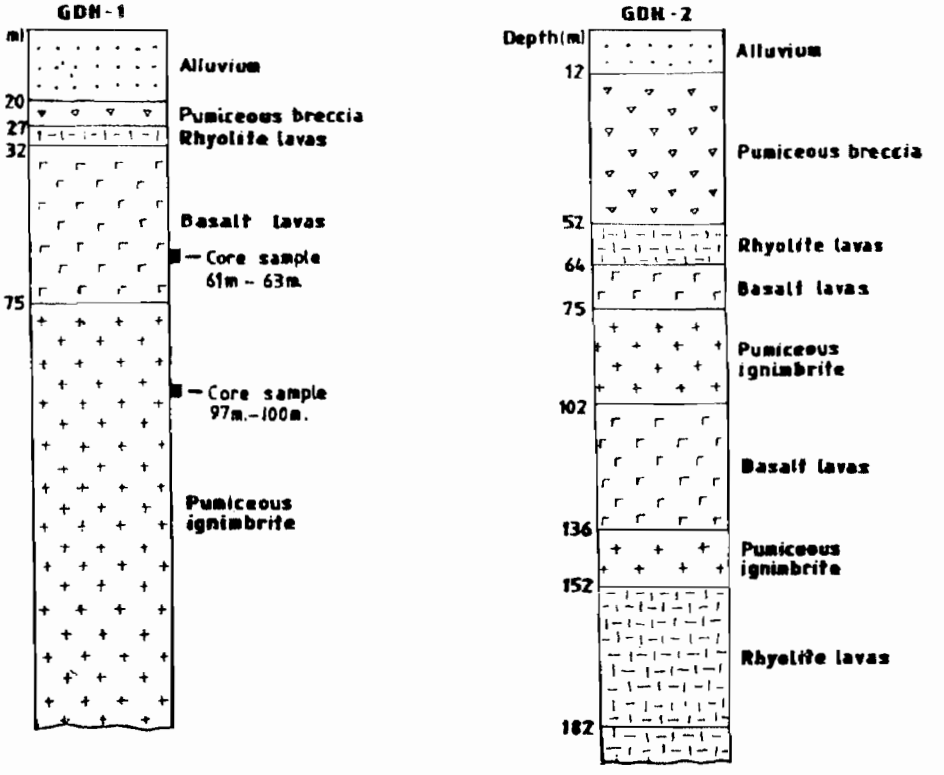

Fig. 5. Geological section in GDH-I and GDH-2 (Gedemsa caldera).

Aluto volcano

The Aluto volcanic complex is a Quaternary volcanic centre located along the Wonji Fault Belt in the central sector of the MER (Fig. 6). The geology of this complex is relatively well-known from surface mapping supplemented by data on the deep stratigraphy and structure from eight deep exploratory wells (Fig. 7) that were sunk to depths ranging from 1300 to 2500 m.

According to Gianneli and Meseret Teklemariam (1993) the oldest outcropping rocks in the area are found at the adjacent eastern rift escarpment and consist mainly of silicic volcanics commonly known as the Tertiary ignimbrite unit. This unit is overlain by a fissural basaltic unit known as Bofa basalt, which in turn is covered by sediments of lacustrine origin that extend over large areas of the rift floor. The volcanic products of Aluto volcanic centre itself consist of a succession of ash-flow tuffs, silicic tuff breccias, silicic domes and unwelded pumice flows. These volcanic products are very young and are associated with surface thermal manifestations that consist of hot springs and fumaroles with temperatures up to 95° C, steaming grounds, silica sinter and travertine deposits. The hydrothermal deposit temperatures measured in the deep exploratory wells range from 88 to 335° C (Gianneli and Meseret Teklemariam, 1993).

The alteration observed in the studied samples from Aluto include an upper facies characterized by intermediate and propylitic assemblages. Intermediate argillic facies are typically represented by smectite group clay minerals; alteration intensity is variable, from incipient groundmass argillification to almost pervasive metasomatism. The latter is best developed in rock units originally very rich in glass. Propylitic alteration includes the characteristic minerals, calcite, chlorite, adularia, quartz and epidote. The metallic minerals found in the studied samples mostly include oxides and sulphides. The oxides consist of magnetite, ilmenite, hematite and Ti-oxide. The sulphide minerals are pyrite, chalcopyrite, sulphosalts possibly Pb. Pyrite is the most abundant.

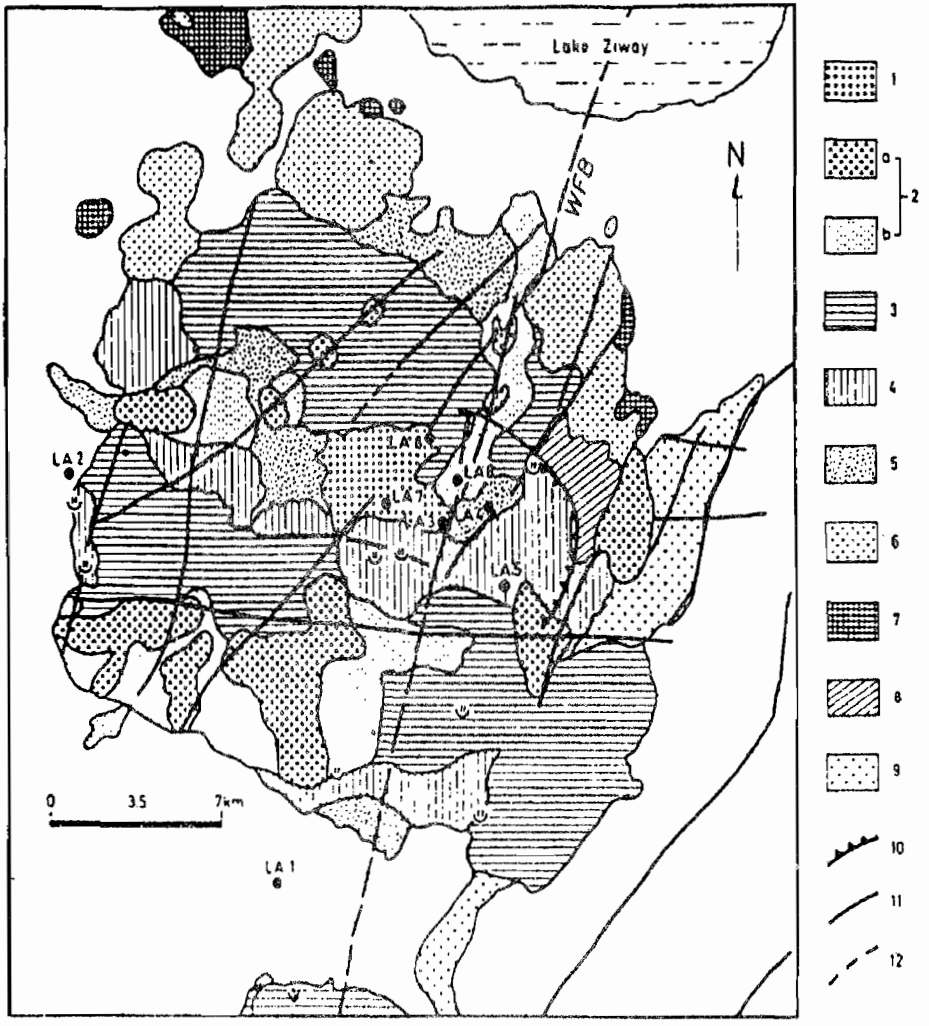

Fig. 6. Geological map, deep well (LA) location and thermal manifestations of the Aluto-volcano. Legend: 1, Alluvial deposits; 2, Peralkaline rhyolite (a) and pumice (b); 3, Peralkaline rhyolite dome; 4, Rhyodacite dome; 5, Awarfu ignimbrite; 6, Rhyolite; 7, Hyaloclastite; 8, Collapsed pre-Aluto volcano; 9, Bofa Basalt; 10, Caldera rim; 11, Faults; 12, Inferred faults; WFB, inferred wonji fault belt (after ELC, 1986).

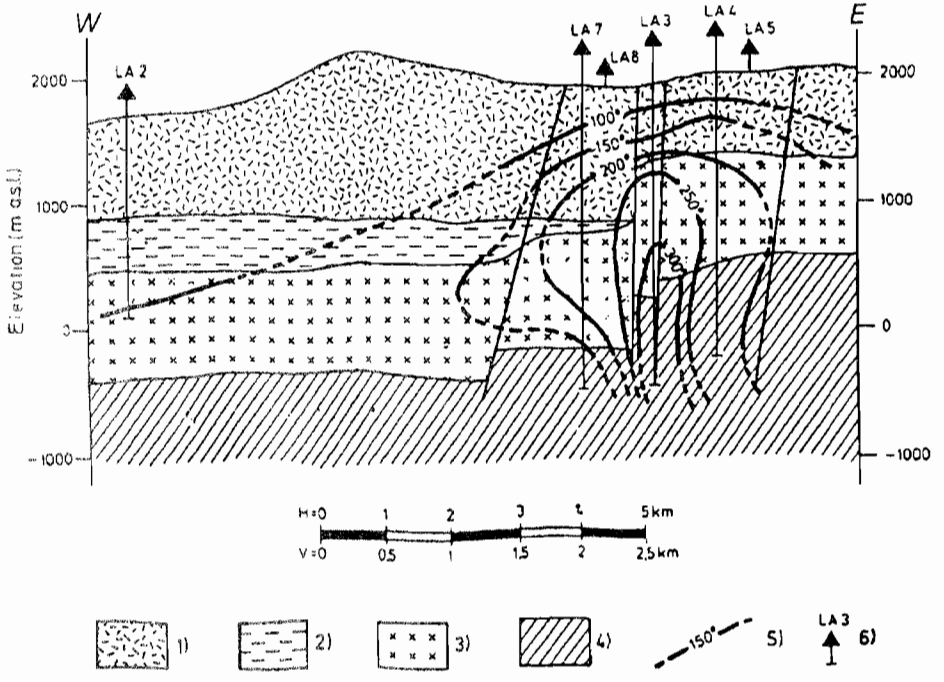

Fig. 7. E-W geological crossection across Aluto volcano (after ELC, 1986). (1, Ignimbrite; 2, Peralkaline rhyolite; 3, Bofa basalt; 4, Collapsed per-aluto volcano; 5, Temprature gradient; 6, Bore hole number.

Gedemsa caldera is the northernmost studied area in the MER where epithermal mineralization occurs. Rhyolite lavas, ignimbrite and pumice deposits represent the host rocks. The alteration belongs to the low sulphidation type. This area appears to be the most promising among the low sulphidation occurrences. The alteration forms a roughly NW elongated area some 5 km long and several hundred metres wide. Propylitic alteration, which is largely affected by later intermediate argillic alteration, surround the zone of potassic alteration. Several thin quartz adularia veinlets cut the zone of potassic alteration. The occurrences are formed of crust form quartz and granular quartz. Carbonates and clay minerals are also present. The ore mineral assemblage includes pyrite, chalcopyrite, enargite, iron oxide minerals, epidote, chlorite and gold. In the western part of the caldera, pyrite occurs in fractured propylitized rhyolite, with narrow zones of potassic alteration and development of intermediate argillic

alteration. In the fractures, thin veins of cavernous quartz with abundant copper sulphide dissemination occur.

The Tendaho graben

This graben is found further north in the Afar Depression. It is a NW-SE trending graben about 50 km wide and is the southern extension of the Afar active spreading zones where the active Erta Ale-Manda Hararo volcanic ranges are situated. The Afar axial ranges are considered to be the exposed equivalents on land of the Red Sea oceanic spreading ridges (Barberi and Varet, 1977).

The Tendaho graben exposes a thick succession of basalt flows of Pliocene age (known as the Afar Stratoid Series) at its borders. The graben is filled with thick lacustrine and alluvial deposits consisting of siltstone and sandstone. Very young basaltic flows and scoria cones (the Afar axial ranges) have been emplaced on top of the graben volcaniclastic sediments. The axial zone is also characterised by the presence of open fissures and numerous active faults which as a whole define the sites of active spreading.

The fissures and faults are evidence of active and fossil hydrothermal deposits which extend for several kilometres along strike. In fact, the most interesting feature of this area is the extensive hydrothermal activity which is controlled by NW-SE trending normal faulting. In, the Tendaho rift, the hydrothermal activity in the area extends for several kilometres following a general NW-SE trend and consists mainly of steaming grounds. Several veins preferably cut the rocks undergoing potassic alteration. These veins, with variable strike between NW-SE, range from veinlets a few meters long and a few centimetres thick to bodies several hundreds of metres long. The quartz forming in these veins may be chalcedony near the walls, but commonly the central part of the veins is crystalline and colourless. The alteration is manifested by the presence of mineral assemblages including chlorite, smectite, vermiculite, epidote, adularia and quartz. The sulphide minerals include pyrite, galena, chalcopyrite, stibnite and covellite (Aquater, 1996).

Petrological notes on the analyzed samples

According to descriptions by several workers Di Paola (1972), Peccerillo *et al.* (1995), Giday Woldegabriel *et al.* (1990), the volcanic rocks of the above described formations range in composition from alkali olivine basalts to peralkali rhyolite and have the following general petrographic features:

Ignimbrites
These rocks show a remarkable uniformity of composition over large areas. They are porphyritic peralkaline rhyolites with abundant glassy matrix usually constituted by a very fine glassy dust. The common phenocrysts are anorthoclase, acmite and fayalite. Lithic fragments are abundant in the ignimbtites.

Peralkaline rhyolite
These rocks are represented by lava flows, lava domes and pumice falls and flows. Petrographically, they appear to be always highly glassy, with variable contents of the following minerals: alkali feldspar, generally anorthoclase, acmite, alkali amphibole (riebeckite) and rare fayalite and quartz.

Basalts
In the studied area, the basalts are usually holocrystalline and they show typical features of transitional basalts with alkaline affinity. The mineralogical assemblage is the following: magnesian olivine, clinopyroxene of augite type, calcic plagioclase, magnetite, ilmenite and rare small apatite crystals.

At Tendaho, the sedimentary sequence in which TD1 core samples were recovered consists of mainly brown to light brown siltstones and grey to greenish-grey, sometimes laminated siltstones with variable calcareous component and fine-grained matrix. Basalts, belonging to the Axial Ranges and those belonging to the Afar Stratoid series show moderately porphyritic intergranular/sub-oplytic texture. The phenocrysts include: olivine, clinopyroxene sometimes titaniferous and basic plagioclase (labradorite).

ANALYTICAL METHOD AND RESULTS

A total of 579 core and cutting samples were analyzed for gold by ICP-MS method at the University of Cagliari, Italy. The applied analytical method is a modification of that proposed by Gowing and Potts (1991). The following modification was found useful for a first rapid screening of samples. Twenty millilitre of freshly prepared aqua regia was added to the powdered sample (10.0 ± 0.1 g) in a 500 ml graduated Erlemmeyer flask. The flask was covered with a watch glass and the mixture stirred on a magnetic stirring table (15 positions) for 30 minutes at room temperature. The mixture was diluted to

volume after addition of 50 ppb of Indium as an internal standard and filtered (20 ml) for ICP-MS gold determination.

The detection limits were calculated at ten times the standard deviation of the blank (11 replicates) divided by the sensitivity and multiplied by the dilution factor (50), which was about 2 ppb.

The precision of the analytical method was evaluated at two different Au concentration levels by leaching two samples, subjected to 11 replicates both (Table 1).

Table 1. Gold concentration levels subjected to replicates.

	Sample 1	Sample 2
Average	240 ppb	11 ppb
Standard Deviation	6.6 ppb	1.6 ppb
Relative standard deviation	2.74%	14,6%

Analytical accuracy was assessed by comparison of the results obtained with the certificate of analysis for two Reference Standard Materials (Table 2).

Table 2. Comparison of results with analysis of reference standard materials.

Reference material	Au certified	Au found	relative error	No of replicates
Gold Ore MA-2	1860 ppb	1890 ppb	1.6%	3
Platinum ore SARM-7	310 ppb	319 ppb	2.9%	3

Analytical results obtained in this work are partly presented in Table 3. Analyses of a total of 579 core and cutting samples collected from 18 deep holes from the studied localities showed gold contents that range from hundreds of ppb to 440 ppb (Table 3). Concentrations ranging from 120 to 300 ppb are very common throughout the geological profiles particularly at Corbetti and Gedemsa calderas and Tendaho graben. Gold content, although irregular or erratic, commonly exceeds 150 ppb both in compact rocks and in pumice

fragments at Corbetti. At Gedemsa caldera, gold content ranges from 100 to 440 ppb. On Aluto volcano, gold value ranges from few ppb to 140 ppb while analysis of a sample from a core at Tendaho (TD1) range in value from 100 to 200 ppb Au.

The mean gold content from the above localities exceeds the maximum gold values reported in Boyle (1979; 1987): 3 ppb for rhyolite; 5 ppb for the upper lithosphere. Nearly all the analyzed samples showed high anomalous values starting from a depth of four metres downwards.

Table 3. Gold concentrations (in drilled cores and cuttings) at CTG (Corbetti caldera), GDH (Gedemsa caldera), LA (Aluto volcano) and TD (Tendaho graben).

No.	Label	Depth(m)	Au (ppm)	Lithology
275	CTG -7	27	166	rhyolite lava
276	CTG -7	30	257	rhyolite lava
277	CTG -7	43	295	rhyolite lava
278	CTG -7	49	155	rhyolite lava
279	CTG -7	52	404	rhyolite lava
280	CTG -7	55	61	pumiceous ignimbrite
281	CTG -7	58	10	pumiceous ignimbrite
282	CTG -7	64	234	pumiceous ignimbrite
283	CTG -7	67	86	pumiceous ignimbrite
284	CTG -7	69	262	pumiceous ignimbrite
285	CTG -7	72	51	basic tuff
286	CTG -7	75	12	basic tuff
287	CTG -7	78	133	basic tuff
288	CTG -7	81	287	basic tuff
289	CTG -7	84	13	rhyolite lava
290	CTG -7	87	90	rhyolite lava
291	CTG -7	90	10	rhyolite lava
292	CTG -7	93	62	rhyolite lava
293	CTG -7	96	142	lake sediment
294	CTG -7	99	108	lake sediment
295	CTG -7	102	287	lake sediment
296	CTG -7	105	118	basalt with thin rhyolite
297	CTG -7	11	74	basalt with thin rhyolite

Table 3. (Contd).

No.	Label	Depth(m)	Au (ppm)	Lithology
298	CTG -7	114	86	basalt with thin rhyolite
299	CTG -7	135	107	basalt with thin rhyolite
300	CTG -7	138	158	basalt with thin rhyolite
301	CTG -7	141	11	basalt with thin rhyolite
302	CTG -7	144	70	basalt with thin rhyolite
303	CTG -7	147	236	basalt with thin rhyolite
304	CTG -7	158	55	basalt with thin rhyolite
305	CTG -7	162	34	basalt with thin rhyolite
306	CTG -7	174	140	basalt with thin rhyolite
307	CTG -7	177	208	basalt with thin rhyolite
308	GDH -1	6	178	Alluvium
309a	GDH -1	9	61	Alluvium
309b	GDH -1	9	ND	Alluvium
310	GDH -1	21	272	pumiceous breccia
311	GDH -1	28	143	rhyolite lava
312	GDH -1	31	99	rhyolite lava
313	GDH -1	34	46	Basalt lavas
314	GDH -1	40	28	Basalt lavas
315	GDH -1	49	210	Basalt lavas
316	GDH -1	55	58	Basalt lavas
317	GDH -1	58	101	Basalt lavas
318	GDH -1	67	56	Basalt lavas
319	GDH -1	73	161	Basalt lavas
320	GDH -1	82	99	pumiceous ignimbrite
321	GDH -1	88	146	pumiceous ignimbrite
322	GDH -1	97	173	pumiceous ignimbrite
323	GDH -1	97-100	172	pumiceous ignimbrite
324	GDH -1	121	99	pumiceous ignimbrite
325	GDH -1	130	45	pumiceous ignimbrite
326	GDH -1	139	232	pumiceous ignimbrite
327	GDH -1	145	130	pumiceous ignimbrite
328	GDH -1	154	110	pumiceous ignimbrite
329	GDH -1	157	106	pumiceous ignimbrite
330a	GDH -1	163	142	pumiceous ignimbrite
330b	GDH -1	163	64	pumiceous ignimbrite
331	GDH -1	172	131	pumiceous ignimbrite

Table 3. (Contd).

No.	Label	Depth(m)	Au (ppm)	Lithology
332	GDH -1	181	57	pumiceous ignimbrite
333	GDH -1	184	98	pumiceous ignimbrite
334	GDH -2	6	56	Alluvium
335	GDH -2	9	266	Alluvium
336	GDH -2	30	312	pumiceous breccia
337	GDH -2	36	165	pumiceous breccia
338	GDH -2	39	215	pumiceous breccia
339	GDH -2	45	195	pumiceous breccia
340	GDH -2	51	177	pumiceous breccia
341	GDH -2	60	77	rhyolite lava
342	GDH -2	63	116	rhyolite lava
343	GDH -2	69	97	Basalt lavas
344	GDH -2	72	155	Basalt lavas
345	GDH -2	75	110	Basalt lavas
346	GDH -2	87	95	pumiceous ignimbrite
347	GDH -2	90	97	pumiceous ignimbrite
348	GDH -2	96	90	pumiceous ignimbrite
349	GDH -2	102	109	pumiceous ignimbrite
350	GDH -2	108	56	Basalt lavas
351	GDH -2	111	95	Basalt lavas
352	GDH -2	114	56	Basalt lavas
353	GDH -2	120	235	Basalt lavas
354	GDH -2	123	214	Basalt lavas
355	GDH -2	129	75	Basalt lavas
356	GDH -2	138	45	pumiceous ignimbrite
357	GDH -2	141	182	pumiceous ignimbrite
358	GDH -2	144	131	pumiceous ignimbrite
359	GDH -2	147	187	pumiceous ignimbrite
360	GDH -2	150	145	pumiceous ignimbrite
361	GDH -2	152	46	pumiceous ignimbrite
362	GDH -2	156	51	rhyolite lava
363	GDH -2	159	12	rhyolite lava
364	GDH -2	162	302	rhyolite lava
365	GDH -2	165	250	rhyolite lava
366	GDH -2	168	141	rhyolite lava
367	GDH -2	171	83	rhyolite lava

Table 3. (Contd).

No.	Label	Depth(m)	Au (ppm)	Lithology
368	GDH -2	177	105	rhyolite lava
369	GDH -2	180	103	rhyolite lava
370	LA-2	1250-1253	135	Bofa basalt
371	LA-6	2200-2203	144	rhyolite lava
372	LA-4	615-617	79	Unconsolidated ash
373	LA-7	550-554	85	Lithic tuff
374	LA-2	1600-1601	107	Bofa basalt
375	TD-1	805-808	118	Basalt lava
376	TD-1	1550-1551	117	Basalt lava
377	TD-1	1588-1597	223	Basalt lava
378	TD-1	1600-1650	108	Basalt lava
379	TD-1	1755-1800	204	Basalt lava
380	TD-1	1855-1900	108	Basalt lava
381	TD-1	1900-1950	200	Basalt lava
382	TD-1	1955-2000	129	Basalt lava
383	TD-1	2009-2017	179	Basalt lava
384	TD-1	2055-2100	156	Basalt lava
385	TD-1	2105-2150	149	Basalt lava

ND, no data.

DISCUSSION

The results reported in this work represent the first phase of studies on epithermal occurrences within the main Ethiopian Rift (MER) and Afar. Much work has to be done in order to arrive at a reasonably well-documented synthesis. However, a working hypothesis can be attempted as a basis for future detailed studies from the obtained observations and results. The different associations among ore mineral paragenetic assemblages and alterations seem to reflect different levels of mineralization. This is shown at Corbetti and Gedemsa which are hosted in similar volcanic systems. At Corbetti the occurrence of base metals is accompanied essentially by propylitic alteration, while at Gedemsa, precious metals and quartz adularia occur, in association with potassic and argillic alterations. Thus the low sulphidation type occurrences are in good agreement with proposed schemes for epithermal mineralization

(*e.g.*, Hollister, 1985; Heald *et al.*, 1986). Furthermore, the fact that the mineralization is intimately related to potassic alteration is similar to that described by Sander and Einaudi (1990) for Round Mountain, Nevada.

Gold most probably originates from Precambrian basement, which is presumed to extend under the rift floor. Hydrothermal fluids rise through a network of fractures found within and outside the caldera, provided that a major fracture system is present that should serve as a plumbing system.

In the Corbetti caldera, one possible source of the fluids may have been the two rhyolite domes near the road just north of the steaming ground structure which apparently represent an intersection between the N-S fault structure (Fig. 2) and a contact between pyroclastic and hard, impervious compact rocks. This fluid channel way is marked by the abundant silica in crustation of the surfaces. Other similar structures capable of driving solutions might exist that potentially localize sites of gold enrichment. Irregular fracture systems within the caldera cause sporadic alteration and variable gold values in the same rock unit. The youngest pumice unit appears fresh (except where fractures offer reactive channels, *e.g.*, steaming ground area), although the gold content is comparable to that of the underlying rocks. This may have resulted from the almost neutral fluid because buffered by alkalis in underlying rocks, but still containing gold, permeated through the interface of rock pumice and spread through the unconsolidated, highly permeable material such as pumice. A further expansion, resulting in an adiabatic drop in pressure and temperature would enhance the precipitation of gold from the circulating solution. Mixing with surface water might also occur, that recharges the ground water body which occurs along the interface between the pumice-hard rock. The high precipitation characterising the area, the high permeability of the surface and the low permeability of the underlying rocks all favour this model. The wide surface area offered by the pumice and its glassy nature, allow adsorption phenomena in the entire pumice unit.

As far as the age of epithermal mineralization in the rift is concerned, no quantitative data are yet available. However, it has been established that in all areas, where gold occurrence has been documented, the host rocks are ignimbrites, rhyolite lavas and pumice deposits, with subordinate basaltic rocks. Thus, the epithermal occurrences are mostly hosted in acidic rocks emitted from central volcanoes during Late Quaternary times, *i.e.*, younger than 0.8 Ma.

The overall characteristics of the known occurrences and the evolution of the central volcanoes within the rift and the associated epithermal phenomena apparently define an individual, homogeneous metallogenic province within the rift. Obviously, it is too early to give any economic evaluation, but the field and analytical data appear encouraging for the development of exploration and a preliminary estimate for gold, at least in the Corbetti, Gedemsa and Tendaho prospects.

For instance, taking an average value of 100 ppb for the gold dispersed in the upper uniformly spread unwelded pumice unit having an average thickness of 40 m over a surface area of 50 km^2, the total reserve (assuming a specific gravity of 0.9 for pumice) can be calculated to over 200 tons in just one of the calderas alone, *i.e.*, a gold reserve level of an important mine.

At current mining exercise, 0.1 g/t average gold content is too low for the wide pumice layer to be considered as economical. It is to be noted, however, that neither the bore holes used for the present evaluation were strategically located to intersect known fluid driving structures nor was it possible to have fully representative composite core samples for assay. If systematic geophysical and exploration drilling directed for gold were done, the subsequent analysis may enable to identify high grade gold concentration target areas even at shallow depth.

As a conclusion, this is the first indication of epithermal gold resources in the Ethiopian rift and this might be an important new target for exploration.
The situation of East African rifts, not yet considered as a possible site for this kind of mineralization, should be carefully assessed. A fascinating field of mineral prospecting can be envisaged in these wide volcanic areas of Ethiopia and other East African countries.

ACKNOWLEDGEMENTS

This research was funded by the Ethio-Italian University Cooperation Programme. Special thanks are to the Ethiopian Institute of Geological Survey which provided the necessary data pertinent to the present study. The author is especially indebted to Professor S. Pretti of the University of Cagliari, Italy, and Dr Gezahegn Yirgu, Department of Geology and Geophysics, AAU, for the many thorough, scholarly

discussions on earlier versions of the manuscript. Special thanks are also to Alessandro Rivoldini of the University of Cagliari, Italy for analysing all the samples.

REFERENCES

1. Aquater (1996). Tendaho Geothermal Project, final report. Aquater, Italian Ministry of Foreign Affairs, Vol. 1, pp. 1–44.
2. Barberi, F. and Varet, J. (1977). Volcanism of Afar: Small-scale plate tectonic implications. *Bull. Geol. Soc. Amer.* **88**:1251–1266.
3. Boyle, R.W. (1979). *The Geochemistry of Gold and its Deposits*. Canada, pp. 280–584.
4. Boyle, R.W. (1987). *Gold: History and Genesis of Deposits*. Ottawa, Ontario, Canada.
5. Burke, K.C., Kidd, W.S.F., Turcotte, D.L., Dewey, J.F., Mouginis-Mark, P.J., Parmentier, E.M., Sengor, A.M.C. and Tapponier, P.E. (1981). Tectonics of basaltic volcanism. **In**: *Basaltic Volcanism on the Terrestrial Planets,* pp. 803–898. Lunar and Planetary Inst. Houston, Texas, Pergamon Press, New York.
6. Di Paola, G.M. (1972). Geology of the Corbetti caldera area (Main Ethiopian Rift). *Bull. Volcanl.* **35**:497–506.
7. ELC (1986). Exploitation of Langano-Aluto geothermal resources. Electroconsult (ELC), Feasibility report. Milano, Italy.
8. Giday Woldegabriel, Aronson, J.L. and Walter, R.C. (1990). Geology, geochemistry and rift basin development in the central sector of the Main Ethiopian Rift. *Bull. Geol. Soc. Amer.* **102**:439–458.
9. Gianneli, G. and Meseret Teklemariam (1993). Water-rock interaction processes in the Aluto-Langano geothermal field (Ethiopia). *Jour. Volcano. Geotherm. Rese.* **56**:429–445.
10. Gowing, C.J.B. and Potts, P.J. (1991). Evaluation of a rapid technique for the determination of precious metals in geological samples based on a selective aqua regia leach. *Analyst* **116**:773–779.
11. Harris, N.B.W., Pearse, J.A. and Tindle, A.G. (1986). Geochemical characteristics of collision zone magmatism. Geol. Soc. Spec. Publ. No. 19. Blackwell, London, pp. 67–81.
12. Heald, P., Hayaba, D.O. and Foley, N.K. (1986). Comparative anatomy of volcanichosted epithermal deposits: Acid-sulphate and Adularia-sericite types. *Econ. Geol.* **82**:1–26.

13. Hollister, V.F. (1985). Models of precious metal epithermal deposits. **In:** Discoveries of Epithermal Precious Metal Deposits, pp. 9–14, (Hollister, V.F., ed.), Society of Mining Engineers, New York.

14. Peccerillo, A., Gezahegn Yirgu and Dereje Ayalew (1995). Genesis of acid volcanics along the Main Ethiopian Rift - A case history of the Gedemsa volcano. *SINET: Ethiop. J. Sci.* **18**:23–50.

15. Sander, M.V. and Einaudi, M.T. (1990). Epithermal deposition of gold during transition from propylitic to potassic alteration, Round Mountain, Nevada. *Econ. Geol.* **85**:285–311.

16. Solomon Kebede (1987). Stratigraphy and results of temperature measurement in shallow drill holes at Corbetti caldera. Preliminary report. Geothermal Exploration Project, Ethiopian Institute of Geological Surveys.

SINET: Ethiop. J. Sci., 24(1):93–104, 2001
 ISSN: 0379–2897

Short communication

THE IMPACT OF UNCONTROLLED WASTE DISPOSAL ON SURFACE WATER QUALITY IN ADDIS ABABA, ETHIOPIA

Tamiru Alemayehu

Department of Geology and Geophysics, Faculty of Science, Addis Ababa University
PO Box 1176, Addis Ababa, Ethiopia, E-mail: dgg@telecom.net.et

ABSTRACT: The main threat to the surface water quality in Addis Ababa is environmental pollution derived from domestic and industrial activities. Due to the inadequacy of controlled waste management strategies and waste treatment plants, people are forced to discharge wastes both on open surface and within water bodies. Uncontrolled (improper) waste disposal has deteriorated the quality of surface water (streams, rivers, reservoirs) by changing the chemical, physical and organoleptic properties of water. Chemical analyses of surface and shallow groundwater samples taken at various points along streams and different springs show that the level of unwanted chemical constituents such as nitrate and chromium, for example, are higher than the background level. Among the main causes are poor economy and lack of proper waste disposal systems that lead the residents to dump wastes illegally within the water bodies. Important measures to alleviate the problem are to develop the environmental awareness of the residents, proper control on industries, establishment of a widespread waste collection system and improved landfill technology.

Key words/phrases: Addis Ababa, Akaki river, toxic substances, uncontrolled waste disposal, water quality

INTRODUCTION

The city of Addis Ababa is one of the fast expanding cities in the country and presently covers an area of about 500 km^2. In many developed countries, proper urbanization takes into consideration equivalent growth in waste removal facilities. In the case of Addis Ababa, the waste collection system (both solid

and liquid) did not progress in proportion to its expansion and consequently the impact of these wastes on the water environment is increasing.

Groundwater from borehole or spring is the source of drinking water in the peripheral parts of the city, where there is a shortage of a municipal water supply network. These supplies also provide the population with water during the failure of the distribution network fed by the reservoirs.

In the city, streams and rivers receive the major part of the waste produced by the residents. In the southern part of the city the same rivers serve for various purposes such as horticulture, drinking water for cattle, washing, and for other domestic activities.

A systematic environmental study has not been carried out in the city so far. The few relevant studies include that of EPA (1997), where the Chemical Oxygen Demand (COD), Biological Oxygen Demand (BOD) and Dissolved Oxygen (DO) at limited sampling points on Big Akaki, Little Akaki and Kebena rivers, are presented and that of Adane Bekele (1999) who carried out regional sampling and presented analytical data on industrial effluents for some streams in the city.

The present work is aimed at evaluating the impact of uncontrolled waste disposal on surface water quality in Addis Ababa in an attempt to raise awareness on environmental protection in Ethiopia in general and in Addis Ababa in particular. In this regard the paper characterizes the surface water on the basis of anthropogenically induced chemical constituents. Its further impact on the shallow groundwater system is also assessed.

BACKGROUND

Geological setting

From geological point of view, the Addis Ababa region is constituted of volcanic rocks and minor amounts of fluvial sediments. Distinct volcanic centres of Plio-Pleistocene age include Mt. Wochacha (3385 m a.s.l), Mt. Yerer (3100 m a.s.l), and Mt. Furi (2839 m a.s.l). The northern part of the region is made up of Cenozoic flood basalts, felsic flows and intrusions overlain by shield volcanics. The main lithologies are basaltic, rhyolitic and trachytic, trachy-

basaltic lava flows and welded tuffs found at different localities and ages. They are comprised between 27 Ma and 3.2 Ma (K/Ar) (Haile Selassie Girmay and Getaneh Assefa, 1989), and are highly fractured and weathered. The main tectonic structures include small-scale joints, fractures and major normal faults such as the Filwoha Fault that was formed between 5-6.4 Ma (Haile Selassie Girmay, 1985). These features are parallel to the faults in the Ethiopian Rift and represent the western rift boundary in the region.

Surface water system

Akaki river and four water reservoirs, namely Legedadi, Gefersa, Dire and Aba-Samuel, represent the main surface water bodies within and in the vicinity of Addis Ababa. Basically the Akaki river has two main branches: the Big Akaki and the Little Akaki. The Big Akaki river has many tributaries among which Ginfile, Kebena, Kechene, Kurtume and Yeka are all found within the eastern part of the city boundaries. The Little Akaki river basin covers the western part of the city (Fig. 1). During the rainy season the city appears cleaner from wastes as it is located on sloppy ground that increases the velocity and hence the mobility force exerted by the surface runoff, which takes away the wastes. Even though rivers and streams represent self-renewing resources, continuous input of wastes may change them into natural sewerage lines.

Surface water is the main receiver and transmitter of pollutant into the groundwater body. Hence, protection of surface water from pollution is directly related to the protection of groundwater system. It is clear that groundwater and surface water commonly form a linked system through the geologic medium. In this case, pollutants may be transferred easily through fractures, where soil cover is absent, in the upper and central part of the city. Porous geologic materials like alluvial deposits and weathered rock profiles have considerable self-purifying capacity and take out unwanted constituents including bacteria.

Waste disposal system

The most widespread waste disposal mechanisms in the city may be categorized as uncontrolled (improper) waste dumping. Forms of improper waste disposals commonly practised in the city include defective septic tanks, open dumps, surface impoundments and land application.

According to NOR consultants (1982), the solid waste distribution in the city consists of: domestic waste (76%), street sweepings (6%), commercial wastes

(9%), industrial wastes (5%), wastes from hotels (3%), and wastes from hospitals (1%). The data on housing show that a total of 380307 housing units are found in the city out of which 74.1% have a toilet facility. About 63.2% of these are dry toilets.

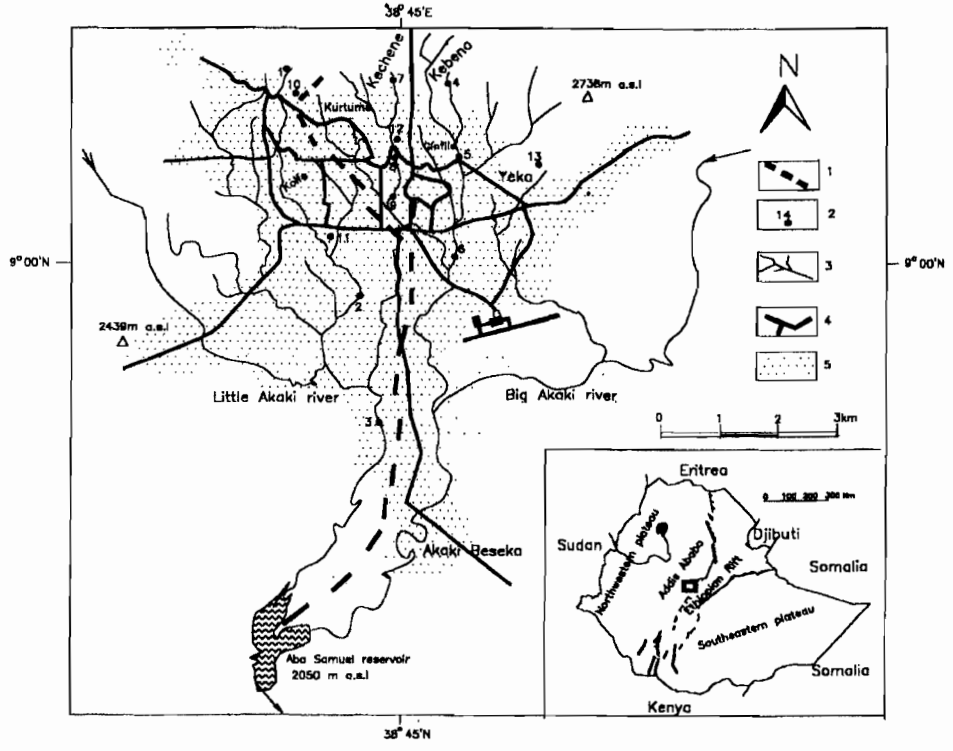

Fig. 1. Location map of streams and sampling points. 1, Surface water divide between Big and Little Akaki rivers; 2, Sampling points and sample numbers; 3, Stream network; 4, Major roads; 5, Urban area.

A report of the Central Statistics Authority (1999), showed that 65.3% of the total industry in the country is found in Addis Ababa. Industrial centres play a role in polluting surface and ground water unless managed and designed with appropriate waste water purifying plants.

From visual observation in the city it is possible to say that the distribution and the services of municipal garbage tanks are not adequate. Hence, the residents have no choice but to discharge domestic refuses where there is open space, along roadsides, bridges and culverts, and directly into streams. The accumulation of solid wastes out of the permitted sites attracts rodents, insects and scavengers that pose health risk to residents.

Some of the reasons for illegal dumping are inadequacy of garbage tanks, delay of pickup services for trash and the lack of environmental awareness.

Land use in the city

The main land use pattern in the city embraces residential areas, market quarters, industrial zones, agricultural areas, forest, and quarries. The rapid urbanization requires wide areas for various purposes and hence the size of the city is increasing at high rate. Presently industrial areas are located in the southern sector along the river channels and in the outskirts of the city. The central part of the city includes residential quarters, governmental offices, churches, schools and colleges, airports, parks, sport grounds, and various sized markets. About 0.3 km^2 of land south west of the city serves as waste dumping site.

SAMPLING AND ANALYSIS

After thorough evaluation of surface water systems and hazard centres, water sampling points were identified (Fig. 1) to assess the extent of water pollution. Two to three water samples were collected in June 1999 at one time (before noon) at different points along the length of each stream found in the city. Appropriate plastic bottles and gloves were used for sample collection. This technique was designed to investigate the enrichment and/or depletion of chemical constituents in the surface waters. For comparative purposes some of the major springs found in the city have also been considered. The current work is intended to investigate spatial variation of the chemical constituents.

The samples have been analyzed for major element and selected trace elements at the Department of Geology and Geophysics, Addis Ababa University. The instruments used for analysis are Perkin-Elmer UV/VIS spectrophotometer and atomic absorption spectrophotometer. On site measurement of pH was carried

out by digital microcomputer pH meter. The data were analyzed with an accuracy range of 0.56 % to 10.39%. The reported percentage values represent calculated error band for different cations and anions.

Bacteriological analysis of few water samples has been carried out in the Central Laboratory of Ethiopian Food and Nutrition Study.

RESULTS AND DISCUSSION

The analytical results corresponding to all samples collected from streams and selected springs are presented in Table 1. The data show relatively high concentrations of Cl, NO_3, COD, Cr, and Mn presumed to have been released from both domestic and industrial activities.

Little Akaki river receives large part of the waste released from the west-central part of the city including the big market centre "*Merkato*" and from a number of factories including a winery, a brewery, a soft drink factory, a liquor factory, several tanneries, a slaughterhouse, and others. This is clearly shown by the concentration of chemical constituents like Cl, Mn and Cr that increase downstream. The high abundance of such chemical constituents that do not concentrate naturally is strong evidence of water pollution by industrial wastes.

The Biological Oxygen Demand (BOD) and Chemical Oxygen Demand (COD) values in the upstream samples are low (8–11 mg/l). This indicates unpolluted environment with high dissolved oxygen in the water. The Big Akaki river has a BOD value of 13 mg/l (Table 2) at the inlet to the Aba Samuel reservoir, while the sample taken from the reservoir outlet shows low value of BOD (0.8 mg/l). This suggests that Aba Samuel reservoir acts as an oxidation chamber in which the water regenerates its dissolved oxygen content. During the site visit, fish and insects were observed in the reservoir, which could indicate the regeneration of dissolved oxygen in the water. From the variation of BOD, it is possible to note that Little Akaki river is more polluted than the Big Akaki river and has high nutrient enrichment and consequently low dissolved oxygen.

Table 1. Analytical results for the stream and spring samples. Zero values represent below detection limit (Analysis in June 1999).

Chemical parameters	Kolfe stream			Kebena stream			Kechene stream			Springs			
	Minch Saloon	Near Kera	Near Behere Tsige	Up stream	Near German Embassy	Near Urael Church	Up stream	Near Ras Mekonen Bridge	Near Zewditu Hospital	Addisu Gebeya	Lideta	Ras Mekonen Bridge	Yeka North
Sample No.	1	2	3	4	5	6	7	8	9	10	11	12	13
PH	6.1	7.68	7.51	6.08	7.22	7.48	6.5	7.63	7.6	6.32	6.49	6.31	5.86
Na mg/l	31	76	90	15	74	28	12	45	44	33	31	38	8.2
K mg/l	3	28	24	6	21	17	7	24	23	8	4	3	6
Ca mg/l	25	53	50	15	67	36	7	43	44	22	48	100	6
Mg mg/l	12	26	23	5	35	15	3.6	24	23	11	28	60	21
HCO_3 mg/l	57.96	219.7	176.7	6.1	219.7	122.04	18.31	152.6	158.7	30.5	146.4	61.02	42.71
Cl mg/l	49.5	109.9	102.5	8.6	106	34.2	3	70	40.6	34	194	56.5	2.2
SO_4 mg/l	Nd	8.3	0.44	23	19.7	9.26	10.2	22.11	24.11	6.5	23.1	19	0
PO_4 mg/l	0.13	3.65	3.03	Nd	Nd	2.09	0.29	3.54	3.78	0.89	0.21	0.12	0.11
NO_3 mg/l	86.19	23.51	9.66	531	188.14	8.96	99.6	17.3	9.53	184.6	728.21	481.41	55.34
SiO_2 mg/l	55.5	32.9	16.23	27	34.1	33.6	25.2	47.2	47.08	30	87.5	69.9	49.2
COD mg/l	8	80	24	14.4	27.2	20	16.5	46.12	40	17.6	11.2	6.4	20.8
Cr μg/l	0	5.5	14.1	0	0	0	5.76	0	0	0	1.88	1.18	0
Mn μg/l	34.1	123-0.2	1756.7	12.3	6531.6	1219.01	63.115	1141.6	1550.8	128.6	0.303	21.47	22.6
Ni μg/l	44.5	9.2	4.8	0	0	0	0	0	0	0	0	0	0
Zn μg/l	0	0	0	0	0	0	54.21	0	81.53	0	0	0	0
As μg/l	0	0	2.3	1.24	0	0.59	1.005	0.126	0.096	0	0.9979	0	0
Pb μg/l	0	0	0	0	0	0	7.873	0	0	0	0	0	0

Table 2. Biological oxygen demand, chemical oxygen demand and dissolved oxygen concentration in surface water bodies in Addis Ababa (taken from EPA, 1997).

	Sample location	BOD mg/l	COD mg/l	DO mg/l
Little Akaki Basin	Tributary of Little Akaki near Asko Shoe factory	8	48	6.9
	Little Akaki near ALERT bridge	8	23	5.8
	Little Akaki After MedhaneAlem high school bridge	301	621	0
	Little Akaki near Mekanissa bridge	19	56	4.4
	Little Akaki near Mekanissa liquor factory bridge	254	375	1.3
	Little Akaki inlet to Aba Samuel lake	321	708	0
	Outlet from Aba Samuel lake	0.8	15.6	7.4
Big Akaki Basin	Kebena at French Embassy bridge	11	43	6.8
	Kebena at Bole bridge	29	105	7
	Big Akaki inlet to Aba Samuel lake	13	28	5.2
	Outlet from Aba Samuel lake	0.8	15.6	7.4

The samples analyzed from springs contain extremely high NO_3 concentration as much as 728 mg/l. It is assumed that these are the result of leaking septic systems. A guideline maximum value of 50 mg/l of nitrate as NO_3 is recommended by WHO (1984) for drinking purpose. However, springs strongly contaminated by nitrate are used by residents for drinking. According to WHO (1984), high nitrate level causes methaemoglobinaemia in infants and in older age groups and may be associated with certain forms of cancer. All streams in the southern part of the city and the Aba Samuel reservoir show strong eutrophication process that has reduced the nitrate concentration in the water.

Manganese was found to be more concentrated in the surface water bodies than in the groundwater reservoirs. This may be partly attributed to retention of Mn by thick alluvial sediments. Manganese concentration higher than 0.1 mg/l is considered unsafe for industrial and domestic use (WHO, 1984). However, in some streams the concentration reaches as much as 6.54 mg/l (Sample No.5).

Spring samples (12 and 13) have high levels of Cr and are probably fed by Cr-rich streams that have been contaminated by surface waste. This is presumably because Cr sinks into the shallow groundwater system through fractures and feeds the Cr rich springs.

Chloride increases downstream faster than any other analyzed constituent from 49 mg/l (Sample No.1) to 109 mg/l (Sample No.2) in Kolfe stream; from 8 mg/l (Sample No. 4) to 106 mg/l (Sample No. 5) in Kebena stream; from 3 mg/l (Sample No. 7) to 70 mg/l (Sample No. 8) in Kechene stream. It is anticipated that the main sources for Cl anomalies could be domestic sewages, leather works, and slaughterhouses all of which release substantial amount of Cl into the surrounding water bodies.

Correlation coefficients (r) are determined for the selected pairs of anions (Fig. 2). A correlation value above 0.35 for Cl vs. NO_3 indicates that groundwater probably has been affected by domestic waste (Pacheo and Cabrera, 1997 and references therein). Water samples from springs have Cl vs. NO_3 correlation coefficient of 0.9026 indicating nitrate pollution derived from defective septic systems and not from agricultural runoff as the samples are collected from urban areas. For plots a, b, c, in Fig. 2 the parameters considered have a correlation indicating probably a similar source. As shown in Figure 2d, chloride increases downstream as NO_3–N decreases resulting in a negative correlation.

The bacteriological analyses revealed that at the inlet of the Aba Samuel reservoir Big Akaki river has 1010 Total Coliform per millilitre of water, while Little Akaki river contains Too Many Bacteria to count (TMC) which is above the counting range. The result indicates that Little Akaki river is more polluted than Big Akaki river. The Lideta spring, which is used as holy water (serves also for drinking purpose) contains 290 Total Coliform per millilitre of water. This is well above the standard limit (10 Total Coliform/ml) set by WHO. The same spring also contains elemental level of *E. coli*, a bacteria that causes disease.

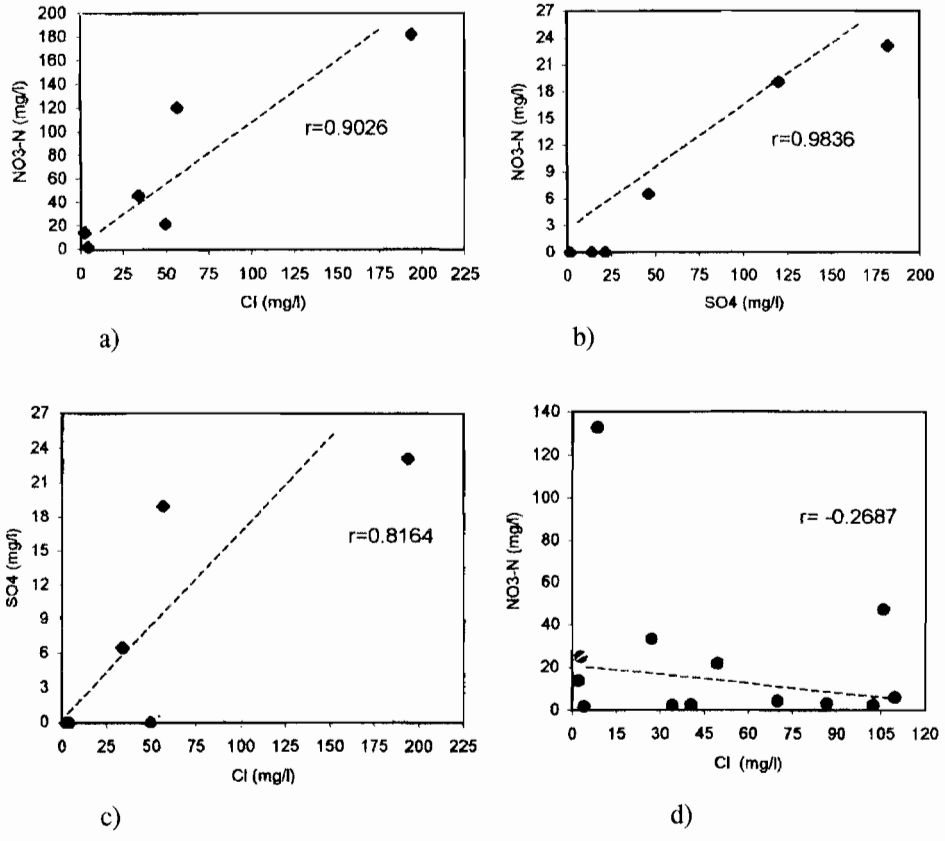

Fig. 2. Chemical constituents with correlation coefficient for spring samples (a, b, c) and stream samples (d).

CONCLUSIONS

The present environmental study in the city of Addis Ababa has demonstrated that improper and continued disposal of domestic and industrial wastes represent a serious threat to surface and groundwater systems. The results of analysis of samples from different location points indicated that there are high levels of

chromium, manganese and nitrate in shallow groundwater infiltrated from contaminated surface water.

Comparison of concentration of toxic chemicals, nutrient enrichment and bacterial population revealed that Little Akaki river is more polluted than the Big Akaki river. The shallow groundwater fed by the Little Akaki river also contains high pollutant load.

The main problem that may arise from uncontrolled dumping of wastes is the infiltration by rainwater of hazardous chemical constituents and bacteria of health significance. It is therefore suggested that appropriate water treatment is necessary before water from shallow boreholes are made available for drinking.

As practised elsewhere in big cities around the world, a reduction in water pollution in Addis Ababa can be attained through the construction of low cost sewerage lines, proper control on industrial effluent, well developed and regulated garbage collection systems, establishment of proper landfill facilities and developing the environmental awareness of the population, in addition to empowering the local authorities to take an active participation in waste disposal regulations. The systematic application of these controlling mechanisms could cut down the surface and ground water pollution in the city.

REFERENCES

1. Adane Bekele (1999). Surface water and groundwater pollution problems in the upper Awash River basins. Master Thesis. University of Turku, Finland.
2. Central Statistics Authority (1999). The 1994 Population and Housing Census of Ethiopia, Results for Addis Ababa, April 1999, Addis Ababa.
3. Environmental Protection Authority, EPA (1997). Preliminary survey of pollutant load on Great Akaki, Little Akaki and Kebena rivers, March 1997. Unpublished Report.
4. Haile Selassie Girmay (1985). Shallow resistivity investigations in the Filwoha Fault. M.Sc. Thesis, Addis Ababa University.

5. Haile Selassie Girmay and Getaneh Assefa (1989). The Addis Ababa-Nazaret Volcanics: A Miocene-Pleistocene volcanic succession in the Ethiopian Rift. *SINET: Ethiop. J. Sci.* **12**(1):1–24.

6. NOR consultants (1982). Addis Ababa solid waste management study. Unpublished Report.

7. Pacheo J.A and Cabrera A.S. (1997) Groundwater contamination by nitrates in the Yucatan peninsula. *Hydrogeology Journal* **5**(2):47–53.

8. World Health Organization, WHO (1984). Guidelines for drinking water quality. Volume 2, health criteria and other supporting information, Geneva.

SINET: Ethiop. J. Sci., 24(1):105–112, 2001
 ISSN: 0379–2897

Short communication

TEST OF ENDOTHELIAL MONOLAYER INTEGRITY IN THE PRESENCE OR ABSENCE OF ENDOTOXIN AND ANTI-TNF-α MONOCLONAL ANTIBODIES

Andualem Mossie [1], Stefan Eriksson [2], Hassen Taha Sherief [3,*] and Legesse Zerihun [3]

[1] Department of Physiology, Jimma Health Science Institute
PO Box 378, Jimma, Ethiopia

[2] Department of Physiology and Pharmacology, Karolinska Institute
Post address 171 77, Stockholm, Sweden

[3] Department of Physiology, Faculty of Medicine
PO Box 9086, Addis Ababa, Ethiopia

ABSTRACT: Monolayer cultures of human umbilical vein endothelial cells were established and tested for the effects of endotoxin treatment and anti-TNF-α monoclonal antibodies following endotoxin treatment on albumin permeability and electrical conductance. Application of 40 $\mu g(ml)^{-1}$ of endotoxin on human umbilical cord endothelial cell culture monolayer increased transendothelial albumin permeability significantly ($P<0.001$) and decreased transendothelial electrical resistances significantly ($P<0.001$). When 10 $\mu g(ml)^{-1}$ of anti-TNF-α monoclonal antibodies was added after endotoxin, the effects of the latter on albumin permeability and electrical resistance were significantly decreased ($P<0.001$). This suggested that the monolayer sheet can be disturbed by endotoxin-induced TNF-α from endothelial cells. TNF-α can disintegrate the endothelial cell monolayer during septicemia. This can be abrogated using anti-TNF-α monoclonal antibodies.

Key words/phrases: Anti-TNF-α monoclonal antibodies, electrical resistance, endothelial monolayer, endotoxin, permeability

* To whom all correspondence should be addressed.

INTRODUCTION

Endothelial cells are found to be physiologically and metabolically dynamic, capable of performing a number of important functions in the body such as mediation of the regulation of blood pressure, and control of blood coagulation. In order to study them in detail, it is possible to isolate the cells from blood vessels using digestive enzymes such as collagen and tripsin, and grow them in culture flasks using appropriate media containing antibiotics. Endothelial cells grown on culture as a continuous sheet-like monolayer can be used as model for capillaries.

Endothelium is a single layer of epithelial cells that lines the inner wall of blood vessels. In the past, endothelial cells were perceived as passive, metabolically inert and permeable barriers. However, they are now known to be metabolically and physiologically dynamic having multiple functions (Curzen *et al.*, 1994).

In order to maintain the potency of blood vessels and the fluidity of the circulating blood, endothelial cells synthesize and release a number of anticoagulants including thrombomoduline, heparin sulphate and prostacyclin (Danner *et al.*, 1991). Endothelial cells can produce precoagulants such as thrombin, factor-II, factor-III, factor-V, platelet activating factor, and van Willebrand factor (Figer *et al.*, 1966). Endothelial cells produce substances that can regulate vascular tone such as endothelium derived relaxing factor, endotheline, and angiotensin converting enzyme (Cruzen *et al.*, 1994).

Endothelium plays an integral role on the acute inflammatory response by producing certain inflammatory mediators such as histamine, serotonin, bradykinin, and prostaglandins (Parrillo, 1993). Endothelium can also express cell surface adhesive substances called selectins (glycoproteins) which can selectively adhere with integrin of neutrophils during transendothelial migration (Hirokawa *et al.*, 1994).

Abnormalities of endothelial cell structure and function contribute to the development of such diseases as thrombo-embolism, atherosclerosis, and vasculities (Castillo and Sanchez, 1993; Bone, 1994).

In order to investigate all these functions of endothelial cells and pathological conditions associated with them, researchers have developed techniques of isolation, purification and culturing of endothelial cells. Endothelial cells can be isolated from pulmonary arteries, aorta, coronary arteries, renal vessels and umbilical vein during delivery (Figer *et al.*, 1966; Booyse *et al.*, 1975). Once isolated, endothelial cells can be cultured on a culture media platted on a membrane support to form a confluent monolayer that represents an *in vitro* capillary model (Booyse *et al.*, 1975; Chuang *et al.*, 1990). This enables one to measure an *in vitro* transendothelial migration of neurotrophils, and permeability for macromolecules such as plasma proteins. All measurements of transendothelial electrical resistance are means of testing endothelium monolayer integrity (Baetscher and Brune, 1983; Chuang *et al.*, 1990).

Endotoxin, a lipo-polysaccharide (LPS) in its chemical nature, is a cell wall component of Gram-negative bacteria. It can stimulate macrophages, neutrophils and endothelial cells to produce such cytokins as TNF-α and II-1. These cytokines are chemo-attractants for neutrophils during inflammation and they are also known to be central mediators of septic shock (Tracey and Fong, 1987). Endothelial cells, in response to endotoxin, TNF-α and II-1, are well known to produce large amount of endothelium derived relaxing factors (EDRF). EDRF is now known to be nitric oxide (Hirokawa *et al.*, 1994). Nitric Oxide is a potent vasodilator biological molecule and it is suspected to be the ultimate mediator of septic shock (Moncada *et al*, 1991; Castillo and Sanchez, 1993; Bone, 1994). During septic shock, the capillary endothelial permeability is pronounced resulting in hypotension secondary to fluid extravasation (Baetscher and Brune, 1983). Researchers suggested that all those cascades of events for the genesis of sepsis can be abrogated if anti-TNF-α monoclonal antibodies are applied on *in vitro* model (Tracey and Fong, 1987; Lowery, 1993).

The objective of the present work is to test the hypotheses that:

1. endotoxin increases albumin passage through the endothelial monolayer;
2. endotoxin decreases transendothelial electrical resistance; and
3. anti TNF-α monoclonal antibodies decrease or revers the above two effects of endotoxin.

MATERIALS AND METHODS

Human umbilical vein endothelial cells were isolated with the help of trypsin enzymatic digestion of the intima. The endothelial cells were grown in a culture flask following the standard procedures adapted from Maryama (1963). The culture media was consisting of a 1:1 mixture of M-199 & RPM 1640 (containing L-glutamine, GIBCO) supplemented with 20% heat inactivated fetal calf serum (GIBCO). After the initial culturing of the endothelial cells in a monolayer, the culture was detached using trypsin (0.25%) in order to transfer them to another culture plate (Fig. 1a) in serial passages. The trypsinized endothelial cells in suspension were seeded over polycarbonate filter membrane support and kept in the incubator. After six days, the formation of endothelial monolayer was examined under high power objective microscope to check if it was ready for experimentation.

Test of endothelial monolayer permeability for albumin

To evaluate the functional integrity of human umbilical vein endothelial cell monolayer, 30 μl of ^{125}I labelled human serum albumin in 10% fetal calf serum was added to 100 μl medium in the upper compartment (Fig. 1a). Thirty minutes later, a 30 μl sample was taken from the lower chamber beneath the filter for ^{125}I labelled albumin determination using LKB-1240 Gamma counter. The ratio of the total count added to the upper chamber to the total count in the lower chamber is indicative of the percent albumin diffusion. This was calculated using the following formula:

$$\%Diffusion = \frac{Total\ count\ in\ the\ lower\ chamber}{Total\ count\ added\ on\ the\ upper\ chamber} \times 100$$

Measurements were made four times at the interval of 30 minutes. Transendothelial albumin permeability was challenged by adding 40 $\mu g(ml)^{-1}$ endotoxin alone and endotoxin with 10 $\mu l(ml)^{-1}$ anti-TNF-α monoclonal antibodies after endotoxin.

Transendothelial electrical resistance measurement

Transendothelial monolayer electrical resistance was measured with a volt metre using two miniature AgCl electrodes. One electrode was placed in the upper chamber (Fig. 1b). Readings in ohms were taken directly from the ohmmeter.

The known resistance of the filter membrane support was subtracted from the total resistance in order to determine the resistance of the endothelial cell monolayer. Resistance measurements were done before and after the addition of endotoxin alone as well as after the addition of endotoxin plus anti-TNF-α monoclonal antibodies.

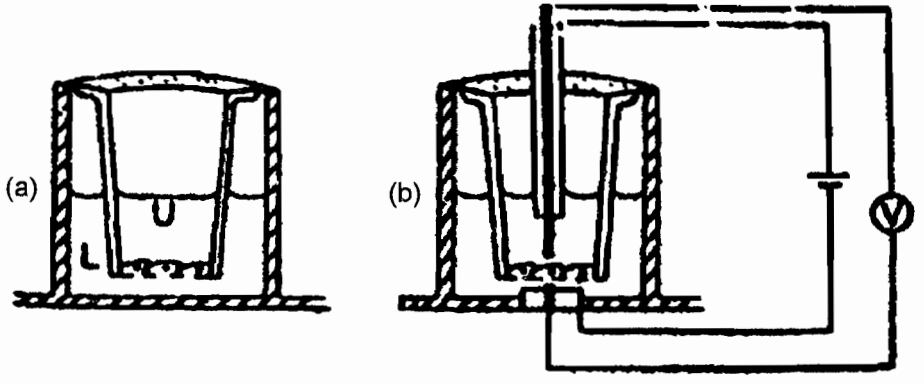

Fig. 1. Schematic view of the assay system for measuring the permeability (a) and trans-endothelial electrical resistance (b) of monolayers of human umbilical vein endothelial cell culture (L, lower chamber; U, upper chamber).

RESULTS AND DISCUSSION

Results of transendothelial permeability for albumin and transendothelial electrical resistance were recorded from ten repeated measurements and presented in graph forms as shown in Figs 2 and 3, respectively.

Following controlled measurement, it was found that endotoxin (LPS) increased significantly ($P < 0.001$) albumin passage through the monolayer. Endotoxin stimulates endothelial cells and macrophages to present TNF-α, which in turn disrupts monolayer integrity, increasing its leakiness, leading to hypotension. The above finding is supported by Furie *et al.* (1987) suggesting that during bacterial infection of the human body, both trans-capillary neutrophil migration and leakiness to plasma proteins will be increased secondary to this fluid extravasation, as a consequence of which circulatory shock will develop.

As shown in Fig. 2, the effect of endotoxin (LPS) was antagonized by anti-TNF-α monoclonal antibodies. A ten μl(ml)$^{-1}$ anti-TNF-monoclonal antibodies decreased albumin flux significantly ($P < 0.001$).

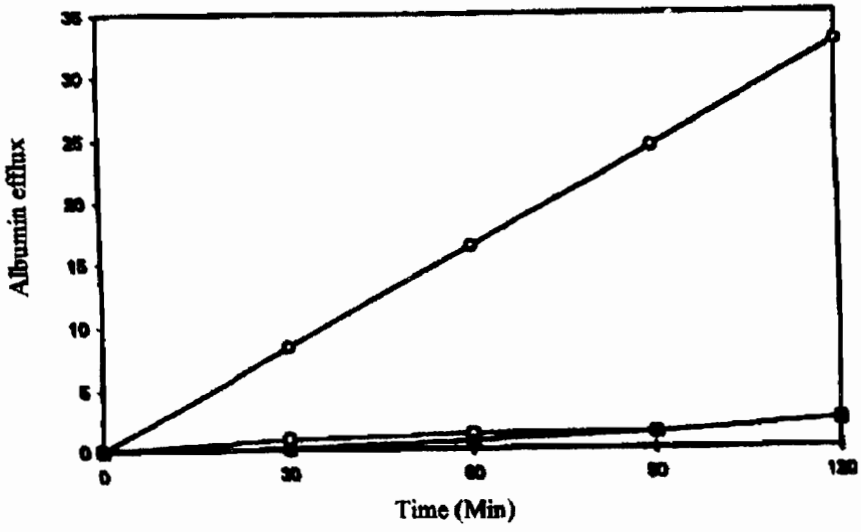

Fig 2. Albumin permeability of endothelial cell culture. The time source change in albumin permeability of monolayer culture of endothelial cells following the application of endotoxin (LPS, 40 μl) alone (—○—), endotoxin plus anti-TNF-α monoclonal antibodies (—□—) and control values recorded in the absence of test chemicals (—△—).

Transendothelial electrical resistance measured before and after the endothelial cell monolayer was treated with LPS [40 μl(ml)$^{-1}$] decreased apparently because LPS disintegrated the confluent endothelial monolayer of the culture (Fig. 3). This effect is significantly reversed by treatment with anti-TNF-α monoclonal antibodies.

In conclusion, endotoxin increases albumin permeability of cultured endothelial cell monolayer. This is because LPS and cytokines such as TNF-α and interleukin alter endothelial cell permeability. Anti-TNF-α monoclonal antibodies reverse the endotoxin-mediated increase in endothelial permeability and decrease in electrical resistance, suggesting that endothelial cell monolayer functional integrity alteration is mediated via TNF-α.

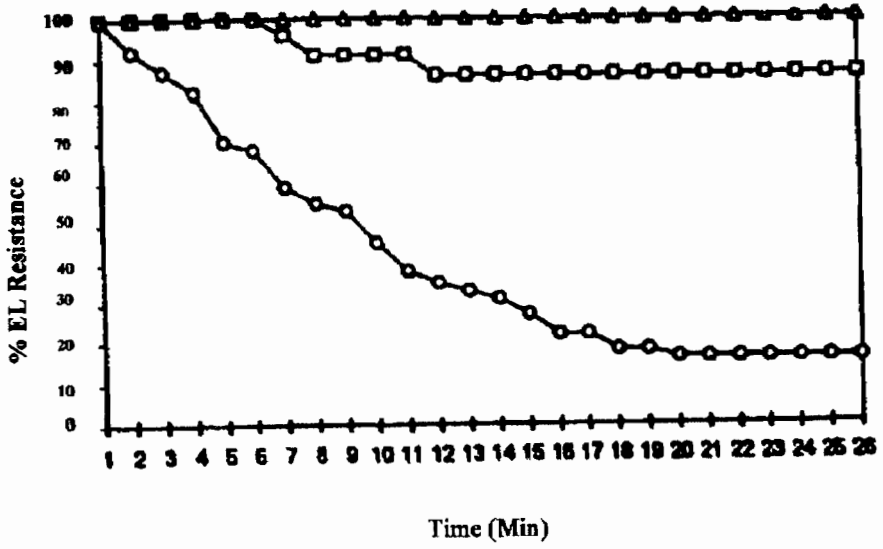

Fig. 3. Electrical resistance of endothelial cell culture. The time course change in electrical resistance of monolayer culture of endothelial cells following application of endotoxin (LPS, 40 μl) alone (—○—), endotoxin plus anti-TNF-α monoclonal antibodies (—□—) and control values recorded with isotonic saline (—▵—).

ACKNOWLEDGEMENTS

This experiment was done in Sweden, Karolinska Institute, Department of Physiology. We thank all people working in the cell culture lab who helped us carry out this experiment.

REFERENCES

1. Baetscher, M. and Brune, K. (1983). An *in vitro* system for measuring endothelial permeability under hydrostatic pressure. *Exp. Cell Res.* **148**:541–547.
2. Bone, R.C. (1994). Sepsis and its complication: the clinical problems. *Crit. Core Med.* **22**:58–512.
3. Booyse, F.M., Sedlak, B.J. and Refelson, M.E. (1975). Culture of arterial endothelial cells: characterization and growth of bovine aortic cells. *Thrombos. Diathe. Haemorrh.* **34**:825–839.

4. Castillo, L. and Sanchez, H. (1993). Septic shock pathogenesis and treatment (abstract). *Indian J. Pediatr.* **60(suppl-3)**:367–369.

5. Chuang, P.T., Cheng, H.J., Lin, S.J., Jan, K.M., Lee, M.M. and Chien, S. (1990). Macromolecular transport across arterial and venous endothelium in rats. *Aterioscler.* **10**:188–197.

6. Curzen, N.P., Grifiths, M.J.D. and Evans, T.W. (1994). The role of endothelium in modulating the vascular response to sepsis. *Clil. Science.* **56**(6):359–374.

7. Danner, F.L., Elin, R.J. and Hosseini, J.M. (1991). Endotoxaemia in human septic shock. *Chest.* **99**:169–175.

8. Figer, D.G., Bimoum, C. and Luttrall, C.N. (1966). Human endothelium in cell culture. *J. Atheros. Res.* **6**:151–163.

9. Furie, M., Naprstek, B.L. and Silverstein, S.C. (1987). Migration of neutrophils across monolayers of cultured microvascular endothelial cells: An *in vitro* model of leukocyte extravasation. *J. Cell Scien.* **88**:161–175.

10. Hirokawa, K.O., Shaughnessy, K., Moor, K, Ramrakha, P. and Wilkins, M.R. (1994). Indication of nitric oxide synthase in cultured vascular muscle cells: the role of cAMP. *Br. J. Pharm.* **112**(2):396–402.

11. Lowery, S.F. (1993). Anticytokine therapies in sepsis. *New horizons* **1**:120–126.

12. Maryama, Y. (1963). The Human endothelial cells in tissue culture. *Zeitsch. für Zellforschung.* **60**:69–79.

13. Moncada, S., Palmere, R.M.J. and Higgs, E.A. (1991). Nitric Oxide: Physiology, Pathology and Pharmacology. *Pharmacol. Rev.* **43**(2):109–136.

14. Parrillo, J.E. (1993). Pathogenic mechanism of septic shock. *N. Eng. J. Med.* **328**:1471–1477.

15. Tracey, K.J. and Fong, Y. (1987). Anti-Cachectin/TNF monoclonal antibodies prevent septic shock during lethal bacteraemia. *Nature* **330**:662–666.

SINET: Ethiop. J. Sci., 24(1):113–125, 2001
 ISSN: 0379–2897

Short communication

THE SYNERGISTIC EFFECTS OF *METARHIZIUM ANISOPLIAE* (METSCHIKOFF) WITH THE ACYL UREA INSECTICIDES TEFLUBENZURON AND DIFLUBENZURON FOR *SCHISTOCERCA GREGARIA* (ORTHOPTERA: ACRIDIDAE)

Emiru Seyoum

Department of Biology, Faculty of Science, Addis Ababa University
PO Box 1176, Addis Ababa, Ethiopia, E-mail: Biology.aau@telecom.net.et

ABSTRACT: The acyl urea insecticide teflubenzuron (=Nomolt ®) caused loss of appetite, ecdysial failure and eventual death in 4th instar *Schistocerca gregaria*. The entomopathogenic fungus *Metarhizium anisopliae* also caused mortality due to mycosis among nymphs of the locust. Enhanced mortality occurred following dual application of the growth regulator and the fungus, which at one combination was synergistic. In another experiment, the fungus was exposed to cuticle treated with acetone (the carrier for the insecticide). This reduced the effectiveness of the fungus. An ultrastructural study showed the effect of the joint application of another acyl urea diflubenzuron (= Dimlin®) and *Metarhizium anisopliae* on locust cuticle. Disruption of the lamellae pattern was observed in some areas of cuticle. This is consistent with localised disruption of chitin synthesized during treatment with Dimlin. This compound, that has a short half-life in the locust, was applied to the food at 5 day interval over a 15 day period. Clearing zones in the cuticle around penetrant hyphae suggested action of cuticle degrading fungal enzymes. These zones were more extensive around gyphae in Dimlin-affected cuticle suggesting possible enhanced hydrolysis of cuticle protein by fungal proteases in the absence of chitin.

Key words/phrases: Diflubenzuron, *Metarhizium anisopliae*, *Schistocerca gregaria*, teflubenzuron

INTRODUCTION

Insects, like other organisms, are more vulnerable to infectious diseases when under stress of malnutrition, crowding, and unfavourable environmental conditions. In particular, insecticides have been observed to act as stressors resulting in increased incidence of natural microbial infection.

A stressor may not cause mortality but can pre-dispose the insect to infection; the converse can also be true. Combined application of entomopathogenic fungi and insecticides as a strategy for pest control has been in use in Eastern Europe particularly in the former Soviet Union between the insect pathogenic fungus *Beaveria bassiana* and different acyl urea insecticides against a number of insect pests on a variety of crops (Ferron, 1978).

There is considerable evidence to show that acyl urea insecticides inhibit the synthesis of chitin (Kerr, 1977). The malformed cuticle that results may prove an easier target for the entry of an entomopathogenic fungus. The cuticle of locusts treated with acyl urea insecticides is prone to fracture in characteristic ways (*e.g.*, Kerr, 1977). This may in particular facilitate fungal penetration during joint applications (Hassan and Charnley, 1989). The present work was carried out during the period of June - October, 1998 to assess the effects of the acyl urea insecticide teflubenzuron (=Nomolt ®) and the entomopathogenic fungus ***Metarhizium anisopliae*** on 4th instar of ***Schistocerca gregaria*** when applied singly and jointly. An ultrastructural study on the effects of the dual application of the insecticide diflubenzuron (Dimilin®) and ***M. anisopliae*** was also carried out.

MATERIALS AND METHODS

The target insect

Schistocerca gregaria was reared according to the method described by Gillepsie *et al.* (1998). Briefly the method can be described as follows: The culture was maintained at constant temperature (27° C) under a 12 hr light and 12 hr dark photoperiod. Insects were kept in metal cages provided with fresh wheat supplemented by wheat bran and tap water. Newly ecdysed 4th instar

nymphs were used in these experiments as the cuticles of earlier instars are too soft to handle during treatments.

***Application of Nomolt as contact poison to 4th instar* S. gregaria**

Applications of Nomolt to fourth instar *Schistocerca* were made topically using a microcap on the ventral side of the abdomen often making the appropriate series of insecticide dilutions in acetone. Acetone was used a carrier because the technical form of Nomolt is hydrophobic and dissolves in acetone only. For all experiments, each concentration (a.i) w/v was kept agitated on a magnetic stirrer to prevent settling out of the suspension prior to use.

***The pathogenic effects of* M. anisopliae *for* Schistocerca**

Conidia of *M. ansopliae* were grown on Sabouraud's dextrose agar (1/4 SDA) in disposable plastic petridishes (9 cm) at 20° C in the dark. The cultures following sporulation were maintained in a refrigerator at 4° C for use within 4 weeks time.

Viability tests were carried out routinely by placing an aliquot of nutrient broth containing $1.5x10^5$ conidia into a sterile cavity microscope slide mounted on a U-shaped glass rod in petridish lined with moist filter paper. The microscope slides were stored at 27°C for 24 hrs. The preparations were observed under a microscope and the germination of 500 conidia was recorded from two microscope slides. Germination was considered to have occurred when the germ tubes were equal to the conidia and when germination was found to be not less than 90% of the conidia counted.

An arithmetic suspensions of *M. Anisopliae* was made up in 0.4% tween 80. Experimental ten 4th instar locusts per treatment were topically dosed on the ventral side of the abdomen with the fungal suspensions.

***Joint application of Nomolt and* M. anisopliae**

The experimental insects (10 insects/treatment) for the joint applications of Nomolt and *M. ansisopliae* were dosed with insecticide dilutions that showed LC10, LC20, LC30, and LC40 in the previous singly applied insecticide treated experiment and acetone for the controls (Table 1(a)) and $2.2x10^5$ conidia/ml which resulted in LC40 in the single treatment (Table 1(b)). For the ultra-

structural studies (see the next section below) 4th instar *S. gregaria* were fed on Dimilin or water (control) treated by spraying on to wheat seedlings grown in green house and the target insects inoculated with the fungus by dipping in *M. anisoplae* (10^8 conidia/ml). All experimental insects were maintained in a Fison's environment cabinet at constant high 39% RH and 28° C temperature, respectively.

Table 1(a)-(b). The toxicity of Nomolt (a) and *M. aniosopliae* (b) 72 hr and, 9 days, respectively to 4th instar S. gregaria.

(a)

Treatment (conidia/ml)	N	% Mortality
0	20	0
$4x10^3$	20	20
$4x10^4$	20	50
$4x10^5$	20	75
$4x10^6$	20	65

(b)

Treatment (mg/ml)	N	% Mortality
Control	20	0
0.036	20	15
0.230	20	40
0.510	20	65
1.020	20	90
3.605	20	8

Results were pooled from two experiments.

Ultra-structural studies on the combined effects of M. anisopliae *and Dimlin on adult* Schistocerca

The third abdominal sternite and associated intersegmental membranes were dissected in Ringer's solution from Dimilin or *Metarhizium* treated locusts, Dimilin and fungus treated individuals from controls (untreated). The samples were fixed in 1.5% gluteraldhyde in sodium (0.2 M) cacodylate buffer at 4% overnight. They were washed with cacodylate buffer and post fixed in 1% sodium tetroxide for 1 hour and washed again.

The samples were placed in resin over-night followed by four changes of pure resin over two days. Tissues were finally embedded in fresh LR white resin in

pre-dried Gelatin Capsules and cured for 24 hrs at 60° C polymerized blocks were cut down with razor blades prior to sectioning using a Reichermuz ultra microtome fitted with glass knives.

The sections (100 μm) were collected on copper 200 mesh grids and stained in 2% aqueous range acetate for 5 min followed by Reynolds lead for another 5 min. They were finally observed using a JEOL 12000 EX transmission electron-microscope at 80-100kv.

Statistical analysis of data

LC50s in dose response experiments with 95% confidence limits were calculated using probit analysis with the aid of Genstat 5 system whereas comparisons of data Table 2(b) were performed using χ^2 test.

Table 2(a). Effect of dual application of Nomolt and *M. anisopliae* on 4th instar *Schistocerca*.

Treatment	N	OM(%) /treatment	CM /treatment
Control	15	1	7
LC10 (I) + LC40 (F)	15	40	35.5
LC30 (I) + LC40 (F)	15	53	49.5
LC40 (I) + LC40 (F)	15	53	49.5
LC10 (I)	15	20	14.0
LC30 (I)	15	33	28.0
LC40 (I)	15	40	35.5
LC40 (F)+acetone	15	13	6.45
LC40 (I)	20	40	40.0 *

* data from Table 1; I, F, LC; OM, CM: Insecticide, Fungus, Lethal Concentration, Observed mortality and Corrected Mortality, respectively.

Results were pooled from two experiments and were corrected for control mortality using Abbot's formula.

RESULTS AND DISCUSSION

Nomolt as contact poison to 4th instar Schistocerca

Topical application of Nomolt to larval *Schistocerca gregaria* resulted in the cessation of feeding activity followed by failure to moult and eventual death. When low doses (0.05 mg/ml) were employed, some of the experimental animals were able to moult but died thereafter. Nomolt caused the highest mortality for the 4th instar *Schistocerca* 72 hrs after application Table 1(a).

The LC50 value was 0.27 mg/ml (95% confidence limits = 0.60 and 0.082). These results are consistent with published results on acyl-urea toxicity against locusts (Wakgari, 1997).

Symptoms of insecticidal action due to Dimilin as seen by Hassan and Charnley (1983) for *Manduca sexta* were however in accord with the effects of Nomolt on locusts, viz failure to moult with high doses, death during moulting in some cases, rupture of cuticle and in insects which succeeded to moult, failure to feed and eventual deaths were seen.

The pathogenic effects of M. anisopliae *on* S. gregaria.

The experiment on the pathogenicity of strain ME1 of *M. anisopliae* to the desert locust larvae was carried out twice using the protocol described in the Material and Methods section. The combined mortality 9 days after inoculation is recorded in Table 1 (b).

The fungus was an effective pathogen of 4th instar *S. gregaria*. The LC50 (mean of two experiments) for mortality was 2.8×10^5 conidia/ml. There was no mortality of untreated insects. No attempt was made in this study to determine causes of death other than from mycosis.

However, bacteria can accompany invading fungal hyphae into an insect cuticle, and thus septicaemia may account for a proportion of experimental deaths (Zachruck, 1974, cited in Hassan, 1983).

***Dual application of Nomolt and* M. anisopliae *on 4th instar* Schistocerca**

The concentration of conidia used for the joint application along with different insecticide dilutions was $2.2x10^5$ conidia/ml which resulted in 40% target mortality when the fungus was applied on its own (Table 1 (b)). The results for the combined application are shown in Table 2(a).

The dual application of insecticide (LC30) + fungus (LC40) caused significantly greater mortality than the fungus only treatment. The insecticide (LC40) and fungus (LC40) and the fungus-only treatments, however, were not significantly different (χ^2 see Table 2(b)).

Table 2(b). Comparison of results of joint application of *M. anisopliae* and Nomolt on 4th instar *Schistocerca*.

Treatment	χ^2
LC10 (I) VS LC30 (I) + LC40 (F)	3.97*
LC10 (I) VS LC40 (I) + LC40 (F)	3.98*
LC30 (I) VS LC30 (I) + LC40 (F)	2.85ns
LC40 (F) VS LC40 (I) + LC40 (F)	0.60ns
LC40 (F) VS LC10 (I) + LC40 (F)	0.60ns
LC40 (F) + acetone VS LC10 (I) +LC40 (F)	3.33*

χ^2, *, ns; Chi-square, significant and non-significant, respectively.

The question is whether the enhanced mortality in first combined treatment amounts to synergy. Harper (1986) has shown that the expected mortality from the combination of two independently acting mortality factors can be predicted by the formula:

$$P = P1 + P2 - P1 \times P2$$

where: P = Predicted decimal percentage kill by the combination
P1 = decimal percentage killed by agent 1
P2 = decimal percentage killed by agent 2

To determine whether the response of the dual treatment is greater than expected, the following Chi-square (χ^2) was applied.

$$\chi^2 = (O-E)^2/E$$

where: O = observed mortality in the combined treatment
E = Expected mortality calculated as P in the last formula.

Applying these two formulae to the present data showed that the observed mortality in the joint treatment is greater than the expected (49.5% vs 43.87%).

In the experiment that provided the result for Table 2 (a), the mortality from fungus alone (dose=$2.2x10^5$ conidia/ml was only 6.45% instead of the predicted 40% (see Table 1(b)). The difference between the two experiments was that in the second the two agents, fungus and insecticide were applied simultaneously and therefore the cuticle was treated with acetone. The inference must be that the acetone had somehow interfered with invasive properties of the fungus. Mathlein (1994) found that conidia of *M. anisopliae* germinated slowly on the regions of the cuticle *moth, Cossus cossus,* that had been treated with lipid solvents. Koidsumi (1957) extracted lipids that were fungicidal or fungitoxic (depending on concentration) from the cuticle of the Japanese Silkworm, *Bombyx mori* and the stem borer *Chilo simplex.* The most active were short chain saturated fatty acids which were presumed to be caprylic or capric acids. Lipids extracted from strains of *B. mori* resistant to *A. flavus* had greater anti-fungal activity than those from susceptible strains (Koidsumi, 1957). Thus the acetone may have removed lipid components of the epicuticle or otherwise altered the chemical properties of the epicuticle sufficiently to interfere with the adhesion of the fungal spore to the cuticle or reduce the availability of the nutrients for fungal germination.

Ultra-structural studies on the combined effects of M. anisopliae *and Dimilin on adult* Schistocerca

Sections were taken from the sternum and intersegmental membranes of insects treated orally with Dimilin. As expected limited disruption of the cuticle structure was observed. Fig. 1(c) shows a micrograph of section taken from intersegmental membrane of adult *S. gregaria* treated with Dimilin and shows

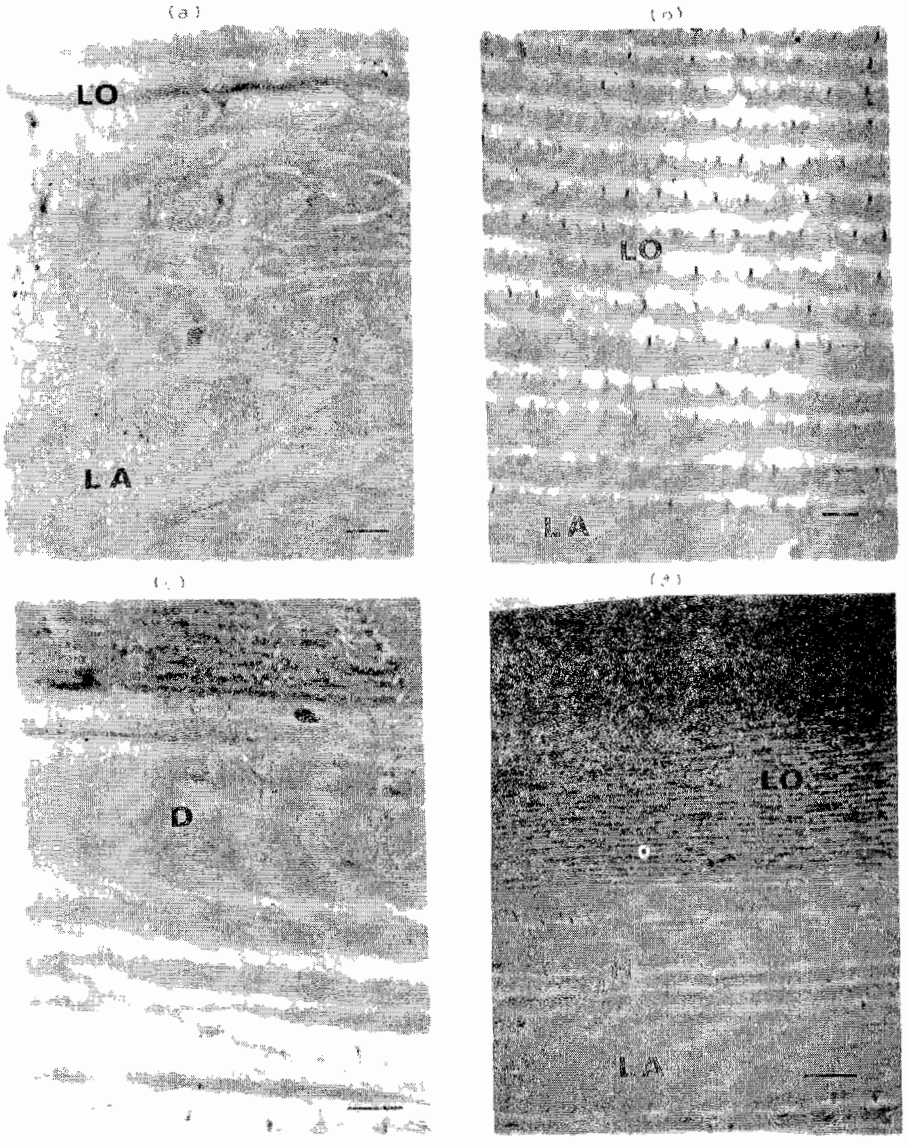

Fig. 1(a-d). Old (lo) and new (la) lamellar structures formed by epidermal cells are depicted in (a), (b) shows normal cuticular layers of old and new lamellae of untreated sections. Disrupted lamellar cuticular patterns due to Dimlin are depicted in (c) and a penetrating hypha (H) is shown in (d).

an area of disorganisation (the formation of cuticular layers and microvilii have been disrupted) (bar = 1μm). Some areas of cuticle from Dimilin-treated locusts e.g. Fig. 1(a) were affected i.e lack normal lamellar cuticular structures like that shown in Fig. 1 (b) was observed but not others e.g., 2 (c). Both Fig. 2 (c) and Fig. 1 (d) show procuticle adjacent to the epidermis, in the former there is no visible effect of Dimilin whereas in the latter there is an area of disorganisation. The fact that post-ecdysial lamellar cuticular pattern was disrupted is consistent with the short half-life of Dimilin in the locust (Kerr, 1977) and may be contrasted with the much more marked effect of Dimilin on post-ecdysial cuticle of *Manduca sexta* (Hassan and Charnley, 1987). The use of acetone was necessary because the technical form of Nomolt was dissolvable in acetone only.

Application of *M. anisopliae* to *Schistocerca* resulted in penetration of the fungus through the cuticle. Typical penetrant hypha can be observed in the procuticle in Figs. 2(a) and 2(b). It is interesting that in Fig. 2(a) the hypha is penetrating through the lamellae rather than parallel with the lamellae in contrast to a previous studies (Hassan and Charnley, 1989). The absence of the lamellar structure adjacent to the hypha is suggestive of the action of cuticle-degrading fungal enzymes. Clearing zones around penetrant hyphae are also apparent in Figs 2(a) and 2(b).

Micrographs of sections taken from Dimilin treated insects inoculated with *M. anisopliae* are shown in Figs. 1(b), 1(c) and 2(d). Fig. 1(b) shows a penetrant hypha surrounded by distinct area of histolysis (compare with Fig. 2(b). However, in Figs. 1(b) and 1(c) the penetrant hyphae are shown surrounded by larger areas of histolysis than in control cuticle in Fig. 1(a). The lamellar structure appears to be disorganized. These observations may be attributed to the effects of Dimlin in that cuticle without chitin may be susceptible to hydrolysis by fungal proteases.

Previous studies on the joint action of *M. anispliae* and Dimlin have shown that the Dimilin treated cuticle is much more susceptible to digestion by fungal enzyme than those non-dimilin treated cuticles (Hassan and Charnley, 1989). In *Marduca sexta* clearing zones around penetrant hyphae are restricted in extent in untreated cuticle possibly due to the molecular weight of fungal enzyme (Charnley, 1984). However in Dimlin-disrupted cuticle, Hassan and

Charnley (1989) found that the procuticle adjacent to the epidermis was virtually completely destroyed, absence of chitin fibrils, presumably aids movement of fungal enzymes through the cuticle.

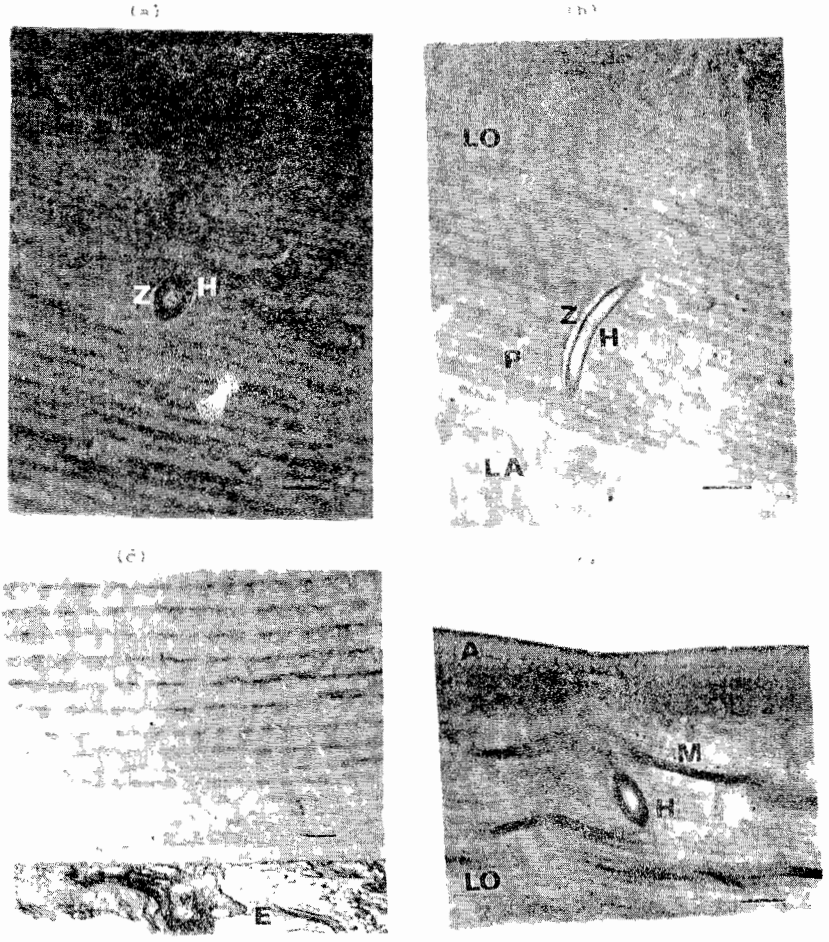

Fig. 2 (a-d). A penetrant hypha (H) and associated zone of hydrolysis (Z) along with a penetrating peg (P) and melanin like material (m) are shown in the old and new lamellae layers of fungus treated sections (a and b) while normal cuticular formation by the epidermal cells (E) is depicted in (C).

The reasons for the reduced effectiveness of Dimilin in the locusts may be that firstly unlike abdominal cuticle of the hornworm, a proportion of the locust cuticle is sclerotized (process of hardening that includes cross-linking of protein with quinones) and thus less available for hydrolysis, and secondly it would be unlikely that gross disruption could occur in the present study since Dimilin was not applied constantly but at intervals of 5 days.

CONCLUSION

Attempts in the present study to improve the general understanding about the role of acyl urea insecticides in inhibition of chitin synthesis on locusts and the synergistic action of the two acyl urea insecticides, Teflubenzuron and Diflubenzuron with the entompathogenic fungus *M. anisopliae* have shown promising results in terms compatibility under laboratory conditions. It is however clear that more work is needed before the use of dual application of the insecticides and the fungus can be contemplated in a programme in Integrated Pest Management (IPM).

ACKNOWLEDGEMENTS

The author is grateful to Dr A.K. Charnely for organizing the research and supervision. The author also thanks Dr Roderick Dillon and Mr Chris Vernard for technical assistance and rearing experimental insects, respectively.

REFERENCES

1. Charnley A.K. (1984). Physiological aspects of destructive pathogenesis in insects by fungi: a speculative review. **In**: *Invertebrate - microbial Interactions,* pp. 229–270 (Anderson, J.M., Rayner, A.D.M. and Walton, D.W.H., eds). Cambridge University Press, Cambridge.
2. Ferron, P. (1978). Biological control of insects by entomopathogenic fungi. *Ann. Rev. Entomol.* **23**:409–442.

3. Gillepsie J. P., Bateman R. and Charnley A.K. (1998). Role of cuticle-degrading protease in the virulence of *Metarhizium* spp. For the desert locust, *Schistocerca gregaria. J. Invertabr. Pathol.* **71**:128–137.

4. Harper J.D. (1986). Practical application for insect control. **In:** *The Biology of Basculoviruses,* Vol. II, pp. 133–155 (Granados, R.R. and Federici, B.A., eds). CRC Press, Boca Raton.

5. Hassan, A.E.M. (1983). The Interaction of the Entomopathogenic Fungus *Metarhizium anisopliae* (Sorokin) and Insecticide Diflubenzuron on *Manduca sexta* (Johanson). PhD Thesis, University of Bath.

6. Hassan, A.E.M. and Charnley, A.K. (1983). Combined effects of deflubenzuron and the entomopathogenic fungus *Metarhizium anisopliae* on the tobacco hornworm, *Manduca sexta.* **In:** *Proc. 10th Int. Congr. Plat Protect.* **3**, p. 790.

7. Hassan, A.E.M. and Charnley, A.K. (1987). The effect of Dimlion on the ultra-structure of the integument of *Manduca sexta. J. Insect Physiol.* **33**:790.

8. Hassan, A.E.M. and Charnley, A.K. (1989). Ultra-structural study of the penetration by *Metarhizium anisopliae* through Dimlin affected cuticle of *Manduca sexta. J. Invertebr. Pathol.* **54:**117–124.

9. Kerr, R.F. (1977). Investigation of locust cuticle using the insecticide Diflubenzuron. *J. Insect Physiology* **39:**39–48.

10. Koidsumi, K. (1957). Antifungal action of cultural lipids. *J. Insect Physiology* **1:**40–51.

11. Mathlein, R. (1994). Gronmykos foros akad au *Metrahizium anisopliae* (Metsch). Sorok. I. Granmykosen som biologiskt insektbekampningsmedel. *Statens Vaxtskyddsanstalt Meddlelande* **43**:1–58.

12. Wakgari, W. (1997). A comparison of efficacies of bran-based baits containing diflubenzuion, tefluenzuion and fenitrothion against desert locust, *Schisocerca gregaria* (Forsk) (Orthoptera: Acrididae). *Int. J. Pest Management* **43:**163–167.

SINET: Ethiop. J. Sci., 24(1):127–131, 2001
 ISSN: 0379–2897

Feature article

LAKE AFDERA: A THREATENED SALINE LAKE IN ETHIOPIA

Abebe Getahun

Department of Biology, Faculty of Science, Addis Ababa University
PO Box 1176, Addis Ababa, Ethiopia, E-mail: Biology.aau@telecom.net.et

ABSTRACT: Lake Afdera is a saline lake located in the Afar region, Northern Ethiopia. Because of its inaccessibility it is one of the least studied lakes of the country. It supports life including three species of fish of which two are endemic. Recently, reports are coming out that this lake is used for salt extraction. This paper gives some insight on the most probable dangers on the ecology of the lake if such activity is allowed to take place before environmental impact assessment was conducted.

Key words/phrases: Afdera, conservation, Ethiopia, fishes, saline lake

INTRODUCTION

Lake Afdera is located some 700 km north of Addis Ababa (12.6°N and 41°E, Fig. 1) at an altitude of 80 meters below sea level. "Afdera" by the local (Afar) language means inaccessible. The depression is under active volcanic and tectonic activities (Williams *et al.*, 1977). The molten black rocks and gravels all around the area and the hot springs that drain the lake, the only source of water other than the scanty precipitation, witness this reality. It is a rainfall deficit area receiving an average annual rainfall of about 100 mm (Wood and Lovett, 1979). A similar isolated and closed lake, Lake Asale, is found north of Lake Afdera at an altitude of 150 m below sea level. Awash River feeds the other lakes in that region (Abbe, Afambo, Bario and Gamari).

The surface area of Lake Afdera is 70 km^2; maximum depth is about 80 m; salinity = 160 gram per litter; conductivity = 250,000 K_{20} ($\mu^S cm^{-1}$); pH = 6.55 (Wood and Talling, 1988). The air, lake water and spring water temperatures in November around noon were 40° C, 33° C and 50° C, respectively. The

very high salinity is accounted by the high evaporative concentration and the lake's geological history of having marine inputs from the Red Sea (Gionfiantini *et al.*, 1973). Unlike the other saline lakes in Ethiopia (Lakes Abijata, Shala, Chitu and Metahara) the pH of Lake Afdera is low in the acidic range.

THE FISH FAUNA

Fishes were collected by the author in the vicinity of one hot spring in the southwestern portion of the lake. It is a location where the freshwater meets the saline lake water. The fishes strategically inhabit areas between the saline waters of the lake and the hot waters of the spring. Seine net (mesh size 6.25 mm) was utilized to collect fishes at this area and three species were identified:

1. *Danakilia franchettii* (Vinciguerra, 1931)

Fishes of this species were first collected by B.R. Franchetti in 1929 and identified as *Tilapia franchettii* by Vinciguerra in 1931. Thys van den Audenaerde (1969) assigned the new genus name *Danakilia*. Fishes of this endemic genus show noted sexual dimorphism and are found in large numbers in the vicinity of the hot springs that flow into the lake.

2. *Lebias dispar* (Rüppell, 1829)

This Killifish (known previously as *Aphanius dispar*) is widely distributed in shores of the Red Sea and Mediterranean Sea.

3. *Lebias stiassnyae* was recently discovered from the lake (Abebe Getahun and Lazara, 2001) and is endemic.

The above fishes were collected from a small segment of the lake (about $100m^2$ area) at the shore where one of the hot springs joins the lake. It is not known whether or not these fishes strive in the interior and even at shores where other springs join the lake. The exact number of springs joining the lake is also not known. Although the lake is reported to be biologically unproductive (Wood and Talling, 1988) no further mention was made as to the extent of its life forms (microbial, phytoplankton, zooplankton and others). Based on the fact that one endemic genus and one endemic species of fishes are identified from

a small portion of the lake, and the lake's isolation for a long time, it is reasonable to suspect that other novel life forms can also be found in this lake.

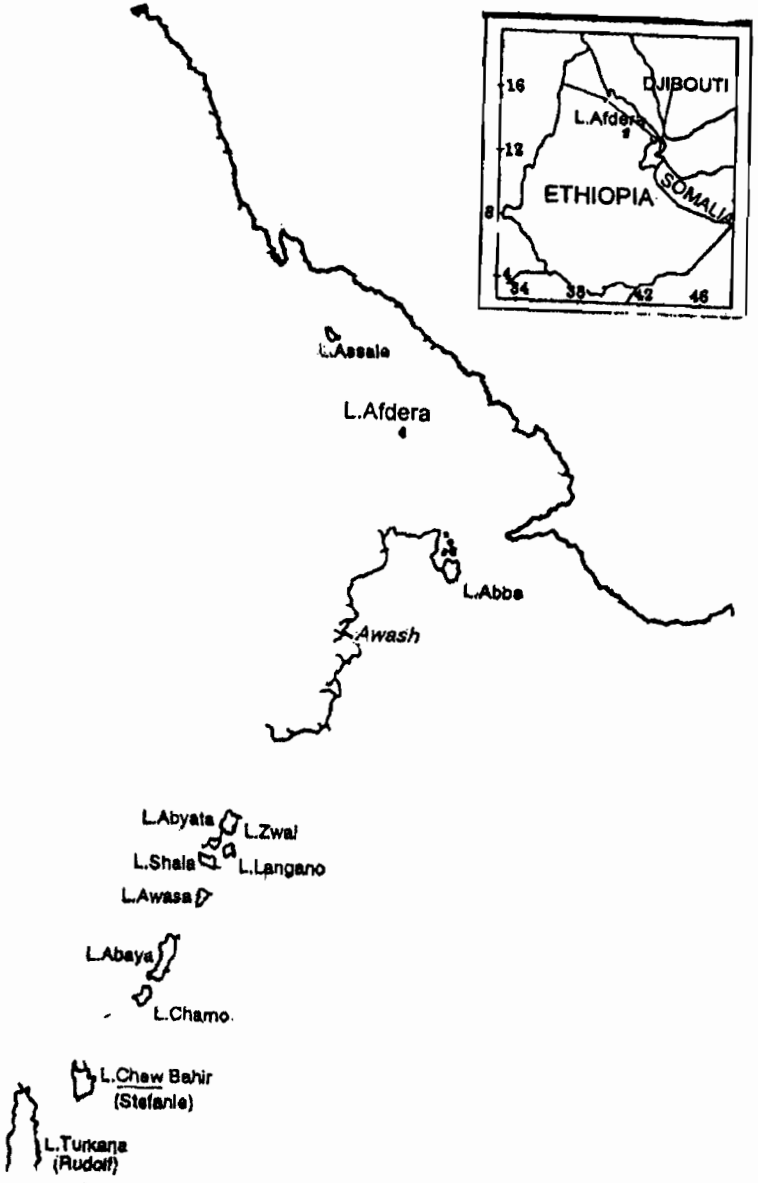

Fig. 1. Geographic location of Lake Afdera.

THREATS TO THE ECOSYSTEM

It is known that many of the streams and some of the lakes of Ethiopia are not well studied for their faunal diversity in general and their fish fauna in particular (Abebe Getahun and Stiassny, 1998). Accordingly, except sporadic visits, there have not been prior ecological and biological studies of Lake Afdera. By the same token, there have not so far been major human activities in and around the lake. However, the lake is facing potential threat now. A new gravel road is under construction to connect the lake to the main asphalt road that goes to the Red Sea port of Assab. One of the objectives is to make the lake a source of edible salt for the presently landlocked Ethiopia and production has already started. Salt extraction needs canalizations of the lake water and, thus, much water level reduction is expected due to large surface area evaporation. Associated with the salt extraction, ,or any activity therein, the spring waters which are the main source of freshwater to the lake and on which the above species of fish depend, could be blocked from entering the lake and thereby affecting life in the Lake.

Therefore, the above economic activity, although vital to the country's needs, has to be undertaken with caution. The ecosystem has to be studied well before implementing such large-scale economic activity on the lake that could affect life forms and the ecosystem at large. It is recommended that a team of scientists should study the impact of this activity and the risks involved pertaining to the loss of biodiversity. Its outcome would be helpful to avert any future demise of this interesting lake, which at present appears to be at risk.

REFERENCES

1. Abebe Getahun and Stiassny, M.L.J. (1998). The biodiversity crisis: The case of the Ethiopian fish fauna. *SINET: Ethiop. J. Sci.* **21(1)**:207–230.

2. Abebe Getahun and Lazara, K.J. (2001). *Lebias stiassnyae*: a new species of killifish from Lake Afdera, Ethiopia (Teleostei: Cyprinodontidae). *Copeia* **1**:150–153.

3. Gionfiantini, R.S., Ferrara, G. and Panichi, C. (1973). Isotopic compositions of waters from the Danakil depression (Ethiopia). *Earth Planet. Sci. Lett.* **18**:13–21.

4. Rüppell, E. (1829). *Atlas zu der Reise im nordlichen Afrika von Eduard Ruppell. Fische des roten Meers*. Gedruckt und in Commission bei Heinrich Ludwig Bronner, Frankfurt am Main. Part II:27–94.

5. Thys van den Audenaerde, D.F.E. (1969). *An annotated bibliography of Tilapia (Pisces, Cichlidae)*. M.R.A.C. Tervuren (Doc. Zool.), 14:x1+450p.

6. Vinciguerra, D. (1931). Spedizione del Barone Raimondo Franchetti in Dancalia. Rettili, batraci e pesci. *Ann. Mus. Civ. Stor. Nat. Giacomo Doria* **55**:104–108.

7. Williams, M.A.J., Bishop, P.M. and Dakin, F.M. (1977). Late quaternary lake levels in southern Afar and the adjacent Ethiopian Rift. *Nature* **267**:690–693.

8. Wood, C.A. and Lovett, R. (1979). Rainfall reliability in Ethiopia, Tables and maps. *SINET: Ethiopian J. Sci.* **2**:111–120.

9. Wood, R.B. and Talling, J.F. (1988). Chemical and algal relationships in a salinity series of Ethiopian inland waters. *Hydrobiologia* **158**:29–67.

SINET: Ethiop. J. Sci., 24(1):133–138, 2001
 ISSN: 0379–2897

Feature article

TWIN CARBON ARC TORCH

David A. Skelskey

Don Bosco Technical School, PO Box 8, Makelle, Ethiopia

ABSTRACT: A simple twin carbon arc torch has been manufactured for the developing world from local materials and applied to brazing and heating in order to offer an alternative to the much more expensive oxyacetylene torch and to the usually environmentally degrading use of charcoal.

Key words/phrases: Arc, brazing, carbon electrode, plasma, torch

DESCRIPTION

The twin carbon-arc torch has been known and used for some time (Brumbaugh, 1976; Nippes, 1985), but in countries of widespread higher technology its predominate applications in heating, brazing, and welding have been supplanted by the highly developed oxyacetylene torch. As seen in Fig. 1, the twin carbon arc torch (henceforth referred to in this article as simply the carbon-arc torch) consists of a hand held apparatus made of two ('twin') carbon or graphite electrodes whose distance from each other (so its arc) is operator controlled. The power of this type of torch comes from an AC or DC arc welder - quite common throughout most of the developing world. The disassembly Fig. 2, shows the simple construction of the locally manufactured carbon arc torch. Welding cables are attached to copper tubing conductors which pass through an insulating asbestos sheet handle and terminate in carbon electrodes. There are finger operated control mechanisms: one which initiates the arc and another which maintains the arc by adjusting the distance between the electrode tips.

Fig. 1. Operator holding a twin carbon-arc torch made from locally available materials.

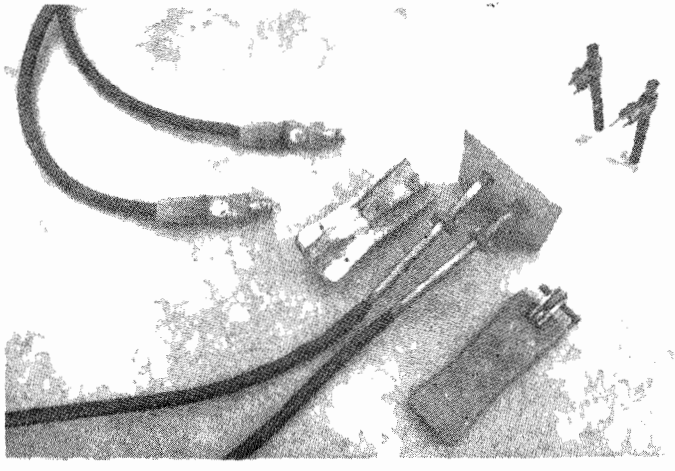

Fig. 2 Twin carbon-arc torch disassembled. Basic materials used for parts are 25 mm^2 multi-strand copper cable, 10 mm in diameter copper tubing, brass rod, asbestos sheet, plastic sheet, and carbon electrodes.

A main attraction of this simple torch is its use of 'freely' available carbon electrodes. This torch uses the anodes (positive electrodes each with a diameter of 8 mm and a length of 55 mm) of used/spent D size dry cells abundant throughout the developing world (see Fig. 3). It is the heat generated by the electric arc between the twin carbon electrode tips that is the heart of the apparatus. A pair of these carbon electrodes will last about 15 minutes while brazing at a typical current of 70 amperes. The carbon electrodes are not to be considered here as consumable electrodes (becoming part of the material heated); because of the high temperatures attained by the arc the carbon electrodes slowly vaporize. The arc is a plasma attaining a temperature of thousands of degrees centigrade depending on the exact region of the plasma. The radiant heat produced by the arc is what the operator of the carbon-arc torch must put to use. Thus it is the skill of its operator that is the prime definer of the applications of the carbon-arc torch.

Fig. 3. The carbon electrodes used by the twin carbon-arc torch come from spent/used D sized dry cell batteries.

USES

Heating

Many smaller metal working shop needs involve the heating of metal in order to bend it or to forge it. Figure 4 shows examples of metals that were heated by the carbon arc torch and then simply bent in the common bench vise. Both where the use of the oxyacetylene torch is prohibitively expensive and where the use of charcoal is not only expensive but environmentally damaging the carbon arc torch may offer a more appropriate alternative method of heating.

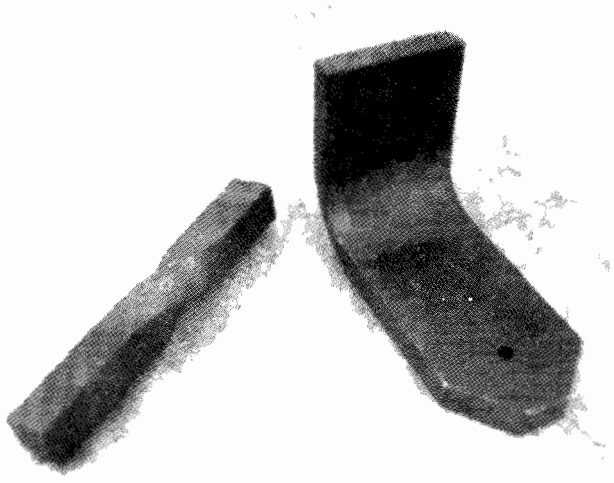

Fig. 4. Steel bars (12 mm x 12 mm, and 8 mm x 40 mm) bent after heating with the twin carbon-arc torch.

Brazing

The main purpose for which this carbon arc torch was developed was simple brazing and braze welding. Figure 5 illustrates sheet metal brazed together using the carbon-arc torch and a pipe fixture braze welded. With care even delicate brazing of small copper tubing can be accomplished with this torch (see Figure 6).

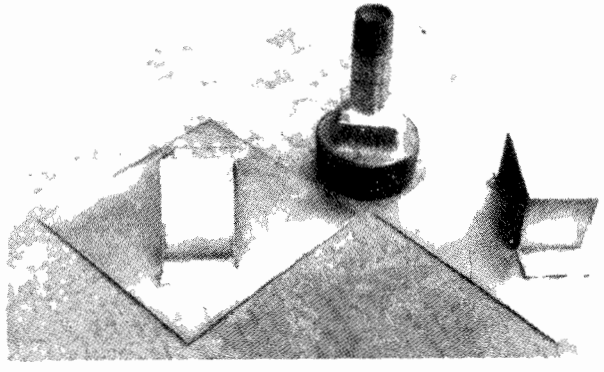

Fig. 5. Sheet steel (0.8 mm thick) brazed together and a piece of ⅜" pipe braze welded into a 1½" plug using the twin carbon-arc torch.

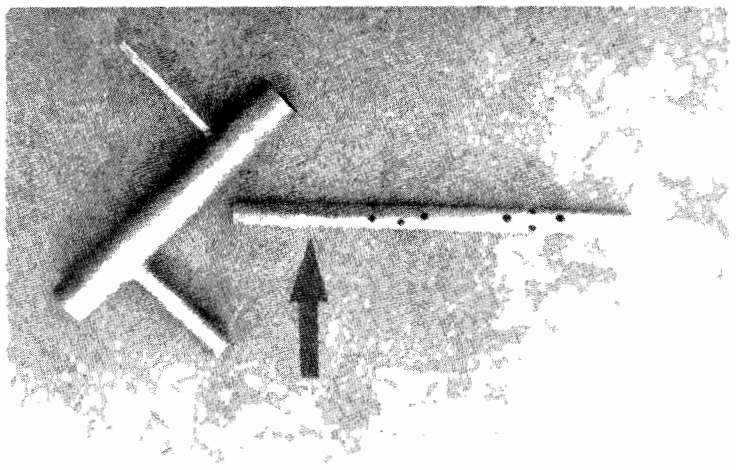

Fig. 6. Using the twin carbon-arc torch pieces of 10 mm diameter and 5 mm diameter copper tubing were brazed at right angles to a piece of 16 mm diameter copper tubing. At the point of the arrow the 10 mm diameter copper tubes were brazed end to end.

ECONOMICS

In the country (Ethiopia) in which this torch was designed the alternative, the oxyacetylene torch, was essentially unavailable on the town level and found in less than 25% of the metal working shops on the city level. A strong argument for the use of the carbon-arc torch is its low cost. Assuming the ownership of a modest electric arc welder, the initial cost of our carbon-arc torch was twenty times less than the simplest oxyacetylene torch apparatus (more than 50% of the cost of the carbon-arc torch consisted in the retail price of 12 meters of welding cable). When considering that for ongoing maintenance there are not the problems of gas tank refills and transportation costs, the carbon-arc torch is vastly cheaper.

As any technical tool the carbon-arc torch needs a bit of patience in the development of skill in its use. The proper setting of the arc welder current comes quickly, but ability to direct the radiant heat of the arc onto the area to be heated comes only with skill and experience. We judge that a determined and competent metal worker/artisan can easily meet such a challenge especially when attracted by the economic benefits.

REFERENCES

1. Brumbaugh, J.E. (1976). *Welders Guide and Handbook.* Audels, D.B. Taraporevala Sons, Bombay, pp. 14, 197–198.

2. Nippes, E.F. (1985). Joining. **In**: *Metals Handbook, Desk Edition*, pp. 308–309, (Boyer, H.E. and Gall, T.L., eds). ASM, Metals park, Ohio.